

**LUMINESCENCE-ACTIVATED CYCLASE ALLOWS LOCALIZED PHOTO AND
CHEMICAL STIMULATION OF cAMP SYNTHESIS**

by

Nyla Naim

BS, State University of New York at Albany, 2012

Submitted to the Graduate Faculty of
the School of Medicine in partial fulfillment
of the requirements for the degree of
Doctor of Philosophy

University of Pittsburgh

2018

UNIVERSITY OF PITTSBURGH
SCHOOL OF MEDICINE

This dissertation was presented

by

Nyla Naim

It was defended on

July 30, 2018

and approved by

Alessando Bisello, Associate Professor, Pharmacology & Chemical Biology

Guillermo Romero, Associate Professor, Pharmacology & Chemical Biology

Jean-Pierre Vilardaga, Professor, Pharmacology & Chemical Biology

Jack Lancaster, Professor, Pharmacology & Chemical Biology

Adam Kwiatkowski, Assistant Professor, Cell Biology

Dissertation Director: Daniel Altschuler, Associate Professor, Pharmacology & Chemical
Biology

Copyright © by Nyla Naim

2018

LUMINESCENCE-ACTIVATED CYCLASE ALLOWS LOCALIZED PHOTO AND CHEMICAL STIMULATION OF cAMP SYNTHESIS

Nyla Naim, PhD

University of Pittsburgh, 2018

Cyclic adenosine monophosphate (cAMP) is a ubiquitous second messenger that regulates cellular proliferation, differentiation, attachment, migration, and several other processes. It has become increasingly evident that tight regulation of cAMP accumulation and localization confers divergent yet specific signaling to pathways downstream. Currently, few tools are available with sufficient spatial and temporal resolution to study location-biased cAMP signaling. Here, we introduce a new fusion protein consisting of a light-activated cyclase (bPAC) and luciferase (nLuc). This novel construct allows dual activation of cAMP production using temporally precise photostimulation or chronic chemical stimulation. Furthermore, we directed this construct to various subcellular compartments to improve spatial resolution. Using a combination of FRET imaging and optogenetics, we investigate location-biased signaling in thyroid epithelial mitogenesis and potential applications of bPAC-nLuc *in vivo*. A better understanding of the physical interactions and dynamics between cAMP and multiple signaling pathways may provide new therapeutic approaches for treating diseases with aberrant cAMP signaling.

TABLE OF CONTENTS

PREFACE.....	XII
1.0 INTRODUCTION.....	1
1.1 CAMP REGULATORY PROTEINS	2
1.1.1 GPCR and Gas Signaling	2
1.1.2 Adenylyl Cyclase.....	3
1.1.3 cAMP-dependent Protein Kinase A.....	4
1.1.4 Exchange Protein Directly Activated by cAMP.....	5
1.1.5 Phosphodiesterase.....	6
1.2 CAMP COMPARTMENTALIZATION PARADIGM	8
1.2.1 Problems with Previous Models of cAMP Diffusion	8
1.2.2 Direct Measurements of cAMP Diffusion	10
1.2.3 cAMP Compartmentalization Model.....	12
1.3 EVIDENCE FOR CAMP COMPARTMENTALIZATION	14
1.3.1 Compartmentalization of Membrane, Cytosol, and Nucleus	16
1.3.2 Small Scale Compartmentalization.....	18
2.0 TSH/CAMP SIGNALING PROMOTES THYROID CELL PROLIFERATION.....	23
2.1 INTRODUCTION	23

2.1.1	TSH is a Master Regulator of Thyroid Function.....	23
2.1.2	TSH Stimulates cAMP-Dependent Proliferation.....	24
2.1.3	Radixin-PKA-EPAC Complex Role in Mitogenesis.....	26
2.2	METHODS.....	28
2.2.1	Cell Culture and Transfection.....	28
2.2.2	Plasmid Construction	29
2.2.3	Immunocytochemistry.....	29
2.2.4	Real-Time FRET Imaging	30
2.2.5	BrdU Incorporation Assay.....	30
2.3	RESULTS	31
2.3.1	Radixin-Associated cAMP Compartment.....	31
2.3.2	N-Radixin Localized cAMP Production Stimulates Mitogenesis.....	34
2.4	DISCUSSION.....	36
3.0	LUMINESCENCE-ACTIVATED CYCLASE ALLOWS DUAL PHOTO AND CHEMICAL ACTIVATION OF CAMP SYNTHESIS	39
3.1	INTRODUCTION	39
3.1.1	Current Methods for Measuring and Modulating cAMP	39
3.1.2	Fluorescence Resonance Energy Transfer Biosensors.....	39
3.1.3	Localized Phosphodiesterase Activity.....	44
3.1.4	Signalosome Disruption	44
3.1.5	Localized Adenylyl Cyclases.....	45
3.2	METHODS.....	48
3.2.1	Cell Culture and Transfection.....	48

3.2.2	Plasmid Preparation.....	49
3.2.3	Lentiviral Infection and Stable Cell Line Generation.....	49
3.2.4	Luminescence Assays	51
3.2.5	Real Time cAMP Imaging – Red Dimerization Dependent Sensor	51
3.2.6	Optogenetic Stimulation.....	52
3.2.7	ELISA	53
3.2.8	Immunocytochemistry.....	54
3.3	RESULTS.....	54
3.3.1	Luminescence-Activated Cyclase Allows Dual Photo and Chemical Activation of cAMP Production.....	54
3.3.2	Luminescence-Activated Cyclase Can Be Localized to Distinct Subcellular Compartments.....	59
3.4	DISCUSSION.....	62
4.0	POTENTIAL APPLICATIONS FOR LUMINESCENCE-ACTIVATED CYCLASE	66
4.1	INTRODUCTION	66
4.1.1	Spatial Regulation of cAMP Synthesis in Thyroid Mitogenesis.....	66
4.1.2	Temporal Regulation of cAMP in GPCR Signaling.....	67
4.1.3	<i>In Vivo</i> Effects of cAMP in B16-F10 Mouse Melanoma Metastasis Model.....	68
4.1.4	Direct Lentiviral Thyroid Injection with Ultrasound Guided Microinjection	70
4.2	METHODS.....	70

4.2.1	PCCL3 EdU Incorporation Assay.....	70
4.2.2	HEK293 Cell Culture and Luminescence	71
4.2.3	FRET Imaging	72
4.2.4	B16-F10 Melanoma Cell Culture	73
4.2.5	Melanoma Metastasis Model	73
4.2.6	Ultrasound Guided Thyroid Microinjection.....	74
4.3	RESULTS	74
4.3.1	bPAC-nLuc Stimulates Thyroid Cell Mitogenesis	74
4.3.2	<i>In Vitro</i> Sustained and Transient cAMP Signaling in HEK293	77
4.3.3	<i>In Vivo</i> Application in Mouse Melanoma Metastasis Model	80
4.3.4	Ultrasound Guided Lentiviral Injection in Thyroid Lobes	83
4.4	DISCUSSION.....	86
4.4.1	Luminescence-Activated Cyclase Stimulation of Thyroid Mitogenesis....	86
4.4.2	<i>In Vitro</i> Sustained and Temporal Signaling of bPAC-nLuc	88
4.4.3	<i>In Vivo</i> Applications of bPAC-nLuc	89
4.4.4	Closing Remarks.....	91
	APPENDIX A	92
	APPENDIX B	101
	BIBLIOGRAPHY	104

LIST OF TABLES

Table 1. List of Arduino-controlled LED system components.....	95
--	----

LIST OF FIGURES

Figure 1. GPCR-mediated cAMP signaling.....	7
Figure 2. Mechanistic models of cAMP compartmentalization.	14
Figure 3. TSH/cAMP-stimulated mitogenic pathway.	28
Figure 4. Targeted FRET sensors demonstrate higher cAMP levels in the Radixin-localized compartments upon TSH stimulation.	33
Figure 5. Cytosolic and N-Rx-localized bPAC stimulates mitogenesis.	35
Figure 6. Fluorescence resonance energy transfer biosensors.....	41
Figure 7. Lentiviral infection of PCCL3 cells.	50
Figure 8. Arduino-compatible LED system and stage.....	53
Figure 9. Luminescent characteristics of bPAC-nLuc fusion protein.....	56
Figure 10. Photo and chemical stimulation activates bPAC-nLuc.	58
Figure 11. Luminescence-activated cyclase can be targeted to different sub-cellular regions.....	60
Figure 12. Stable lentiviral-infected PCCL3 expression and luminescence.....	62
Figure 13. Light and luciferin-activated bPAC-nLuc stimulates mitogenesis.....	75
Figure 14. Localized bPAC-nLuc constructs stimulate proliferation.	77
Figure 15. Luciferin-induced luminescence in HEK293.	78

Figure 16. Light and chemical activation mimic cAMP production phases in PTH receptor signaling.....	79
Figure 17. B16-F10 stable cells used for <i>in vivo</i> study express GFP and bPAC-nLuc.	81
Figure 18. bPAC-nLuc use in the mouse melanoma metastasis model.....	82
Figure 19. Intradermal tumor formation of bPAC-nLuc expressing B16-F10.	83
Figure 20. Ultrasound guided thyroid lobe injection.	85
Figure 21. Diagram of Arduino-controlled LED system.	93
Figure 22. Arduino-controlled system.	97
Figure 23. Portion of Arduino code for LED illumination.	100
Figure 24. N-Rx targeting motif does not alter cAMP affinity.....	102
Figure 25. bPAC expression can be controlled using the DD/shield-1 inducible system.	103

PREFACE

The phrase popularized by Isaac Newton, “If I have seen further it is by standing on the shoulders of Giants,” encapsulates my view as a scientist, particularly after learning the history of the idiom. Most reiterations of this hackneyed phrase exclude the original metaphor by Bernard of Chartres, “We are like dwarfs sitting on the shoulders of giants. We see more, and things that are more distant, than they did, not because our sight is superior or because we are taller than they, but because they raise us up, and by their great stature add to ours.” I find this reminder that we are humbly smaller in perspective compared to the grand body of literature supporting biomedical research. We strive to bring the universe in our heads into something our hands can grasp through innovative and sometimes clumsy ways. We do not aim to be giants; we just want to see a little further. This metaphor suggests that over time some dwarfs become giants, but I think this is a mistake in perspective. The ‘giants’ we see are an amalgamation of many dwarfs who have worked as we have. Thus, I would like to thank my fellow dwarfs who worked with me, provided support and guidance, and helped me see farther.

Dr. Daniel Altschuler and my lab colleagues have been instrumental in carrying out this work and helping me gain independence as a scientist. Jeff Reece developed the Arduino system from scratch and provided excellent training. My committee members continually provide insight into shaping experimental approaches. The Molecular Pharmacology Training Program and Department of Pharmacology have provided ample support and opportunities for developing

my career. I would like to thank my many collaborators and professors who supported this research: Dr. Adriana Larregina and Olga Tkacheva of the Department of Dermatology for teaching methodology and sharing resources for the mouse melanoma metastasis model; Dr. Jian Yu and Nathan Yates of the Department of Developmental Biology for teaching methodology and sharing resources for the ultrasound guided microinjection mouse model; Dr. Jean-Pierre Villardaga and Alex White for conducting FRET experiments in the HEK293 cell model and sharing resources; Dr. Simon Watkins for aid in imaging in EdU-based proliferation assays; and Dr. Davide Calebiro of the University of Würzburg for expanding my training. Furthermore, I would like to thank Dr. Kees Jalink (Netherlands Cancer Institute) for providing the H208 sensor, Dr. Walter Storkus (University of Pittsburgh) for providing the B16-F10 cell line, and Dr. Hak Soo Choi (Harvard Medical School) for providing the T800-F.

Lastly, I would like to thank my favorite dwarfs who stood with me, even on low ground. My husband, Ethan, is the tallest dwarf I know and thus provides the greatest support I could have ever asked for. My parents, sisters, Sifu, friends, and the Fair People of Heidiland have brought me light, laughter, and countless memories which I cherish. Together you make tall.

Work from this thesis surrounding the development of the luminescence-activated cyclase has been submitted for publication at this time.

1.0 INTRODUCTION

Since the discovery of cyclic adenosine monophosphate (cAMP) over 60 years ago, it has been regarded as a critical molecule in basic cell function and human disease (1). cAMP is a key signaling node for multiple pathways including proliferation, differentiation, attachment, and migration. The initial discovery spurred a cascade of breakthroughs such as the isolation of cAMP-dependent protein kinase A (PKA), which formed the major biomedical field of protein phosphorylation (2,3). It filled major gaps in knowledge in G Protein Coupled Receptors (GPCRs) signaling (4-9). Additionally, cAMP regulation was vital to understanding hormone-mediated glycogen metabolism (3). As of now, seven Nobel prizes have been awarded for studies directly tied to cAMP signaling. However, even with a robust history of research, the field still lacks an understanding of how cAMP can activate specific downstream pathways. Fundamental knowledge of cAMP signaling and regulation reaches across disciplines and thus remains essential for biomedical advancement.

One key example that illustrates our gaps in understanding cAMP pathway specificity came early after its discovery. Researchers found cAMP negatively regulated proliferation in lymphocytes, fibroblasts, and several other mammalian cells (10,11). Hence it became a widely accepted dogma that cAMP was an inhibitor of proliferation. However, other groups found cAMP stimulated proliferation in non-dividing lymphocytes and thymocytes (12,13). Since then, multiple cell types have been added to each side and contradicting roles of cAMP have also been

found in other cells processes. This discrepancy demonstrates that the context of cAMP signaling is key to determining downstream effects. Cumulating literatures reveals the stimulus (14-16), cell type (17-21), and disease state of a cell can alter the outcome of cAMP signaling (22). To distinguish the effects of cAMP, careful attention must be given to the conditions of the cell and environment. The regulatory machinery and kinetics of cAMP itself will be reviewed in this section.

1.1 cAMP REGULATORY PROTEINS

1.1.1 GPCR and Gas Signaling

cAMP synthesis is canonically stimulated by G-protein coupled receptor (GPCR) signaling. GPCRs are a class of transmembrane proteins with 7 membrane-spanning helices that transduce extracellular signals to intracellular actions. Upon binding to a ligand at its N-terminus, the receptor undergoes a conformational shift that stabilizes its interaction with the coupled heterotrimeric G protein (23). Activation of the G protein prompts exchange of GDP for GTP and dissociation of the $G\alpha$ GTPase subunit from the $G\beta\gamma$ dimer (24). Of the four $G\alpha$ protein subclasses, two regulate adenylyl cyclases (ACs) (25). $G_{\alpha s}$ stimulates AC whereas $G_{\alpha i}$ inhibits it. While $G_{\alpha i}$ can inhibit a few cyclase isoforms, $G_{\alpha s}$ can stimulate all nine isoforms of transmembrane AC (26). GPCR signaling is regulated by receptor endocytosis. Most activated GPCRs bind the scaffolding protein β -arrestin which sterically blocks G protein interactions and couples the receptor to the endocytotic machinery (27).

1.1.2 Adenylyl Cyclase

Transmembrane ACs exist as dimers with 12 membrane-spanning helices and two cytoplasmic domains, C1 and C2, which form the catalytic pocket for converting ATP into pyrophosphate and cAMP (28,29). GTP-bound G α s activates cyclase through allosteric modulation of the active site (30). Additionally, the pharmacologic agent forskolin can activate cyclase isoforms 1-8 alone or with G α s in a synergistic or additive manner (31). Canonical activation occurs at the membrane, but sustained cyclase activation and signaling can occur from endosomes following the activation and internalization of the GPCR (32-35). Endosomal generated cAMP has been shown to elicit distinct effects from membrane generated cAMP (36).

Another source of cAMP production is soluble AC (sAC or sAC10). As the name implies, this isoform lacks transmembrane domains and can be found throughout the cytosol. sAC is a ~187 kDa dimer containing C1 and C2 catalytic domains similar to transmembrane cyclases (37). However, unlike the transmembrane isoforms it does not respond to G α s or forskolin; instead, it is activated by Ca⁺² and bicarbonate (37,38). sAC is unique in that it is the only isoform that can produce cAMP in non-membrane regions. It has been shown to localize to the cytosol, nucleus, mitochondria, and sub-membrane regions (39-46). While GPCRs classically stimulate transmembrane cyclases, some have shown GPCRs can activate sAC indirectly through Ca⁺² release from the endoplasmic reticulum (47).

Individual cyclase isoforms have been linked to distinct physiological responses. For example, learning and memory (48-51), cardiac myocyte function (52), and olfaction (53) have been linked to specific AC isoforms (54). Some isoforms have been found to localize proximal to specific GPCRs or associate with lipid rafts, suggesting a potential mechanism for how GPCR signaling can activate individual isoforms (55,56). For example, in cardiac myocytes β 1-

adrenergic GPCRs are enriched in caveolae-lipid rafts with AC6; however, the GPCR prostaglandin E2 that localizes in non-raft regions of the membrane does not activate cyclase 6 (57,58). In sum, multiple sources of cAMP reside throughout the cell and AC isoform localization can overlap with specific proteins and protein complexes.

1.1.3 cAMP-dependent Protein Kinase A

Once cAMP is synthesized, cAMP can activate a handful of effector proteins which ultimately lead to a wide array of physiological responses. The first effector identified was cAMP-dependent protein kinase A (PKA), a tetrameric protein consisting of two regulatory subunits and two catalytic subunits (2,59). Binding to four molecules of cAMP triggers dissociation of the catalytic subunits which can then phosphorylate serine/threonine substrates (60). Recently a combination approach using CRISPR-Cas9 genome editing and large-scale mass spectrometry identified 229 PKA target proteins in mouse kidney epithelial cells (61), demonstrating the enormous number of pathways that PKA affects.

The first mention of PKA compartmentalization was in the late 1970s when Corbin et al. (62) identified particulate-bound PKA and cAMP. They noted this localization was advantageous for signaling since it placed the cAMP effector protein near the site of synthesis. Furthermore, after activation at the membrane, the dissociated PKA catalytic domains served as the “mobile” units for activating downstream cytoplasmic proteins rather than cAMP diffusion activating distant PKA. Later, the group of Brunton, Hayes, and Mayer elegantly demonstrated differential activation of PKA in the cytoplasm and sub-plasma membrane region through two different GPCR pathways. They found stimulating prostaglandin E1 increased PKA activation in soluble fractions. However, stimulation of the β -adrenergic receptor, which also elevated cAMP,

increased PKA activation in both soluble and particulate fractions. Furthermore, despite similar levels of cAMP, only β -adrenergic signaling activated glycogen phosphorylase (14,15,63-65). The concept of PKA pools and potential spatial distinction of cAMP activation is still being investigated today.

PKA compartmentalization or its presence in signalosomes is governed by associated scaffolding proteins. PKA localization depends on which A Kinase Anchoring Protein (AKAP) it binds. AKAPs are a diverse family of proteins that has little sequence similarity and are only united by one feature: a 14-18 residue amphipathic helix that binds to the PKA regulatory subunit dimer (66,67). They contain several docking sites, each with a unique set of binding partners such as phosphatases, kinases, small GTPases, guanine exchange factors, phosphodiesterases, membrane receptors, and ion channels (68). Furthermore, AKAPs can adapt multiple conformational states that alter which proteins they bind (69). AKAPs have been found in several compartments including the membrane, nucleus, mitochondria, cytoskeleton, and centrosomes (70) to create dynamic cAMP-sensitive signalosomes throughout the cell. Since PKA can phosphorylate numerous proteins, AKAPs regulate pathway specificity by positioning PKA substrates and cAMP regulatory machinery to foster preferential activation (71). Interestingly, PKA can inhibit its own activation and reduce cAMP levels by blocking AC activation and activating PDEs, both of which are believed to be regulated by AKAP interactions (68,72-74).

1.1.4 Exchange Protein Directly Activated by cAMP

Another major cAMP effector protein is Exchange Protein Directly Activated by cAMP (EPAC). Its discovery 20 years ago identified it as a guanine nucleotide exchange factor (GEF) for the

Rap1 GTPase (75,76). GEFs facilitate GDP dissociation from inactive GTPases, allowing GTP to bind and form an active complex. The C-terminus of EPAC contains a catalytic CDC25-homology domain that is stabilized by the Ras-Exchange Motif domain and Ras-association domain (77). The autoinhibitory N-terminal regulatory region of EPAC contains a cAMP binding domain (CBD), a membrane-anchoring DEP (**D**isheveled-**E**gl-10-**P**leckstrin) domain, and an EBD domain (**E**RM-**B**inding **D**omain) (78,79). EPAC has been found to activate multiple proteins including Ras, Rho GTPases, and phospholipase C- ϵ (80).

The EPAC1 isoform has been identified at the plasma membrane, cytosol, nuclear envelope, and mitochondria (81). EPAC1 localization at the membrane has been described by two different mechanisms which require an intact DEP domain. Studies suggest activated EPAC1 can bind to the membrane directly by interacting with phosphatidic acid (82). EPAC1 can also directly bind to ERM (**E**zrin, **R**adixin, **M**oesin) cytoskeletal scaffolding proteins, which recruit EPAC to the membrane (79,83). Interestingly, phosphatidic acid bound EPAC exhibits even expression along the membrane whereas ERM-associated EPAC forms clusters along the membrane (83). EPAC localization at the nuclear envelope depends on interaction of EPAC1's Ras-association domain which can interact with Ran, a small GTPase that regulates nuclear transport (84). Although more recent studies suggest RabBP2 anchorage of EPAC1 is independent of Ran (83,85). These examples demonstrate spatial regulation of EPAC is critical for its function.

1.1.5 Phosphodiesterase

cAMP is rapidly degraded by phosphodiesterases (PDEs). These enzymes play a major role in shaping the duration of cAMP signaling. PDEs catalyze hydrolysis of the 3' phosphate bond of

cAMP and cyclic guanine monophosphate (cGMP) into 5'-AMP and 5'-GMP, respectively. There are 11 PDE families that of which PDE 1, 3, 4, 7, 8, and 10 preferentially bind cAMP over cGMP (86). Only PDE 4, 7, and 8 are cAMP specific. PDE isoforms demonstrate differential tissue expression as well as distinct localization patterns in cells. For example, PDE8B1 is only expressed in the thyroid and can be found in cytosolic and particulate fractions, while PDE4A is widely expressed throughout the body and can localize in membrane ruffles and bind to scaffolding proteins such as β -arrestin and AKAPs (86). PDE isoforms can have different affinities for cAMP, with some having high affinities in the 10-100 nM range (PDE3 and PDE8) and some having low affinities for cAMP >10 μ M (PDE1A and PDE2) (86,87).

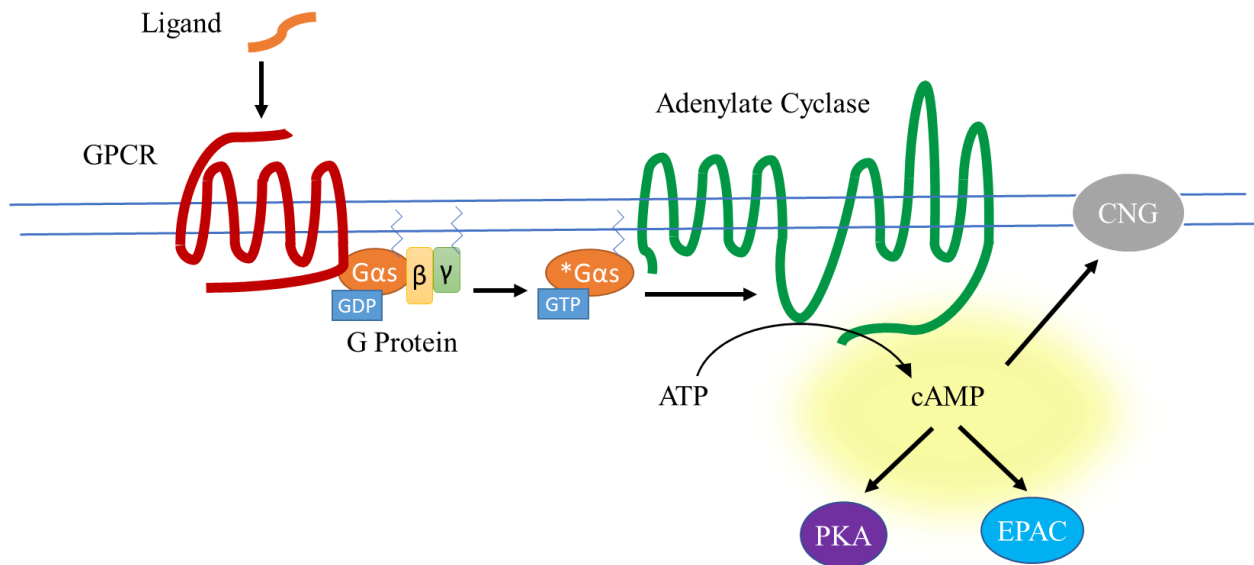


Figure 1. GPCR-mediated cAMP signaling.

Upon binding to its ligand, GPCRs activate heterotrimeric G proteins which exchange GDP for GTP. The heterodimer dissociates, and the active Gαs subunit stimulates adenylyl cyclase production of cAMP. cAMP activates a handful of effectors including PKA, EPAC, and cyclic nucleotide gated channels (CNGs).

1.2 cAMP COMPARTMENTALIZATION PARADIGM

The combination of ACs, PDEs, effector proteins, and scaffolding proteins that regulate cAMP signaling result in three temporal patterns of accumulation: transient, sustained, and oscillating. GPCR endocytosis, PKA-driven negative feedback loops, and PDE activity result in transient spikes of cAMP production (88-91). Several GPCRs exhibit sustained cAMP production (32,33,92-95) and activating mutations in the GPCR pathway can lead to constitutive production of cAMP (96-99). Additionally, cAMP oscillations have been reported in pancreatic β cells (100,101), neurons (102,103), pituitary cells (104), and in myocardial cells (105). In addition to this temporal regulation, spatial regulation was also demonstrated by differential cyclase localization and AKAP signalosomes. Although proximity-based signaling mechanisms may accelerate protein-protein interactions, the characteristics of the small molecule cAMP pose a problem for location-dependent models given the classic paradigm of diffusion.

1.2.1 Problems with Previous Models of cAMP Diffusion

The first studies measuring cAMP diffusion rates in cells measured a diffusion coefficient of $\sim 3 \times 10^{-6} \text{ cm}^2/\text{s}$ (106,107) which was similar to values obtained in aqueous solutions (108). These measurements were taken in amphibian olfactory cilia and cAMP concentrations were measured via voltage changes from cyclic nucleotide-gated channels (CNGs). Chen et. al. performed their studies in the absence of PDE activity and noted that higher levels of cAMP (5 μM) diffused more slowly (107). Thus, they hypothesized this was due to buffering effects of cAMP binding proteins which reversibly bind, thus slowing diffusion. The idea that cAMP diffusion was largely

unimpeded by the intracellular environment became widely accepted. However, experimental evidence for PKA pools seemed to contradict these data.

Mathematical modeling by Rich et. al. suggested if cAMP diffuses through a cell as it does in aqueous solutions, it would not accumulate to effective concentrations for activating effector proteins (109). Transmembrane ACs have a relatively slow rate of catalysis, generating about 59 molecules of cAMP every second (110). The concentration of cAMP, even 5 nm from AC, would be ~10-fold lower than the concentration needed to achieve half maximal activation ($K_{1/2}$) of PKA, ~100-fold lower than the $K_{1/2}$ of EPAC, and ~10,000-fold lower the $K_{1/2}$ of olfactory nucleotide-gated channels (111,112). While comparing protein activation constants does not necessarily recapitulate *in vivo* signaling, there are other problems with the concept of unhindered cAMP diffusion. For example, it could lead to activation of distant effector proteins throughout the cell, contradicting GPCR activation of different PKA pools. Mathematical models indicate co-localization of AC and PDEs are not sufficient for generating physiologically relevant cAMP gradients (113,114). Hence, models relying on proximity alone is not enough for cAMP activation of specific signalosomes.

Rich et. al. compared cAMP concentrations using membrane cyclic nucleotide-gated channels and cytosolic PKA-based FRET (Fluorescence Resonance Energy Transfer) sensors (109). They found under the same stimulating conditions in C6-2B glioma cells that membrane concentrations of cAMP were much higher (>12-fold) than cytosolic levels. Combining this knowledge with their mathematical models formed the two-compartment model of cAMP diffusion (111). The compartments refer to a smaller sub-cellular compartment such as near a site of cAMP production and the larger compartment of the bulk cytosol. The basic premise states cAMP diffusion between the two compartments is restricted or slower than the previously

assumed rate of diffusion. Upon stimulus of cAMP production, the activated cyclase produces cAMP in the smaller first compartment, leading to an initial spike in cAMP accumulation. Then, delayed activation of PDEs and diffusion with the second larger compartment lead to decreased cAMP accumulation in the first compartment. There is a subsequent increase in cAMP accumulation in the cytosol however it does not reach the same maximum as the smaller compartment. Other computational models confirm that a lower cAMP diffusion coefficient (10-100-fold lower) created scenarios where membrane-localized effectors could be activated and physiologically relevant cAMP gradients could form (113,115). Although, some models found they could achieve compartment specific activation using unrestricted cAMP diffusion in their model using high, non-physiological levels of PDE activity and specific cell geometries (116), or using broadly distributed PKA-sensitive cAMP degradation, high cyclase activity, and high PDE activity (117,118). A two-compartment system with restricted diffusion between the membrane and cytosol could absolve proximity-based models for cAMP activation of specific effector pools.

1.2.2 Direct Measurements of cAMP Diffusion

Intracellular diffusion of a molecule or protein depends mainly on three factors: cytoplasmic viscosity, molecular crowding causing collisions, and binding to mobile or anchored molecules (119). Most small molecules exhibit 3 to 8-fold slower diffusion rates in the cytosol compared to aqueous solutions (119,120). The previously measured rates of cAMP diffusion were at odds with budding experimental evidence of GPCR-mediated activation of distinct PKA pools. Mathematical models predicted cAMP diffusion needed to be at least 10-fold slower ($\sim 30 \mu\text{m}^2/\text{s}$) for effective accumulation, activation of effectors, and effective degradation by PDEs (113). The

previously described studies measuring cAMP diffusion relied on indirect methods for measuring cAMP. Recent, advances in live cell imaging have provided more direct measurements of cAMP diffusion and methods to monitor cAMP accumulation with high spatio-temporal resolution.

To more directly measure cAMP diffusion in live cells, Agarwal et. al. used Raster Imaging Correlation Spectroscopy to measure diffusion of a fluorescent cAMP analog, 8-[Pharos-450]-cAMP (ϕ 450-cAMP), in HEK293 cells and adult cardiac myocytes (121). They obtained similar measurements of 5-10 $\mu\text{m}^2/\text{s}$ in both cell types, suggesting cell morphology was not a major factor. Rather, they noted ϕ 450-cAMP co-localized with PKA-RII regulatory units in cardiac myocytes, indicating a majority of the cAMP analog was binding to anchored PKA, particularly at the mitochondria. Consistent with this finding, the rate of PKA-RII diffusion was similar to the diffusion of ϕ 450-cAMP. Disrupting AKAP-PKA binding increased the rate of PKA-RII and ϕ 450-cAMP diffusion to $\sim 33 \mu\text{m}^2/\text{s}$, demonstrating PKA buffering accounts for a 3-fold reduction in cAMP diffusion in adult cardiac myocytes. It is important to note ϕ 450-cAMP is resistant to PDE4 hydrolysis which represents a major source of cAMP regulation.

Another approach to measure cAMP uses FRET biosensors which are dynamic, cAMP-sensitive, fluorescent probes that can be used to extrapolate relative concentrations. Richards et. al. expressed an EPAC-based FRET sensor in adult cardiac myocytes and stimulated cAMP production using a microperfusion apparatus to expose half the cell to β -adrenergic agonists (122). They found cAMP diffused at a rate of 32 $\mu\text{m}^2/\text{s}$ that was independent of cAMP concentration, intracellular acidity, PDE activity, and PKA buffering. Their measurements were similar to diffusion rates of other small compounds; hence they hypothesized a common physical mechanism restricts cAMP diffusion. They found neonatal cardiac myocytes which express far

fewer mitochondria and exhibit lower cellular tortuosity have slightly faster rates of cAMP diffusion (~3-fold). The mechanisms governing cAMP diffusion remained undetermined, however there is consistent evidence that intracellular cAMP diffusion is much slower than in aqueous solutions. This distinction helps bridge the gap between computational predictions and growing experimental evidence for cAMP compartmentalization.

1.2.3 cAMP Compartmentalization Model

cAMP compartmentalization provides a new conceptual framework to investigate signaling specificity. By a functional definition, cAMP compartments are local areas of high concentration that co-localize with cAMP effectors and disruption of these compartments impact specific downstream responses. Some have described cAMP ‘microdomains’ which are compartments that measure micrometers in diameter. The mechanisms governing the formation and maintenance of cAMP compartments are still unclear. Most agree some combination of co-localization of cyclases and effectors, localized degradation, cAMP buffering, cAMP export, and physical barriers contribute (123). Compartmentalization of other second messengers including cyclic GMP, nitric oxide, and Ca^{+2} are also hypothesized to follow these proposed models (124).

Localized cAMP production depends on differential AC isoform localization and activity. Transmembrane isoforms can co-localize with GPCRs through interactions with scaffolding proteins or with lipid rafts of the membrane. Additionally, sAC can localize in various subcellular regions through binding AKAPs. The cAMP compartmentalization model predicts cAMP accumulation near the source of synthesis can reach effective concentrations for activating effector proteins. Furthermore, these effectors are positioned via AKAP or other associated proteins in a manner which favors activation (Fig. 2A). To achieve high cAMP

concentrations, diffusion can be limited by physical and enzymatic boundaries. Physical barriers can include cellular viscosity and tortuosity, cell shape, and potentially barriers from organelles (Fig. 2B). For example, the endoplasmic reticulum can come in close contact with the membrane and potentially impede cAMP diffusion (109). Another model suggests the cortical actin cytoskeleton can serve as a diffusional barrier. Destabilizing actin cytoskeletal organization using latrunculin promoted cAMP diffusion from the membrane to cytosol in a cystic fibrosis cell line; this could be rescued by overexpressing the scaffolding protein Na(+)/H(+) exchanger regulatory factor (NHERF1) to re-establish cytoskeletal organization (125). Sub-cellular regions and compartments can also be protected from cAMP through localized PDE degradation. Multiple studies have shown PDE inhibition increases spreading of cAMP throughout the cell, concluding PDEs act as a barrier to limit diffusion in certain regions (87) (Fig. 2C). Others have found microdomains of low cAMP concentration where PDE functions as a sink (126,127) (Fig. 2D). Another mechanism slowing cAMP diffusion is buffering by cAMP effector proteins which limit the number of free, unbound molecules available (Fig. 2E). Lastly, cAMP can be exported through the cell via multidrug resistant proteins, although the rate of export is relatively slow ($2 \times 10^{-3}/s$) (118,128,129) (Fig. 2F). These fundamental concepts underly the growing experimental evidence for cAMP compartmentalization.

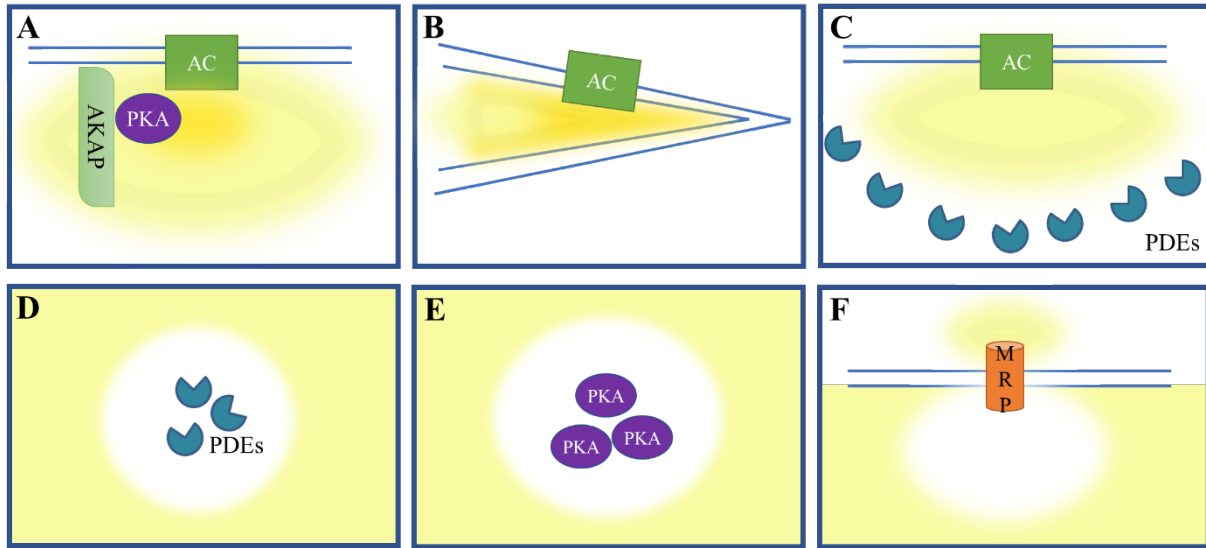


Figure 2. Mechanistic models of cAMP compartmentalization.

(A) Co-localization of ACs and cAMP effectors via AKAPs can favor activation of specific pathways. (B) Physical compartmentalization by cell geometry, viscosity, tortuosity, or organelle barriers can promote cAMP accumulation. (C) PDEs can form barriers which prevent cAMP accumulation outside of compartments. (D) PDEs create compartments with low cAMP, thus protecting effectors from activation. (E) Buffering by cAMP effectors can impede diffusion by limiting free cAMP. (F) MRPs can export cAMP from the cell.

1.3 EVIDENCE FOR cAMP COMPARTMENTALIZATION

Some of the first experimental and visual data supporting compartmentalization of cAMP used FRET-based approaches. Bacsikai et. al. were the first to use cAMP FRET sensors to study diffusion in *Aplysia* sensory neurons using a PKA-based sensor called fluorescein-labeled catalytic subunit and rhodamine-labeled regulatory subunit (FICRhR, pronounced “flicker”) (130). They found serotonin stimulated greater PKA activation in distal processes and minimal activation near the nucleus. They hypothesized this phenomenon could result from several factors: 1) serotonin receptors and/or cyclases were more concentrated at distal processes, 2)

cAMP diffusion was restricted, 3) PDEs exhibit differential effectiveness throughout the cell, 4) the sensor was perturbed in one part of the cell, or 5) the observed cAMP gradient resulted from the higher surface-to-volume ratio in distal processes. Interestingly, they found injected cAMP was freely diffusible ($780 \mu\text{m}^2/\text{s}$), suggesting there were no obvious barriers for cAMP. They further concluded endogenous PDE activity and the sensor alone could not form cAMP gradients; rather, cell geometry was the primary factor establishing the gradient. The substantial discrepancy between physiological stimulus of cAMP gradients and artificial addition of freely diffusing cAMP emphasizes the impact of spatial regulation. While this initial study had a few drawbacks, including potential cAMP buffering by the sensor which could artificially favor gradient formation and microinjection of the sensor could introduce a cAMP sink from the needle (131), it was the first direct evidence of restricted cAMP diffusion.

Zaccolo and colleagues were the first group which combined experimental evidence for cAMP compartmentalization and AKAP-mediated signalosomes (132). They created a PKA-based FRET sensor which relied on dissociation of the regulatory and catalytic domains upon binding to cAMP (89,132). In cardiac myocytes they discovered β -adrenergic receptor stimulation with norepinephrine increased cAMP levels near T tubules/junctional sarcomere membrane compared to the cytosol. These compartments of high cAMP concentration could be as little as $1 \mu\text{m}$ in diameter, hence earning the title of 'microdomains'. Inhibiting PDEs made this signature more evenly diffuse throughout the cell, suggesting PDEs were the main factor limiting cAMP diffusion and maintaining compartmentalization. They additionally hypothesized in their cell model that cyclases constitutively produced cAMP and that low PDE activity maintained basal cAMP levels. A few limitations of the assay are worth considering when interpreting the results. The sensor has slow kinetics since dissociation of the PKA heterotrimer

requires cooperative binding of four cAMP molecules (133). Additionally, intermolecular FRET interactions can occur between clustered sensors, and the sensor retains endogenous PKA activity and localization (133). To prevent sensor co-localization with AKAPs along the sarcomere, they made a truncated version which lacked the AKAP binding motif; however, they did not see the same high concentration cAMP pools. This suggests sarcomeric AKAPs represent a unique compartment for specific PKA activation.

They further refined this study using PKA regulatory RI and RII subunits which bind to different AKAPs in cardiac myocytes (134). PKA-RII is primarily found in particulate fractions of M sarcomeric lines, while PKA-RI localized to Z and M sarcomeric lines. Both anchored to AKAP proteins and demonstrated comparable cAMP binding characteristics. Using the PKA-RI and RII AKAP anchoring motifs, they created RI and RII-targeted FRET sensors for cAMP using an EPAC-based sensor. They found isoproterenol stimulation of β -adrenergic GPCRs primarily activated RII-localized sensors, whereas prostaglandin E1 receptor stimulation primarily activated RI sensors. The cAMP signature for both the RI and RII compartments could be altered by perturbing AKAP binding of the individual sensor or inhibiting a specific, associated PDE isoform. These results demonstrate specific GPCRs can stimulate distinct cAMP pools which in turn selectively activate AKAP-associated PKA isoforms. Additionally, after 25 years, it provided a potential mechanism behind the ‘PKA pool’ observations made by Buxton and Brunton (14).

1.3.1 Compartmentalization of Membrane, Cytosol, and Nucleus

After the initial experiments describing cAMP compartments and microdomains, several other studies have confirmed differential cAMP dynamics between the plasma membrane, cytosol, and

nucleus (115,135-137). These sub-cellular compartments are larger than the aforementioned microdomains, yet they still represent distinct regions where differences in cAMP accumulation have functional effects. Using cAMP FRET sensors localized to the plasma membrane and cytosol, researchers found cAMP accumulates and reaches higher concentrations in sub-membrane regions. For example, prostaglandin E1 signaling stimulates higher amplitudes of sub-membrane cAMP in HEK293 expressing lipidated PKA- and EPAC-based cAMP FRET sensors (137). PKA regulates the gradient formed between the membrane and cytosol through a negative feedback loop. Pharmacological, siRNA knockdown, and dominant negative approaches reveal PKA-dependent activation of PDE4D and PDE4B regulated cAMP levels in the membrane and cytosol, respectively. They hypothesized cAMP forms multiple contiguous compartments with different concentrations which depend on PDE activity. Interestingly, they found cAMP accumulation in the nucleus was higher than cytoplasmic levels and comparable to membrane accumulation. This contrasted earlier work from another group which also studied HEK293 cells. DiPilato et. al. found isoproterenol and prostaglandin E1 stimulates higher cAMP levels in sub-membrane regions, compared to the cytosol and mitochondria-localized sensors; however, cAMP levels in the nucleus were lower than all other compartments measured (136). There was no substantial kinetic delay for cAMP entering the nucleus, but there was a significant delay in nuclear PKA activation compared to cytosolic PKA. The delayed timeframe was consistent with slower translocation of the catalytic subunit from membrane-activated PKA pools rather than direct activation of a nuclear PKA pool (138,139). The presence of cAMP in the nucleus, which demonstrates differential regulation from other sub-cellular compartments, presents an interesting case.

Sample et. al. was the first group to prove a functional pool of nuclear PKA existed. They combined targeted FRET sensors to measure cAMP concentrations and PKA activity with a truncated, catalytically active sAC localized to the membrane, cytosol, and nucleus (135). This technique allowed activation of cAMP production with bicarbonate in different compartments while measuring cAMP and PKA activity in real time. They found cAMP production at the membrane exhibited low nuclear cAMP levels and delayed nuclear PKA activity. The ~20 min delay in PKA activation despite the presence of cAMP in the nucleus was consistent with the cPKA translocation. cAMP production from the cytosol and nucleus exhibited lower membrane cAMP levels, rapid PKA activity in the nucleus (~3-4 min), and faster phosphorylation of CREB. This suggested a pool of PKA was present in the nucleus which is not activated by membrane-localized cAMP production in this model. They further verified the full PKA holoenzyme was present in the nucleus and hypothesized a PDE/AKAP/PKA complex regulated activation in the nuclear compartment.

1.3.2 Small Scale Compartmentalization

Small scale compartments and microdomains have also been identified in membrane lipid rafts, endosomes, presynaptic boutons, AKAP-localized regions, and mitochondria (127,140-144). Collectively these show regions of high or low cAMP concentrations exist and can co-localize with clusters of effector proteins. Again, this is achieved by close physical proximity to cyclases (AKAP/lipid rafts), physical sterics (cell shape), and enzymatic barriers (localized PDE). This section will focus on experimental proximity-based models as it is more relevant to this thesis.

Researchers have proposed lipid-raft and non-raft organization of the plasma membrane could help establish cAMP compartments; however, more comprehensive experimental evidence is

required. Depry et. al. used localized PKA-substrate (AKAR) FRET sensors targeting raft (myristoylated/palmitoylated) and non-raft (farnesylated) membrane regions in HEK293 (145). They found higher basal cAMP activity in raft regions, however their findings could not control for differences in PKA expression in the regions. A complementary study using similarly targeted cAMP FRET sensors in HEK293 found somewhat contrary results concluding basal cAMP levels are higher in non-raft regions. This study further compared raft and non-raft cAMP levels with raft-associated β 2-adrenergic receptor and non-raft associated prostaglandin receptor stimulation (140,146). They found no striking difference between compartments, however interfering with rafts via cholesterol depletion selectively reduced β 2-adrenergic stimulated cAMP levels. Similar studies were conducted in airway smooth muscle cells using targeted cAMP FRET sensors (147). Stimulation of β 2-adrenergic signaling exhibited increased cAMP levels throughout the cell, while butaprost stimulation of prostaglandin receptors increased cAMP levels specifically in non-raft and nuclear localized compartments. Butaprost stimulation in the presence of a PDE4 inhibitor resulted in increased cAMP levels in all measured compartments, including the raft and cytoplasmic regions. Taken together with other studies on this subject, lipid rafts and non-raft membrane organization may provide an environment for effective clustering of GPCRs, associated ACs, and cAMP regulatory machinery for favoring cAMP compartment formation. However, advances in spatial resolution and additional methods for altering raft domains may be needed to substantiate this model.

Combination approaches lead to the most convincing evidence for lipid-raft-mediated cAMP compartmentalization. Averaimo et. al. combined localized FRET measurements, cAMP signaling interference, and stimulation in retinal ganglion cells (148). They hypothesized AC1 localization to membrane lipid rafts represented a potential cAMP compartment which regulates

ephrin-A-stimulated axonal retraction. Using EPAC-based FRET sensors localized to raft and non-raft membrane domains, they found ephrin-A5 stimulated a reduction in cAMP levels specifically in raft compartments. They found mimicking this effect, using a localized cAMP sponge to reduce cAMP levels, produced a similar response. Raft-associated cAMP reduction promoted axon retraction whereas non-raft cAMP reduction did not. Notably, expressing a cAMP binding-deficient mutant of the cAMP sponge did not elicit the same effects, showing their approach did not interfere with compartmentalization. Lastly, they found localized bPAC, when activated transiently, could induce PDE activity and ultimately reduce local cAMP. Reducing cAMP with this method in raft-compartments specifically stimulated axon retraction. While the use of bPAC to reduce cAMP levels is rather unconventional, particularly since their FRET recordings also excited bPAC inadvertently, they were able to distinguish cAMP dynamics in two compartments with close proximity. They further tested this effect *in vivo* to show that the raft-localized cAMP sponge interfered with axon arbor refinement whereas a non-raft localized cAMP sponge and a raft-localized mutant sponge had no effect on axon arbor development.

Others have approached identifying cAMP compartments by probing AC and AKAP-mediated signalosomes. Wachten et. al. investigated AC8-associated cAMP pools by fusing a cAMP FRET sensor to a catalytically inactive AC8 (142). They compared this to membrane (myristoylated/palmitoylated) and cytosolic localized sensors in GH₃B₆ pituitary cells. G α s-stimulated cAMP production increased cAMP levels at the membrane and cytosol, but not in AC8-localized membrane compartments. G α q-stimulated Ca⁺² signaling, which typically inhibits AC5/6, decreased cAMP levels at the membrane and cytosol, but increased cAMP proximal to AC8. Although the AC8 and lipid-modified FRET sensors both reside at the membrane, they

exhibited distinct cAMP dynamics. This provides evidence that AC isoform specific cAMP compartments can exist. AKAP-mediated compartments became a field of study after discovering peptide-based disruption of its interaction with PKA severely hindered PKA activation (67,149). AKAPs are hypothesized to increase local effective concentrations for protein interactions and accelerate activation anywhere from 4 to 20-fold faster than in solution (71). Scott and colleagues identified a signalosome consisting of muscle-specific AKAP (mAKAP), PKA, EPAC1, and PKA-activated PDE4D3 (68). They show PDE4D3 tethering to PKA reduces PKA activation, suggesting this AKAP-mediated signalosome incorporates a negative feedback loop to terminate cAMP signaling. Another example of this is AKAP79 which has been shown to bind β -adrenergic receptors, AC5, and PKA (72,74). PKA phosphorylation of cyclase 5 represses cAMP synthesis, thus creating an environment where GPCR-stimulated cAMP synthesis is quickly downregulated (74). Proximity based models of co-localized sites of cAMP synthesis and cAMP effectors is foundational to the compartmentalization paradigm.

The field of cAMP compartmentalization has made substantial progress in the last two decades largely due to advances in imaging technology. The compartmentalization paradigm is well-recognized; however, it is not fully accepted. Limitations in the methods applied have left a few gaps. For example, the term ‘compartmentalization’ implies these are rigid and static when they are in fact highly dynamic. The borders and size of compartments are not well defined and based on interpretation. Some studies prefer the term ‘location-biased cAMP signaling’ rather than compartmentalization since cAMP is still found throughout the cell and not tightly constrained. Regardless, they all agree uneven distribution of cAMP throughout the cell has potential physiological consequences. Furthermore, concepts from the cAMP compartmentalization paradigm are being applied to disease models (150-152). Since many

cAMP compartments have not yet been explored, there is a clinical need for identifying new compartments. Here, we have characterized a potential Radixin-associated cAMP compartment in thyroid epithelial cells and created novel tools to advance the field.

2.0 TSH/cAMP SIGNALING PROMOTES THYROID CELL PROLIFERATION

2.1 INTRODUCTION

2.1.1 TSH is a Master Regulator of Thyroid Function

The thyroid is a major endocrine gland that regulates cellular metabolism throughout the body. This butterfly shaped organ consists of two lobes, located on either side of the trachea connected by a thin section of tissue known as the isthmus. Each lobe contains follicles lined with epithelial cells that are responsible for producing and secreting thyroid metabolic hormones triiodothyronine (T3) and thyroxine (T4) in response to thyroid stimulating hormone (TSH) (153). TSH is a glycoprotein secreted from the pituitary gland that serves as the master regulator for thyroid function. The ligand binds to its receptor (TSHR) at the basal side of thyroid follicular cells to stimulate multiple cell processes including cell differentiation, attachment, iodine intake, thyroid metabolic hormone production/secretion, and most relevant to this thesis, proliferation (154). Hence circulating TSH levels are carefully regulated by the body through a negative feedback mechanism known as the hypothalamic-pituitary-thyroid axis. Under normal circumstances, the hypothalamus produces the thyrotropin-releasing hormone which stimulates TSH production in the pituitary gland. TSH signaling at the thyroid elevates circulating levels of the thyroid hormones. T3 and T4 then negatively affect hypothalamus production of thyrotropin-

releasing hormone, thus reducing TSH production. This negative feedback axis in addition to other regulatory mechanisms of TSH production result in short pulses of circulating TSH. TSH pulses occur slightly less than every two hours and reach higher amplitudes at night, following a circadian rhythm (155).

As with most highly regulated pathways, irregularities in TSH signaling can lead to thyroid disorders such as hyper/hypothyroidism, goiters, hyperplasia, and adenoma. With improved diagnostic methods for detecting thyroid cancer, the population of affected patients has risen over the last decade (156); hence, the role of the TSH pathway in cell proliferation sparks immediate attention. The next section discusses the major players in TSH-mediated proliferation.

2.1.2 TSH Stimulates cAMP-Dependent Proliferation

The interaction between the TSH ligand and TSHR follows canonical models of GPCR signaling (Fig. 1). TSHR is a classic A family GPCR where TSH promotes the activation of *Gas* and *Gaq/11* (157). Both pathways have been shown to promote proliferation; however, *Gas* shows a higher affinity for TSHR binding and has a well-characterized role in cAMP-dependent proliferation. cAMP signaling transduces most of the effects of TSH on thyroid cells (158). Mutations in this pathway that render constitutive cAMP signaling have been linked to thyroid hyperproliferative disorders. Ledent and colleagues were the first to show constitutive cAMP signaling caused hyperthyroidism and goiter formation in transgenic mice expressing the adenosine A2a receptor (159). This proof of concept was supported by similar studies with constitutive *Gas* activity which instigated hyperfunctioning thyroid adenoma and hyperplasia (160,161). Furthermore, characterization of human thyroid adenomas revealed somatic mutations in the TSHR which exhibit constitutive cAMP signaling (162,163). Patients with McCune-

Albright syndrome, which have an activating G α s mutation, also exhibit goiters and thyroid nodules (97,164,165). Hence, understanding the mechanism regulating cAMP signaling in thyroid proliferation is clinically imperative.

TSH/cAMP stimulated proliferation in thyroid cells additionally requires the presence of a co-mitogen such as insulin, IGF-1, or serum. Roger et al (166) showed TSH alone could not promote proliferation in primary canine thyroid epithelial cells in the absence of insulin or serum. It was later discovered in primary canine thyroid cells that insulin/IGF-1 and TSH/cAMP signaling separately control cell growth and DNA synthesis, respectively (167). Insulin or IGF-1 was required to increase cell mass and had a permissive effect on TSH-stimulated DNA synthesis. This co-mitogen requirement has been shown in several thyroid models (168). The resulting model suggests insulin/IGF-1 stimulates upregulation of cyclin D3 and cAMP-dependent activity is required for forming cyclin D3 complexes with cyclin dependent kinase 4 (CDK4) (169,170). Since TSH specifically promotes the G1 to S phase transition, the next sections will focus on mitogenesis rather than the full spectrum of events throughout cell proliferation.

cAMP exerts its effects on mitogenesis primarily through activation of PKA and EPAC. Studies in several thyroid models show PKA is required for effective stimulation of DNA synthesis, however it does not account for the full effect (171-173). The small Ras-like GTPase, Rap1, was identified as another key factor in TSH-mediated mitogenesis. This helped identify EPAC as a cAMP-dependent GEF which activated Rap upon TSH stimulation. While some reports found the role of EPAC in cell mitogenesis was independent of PKA (174,175), our lab found its effects required PKA activity in PCCL3, an epithelial thyroid cell line derived from rats (176,177). PCCL3 are a unique model for thyroid studies since they retain several characteristics

of thyroid cells including TSH-dependent growth, iodine uptake, and expression of differentiation markers like thyroglobulin and thyroperoxidase (168). PCCL3 are considered pre-cancerous since they require two retroviral oncogenes for transformation, while other thyroid cell lines like FRTL-5 only require one (168,177).

2.1.3 Radixin-PKA-EPAC Complex Role in Mitogenesis

Using the PCCL3 cell line, our lab established a mechanistic model for the role of EPAC in TSH-mediated mitogenesis (176). We found that TSH stimulated EPAC activation of Rap1b. Specific activation of EPAC using the cAMP analog 8-pMeOPT-2'-O-Me-cAMP (178) did not stimulate mitogenesis by itself, however it significantly increased the proliferative effect of the PKA-specific activator 6-Bz-cAMP (179). This suggests EPAC and PKA work in a synergistic manner (176). Using a dominant negative approach, our lab found that expressing a truncated form of EPAC that lacked the catalytic domain but retained the N-terminal DEP domain for localization blocked endogenous EPAC activity and prevented TSH-stimulated mitogenesis. This revealed that EPAC was necessary for transducing TSH/cAMP-dependent mitogenesis and that the location of EPAC was critical for its role.

Searching for potential DEP domain binding partners of EPAC, we identified Radixin in a yeast two-hybrid assay using the N-terminus of EPAC as bait (79). Radixin is an ERM family protein that binds the actin cytoskeleton at its C-terminus and membrane-associated proteins at its N-terminus in its active form (180). In its inactive form, the N and C-termini associate, creating an auto-inhibited closed conformation which prevents actin and membrane interactions (181,182). *In vitro* pulldown assays confirmed the interaction between the N-terminus EBD domain of EPAC and the N-terminal FERM (**F**our.1, **E**zrin, **R**adixin, **M**oesin) domain of

Radixin. EPAC and Radixin co-localize in sub-membrane regions in clusters (79). We further examined whether Radixin served as a scaffolding protein for PKA.

Since the N and C-termini of Radixin can interact, truncated forms of either terminal domain can interfere with ERM function (183,184). Hence expression of a truncated Radixin C-terminal fragment disrupted EPAC localization to sub-membrane clusters. Interestingly, a N-terminal fragment of Radixin did not interfere with EPAC localization or TSH signaling. The Radixin C-terminus disrupted TSH-mediated mitogenesis; however, this could be rescued by expressing a Rap1b mutant. Rap1b expression rescued mitogenesis only when it was constitutively active and had a phospho-mimetic mutation, therefore bypassing the need for EPAC activation and PKA phosphorylation of Rap1b (79). Since disruption of the Radixin complex was rescued by the double mutant Rap1b, the data suggest the only role of the Radixin-PKA-EPAC complex is to position PKA and EPAC in an area of high cAMP for effective transduction of TSH signaling. Hence, we hypothesize a Radixin-associated cAMP compartment plays a role in TSH-mediated thyroid cell mitogenesis. Here, we show evidence for increased cAMP accumulation in Radixin-associated sub-membrane compartments using the N-terminus of Radixin as a novel targeting agent.

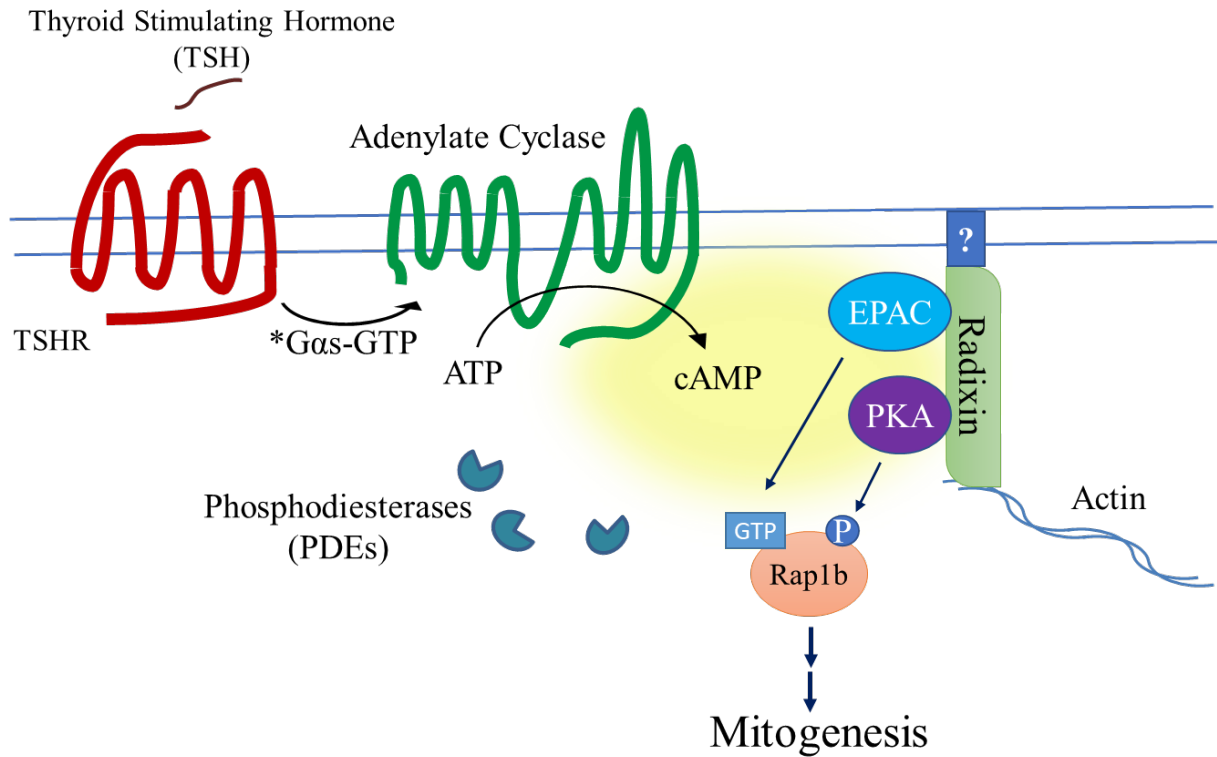


Figure 3. TSH/cAMP-stimulated mitogenic pathway.

TSH binding to its receptor activates Gαs which in turn activates transmembrane ACs. AC converts ATP into cAMP where it activates the GEF EPAC and the kinase PKA which are both anchored by the cytoskeletal scaffolding protein Radixin. EPAC and PKA synergistically promote mitogenesis through their actions on Rap1b. The EPAC-Radixin-PKA complex is hypothesized to co-localize with a region of high cAMP concentration.

2.2 METHODS

2.2.1 Cell Culture and Transfection

The rat thyroid follicular cell line, PCCL3, was grown in F12 Coon's modified media supplemented with 2.68 g/L sodium bicarbonate, 5% fetal bovine serum (FBS), Penicillin/Streptomycin, L-glutamine, and 4 Hormone solution: insulin (1 μg/mL), apo-transferin

(5 µg/mL), hydrocortisone (1 nM), and thyroid stimulating hormone (1 IU/L) (Complete Coon's media). Cells were grown to ~90% confluency before passaging every 2-4 days at 37°C in 5% CO₂, 95% humidified air. For transient transfections, cells were transfected 24 hs after plating using Xtremegene HP (Roche) or Lipofectamine 3000 (Thermo Fisher Scientific) for PCCL3 cells. Cells were cultured for 24 hr and given fresh media.

2.2.2 Plasmid Construction

A codon optimized N-Radixin (N-Rx, amino acids 1-318) sequence for mammalian expression with flanking HindIII sites was synthesized by Geneart. The sequence was subcloned using these cut sites upstream of the Epac1-cAMPs FRET sensor (88). The N-Rx sequence was also subcloned into pcDNA3.1+-bPAC-myc-mCherry (Addgene) using HindIII restriction enzymes. Plasmids pSiren-dsRed and pCMV-myc-empty vector were purchased from Clontech.

2.2.3 Immunocytochemistry

PCCL3 cells were seeded in a 6-well dish on gelatin-coated glass coverslips (25 mm, #1.5, Warner Instruments), transfected, washed with PBS, fixed 10 min in 4% PFA, and permeabilized 10 min with 0.5% Triton X-100. Cells were stained with DAPI, mounted, and imaged on an Olympus Confocal Fluoview FV1000, 60x/NA 1.45.

2.2.4 Real-Time FRET Imaging

1.5×10^6 cells were seeded on 0.1% gelatin-coated glass coverslips for 24 hr, transfected, and given fresh media the next day. Cells were hormone starved for 3 hr prior to imaging in Coon's media with 5% FBS and lacking TSH, Insulin, and hydrocortisone (Starvation Coon's media). Cells were washed twice with PBS and imaged in OptiMEM lacking phenol red on an Olympus IX70 microscope equipped with a Till Poly V monochromator. Images were acquired every 10s with a 60x/1.4 NA oil objective, 8x8 binning and a Hamamatsu CCD camera using 440nm excitation with emission filters 470/30 and 535/30 and dichroic 455 DCXR. Data was collected using Slidebook software containing the appropriate two-channel (intramolecular FRET) or three channel (intermolecular FRET) correction modules (channel bleed-through and direct acceptor excitation). The PDE inhibitor 3-isobutyl-1-methylxanthine (IBMX) is added at the end of each experiment to find the maximal saturation point of the sensor.

2.2.5 BrdU Incorporation Assay

1.5×10^6 cells were seeded on 0.1% gelatin-coated glass coverslips for 24 hr, transfected, and given fresh media the next day. 24 hr after transfection, cells were hormone starved in Starvation Coon's media with 5% FBS for 16 hr. Media was replaced with fresh starvation Coon's media containing 5% FBS and either kept in darkness or stimulated with $4.41 \pm 0.30 \mu\text{W}/\text{mm}^2$ 450 nm light for 500 ms every 15 min over 24 hr (royal blue CREE XTE, LED Supply). The LED control system is described in greater detail in the next chapter. 8 hr after stimulation, 100 μM BrdU was added using a small volume and incorporated over 16 hr. Then cells were washed in PBS, fixed for 10 min in 4% PFA, and permeabilized 10 min in 0.5% TritonX-100. Cells were

washed and incubated with primary antibody anti-BrdU (CapriLogics) in 3% bovine serum albumin with RQ1 DNase I (1:100, Promega), 5mM MgCl₂, and 1mM CaCl₂. Secondary antibody anti-sheep Alexa 488 (1:1000 Jackson Labs) and DAPI were used. Images were acquired using a 20x/0.70 NA HC PLAN APO objective on a Leica DM500B microscope. Images were analyzed in Image J counting % BrdU positive nuclei/total DAPI stained nuclei.

2.3 RESULTS

2.3.1 Radixin-Associated cAMP Compartment

As previously described, the N-terminus of Radixin (N-Rx, amino acids 1-318) did not interfere with EPAC localization or TSH-mediated mitogenesis (79). Thus, it presents a unique opportunity to investigate Radixin-localized sub-membrane compartments. Using an EPAC-based FRET sensor, Epac1-cAMPs (Ep1) (88), we can measure real-time cAMP dynamics in PCCL3 cells. We modified the Ep1 sensor to include the N-Rx motif (N-Rx-Ep1) to target this construct to EPAC-Radixin-PKA compartments (Fig. 4A). The N-Rx-Ep1 sensor co-localizes with Radixin, indicating the membrane targeting mechanism is not limiting (Fig. 4B). We found that adding the N-Rx motif to a similar FRET sensor did not alter cAMP binding affinity (Fig. 24). Consistent with our hypothesis and the two-compartment model, N-Rx-Ep1 senses ~2-fold higher cAMP levels compared to the cytosolic Ep1 sensor (Fig. 4C-D). This higher amplitude is transient and decreases to levels matching the cytosolic sensor. PDE activity is responsible for this decline, particularly PDE4 (data not shown). The differential cAMP dynamics found in

Radixin-localized domains is consistent with the compartmentalization model, hence for conventional purposes we refer to this as the Radixin cAMP compartment.

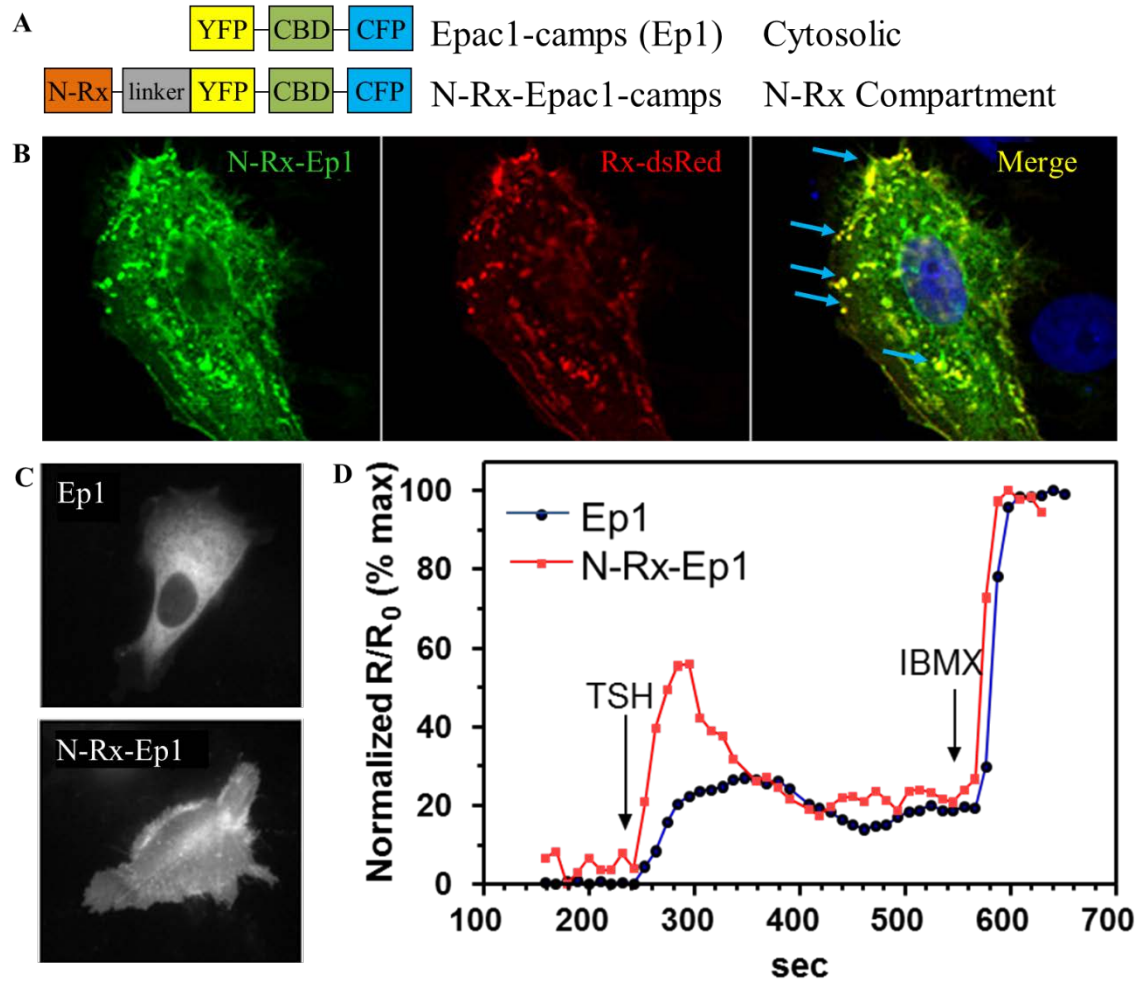


Figure 4. Targeted FRET sensors demonstrate higher cAMP levels in the Radixin-localized compartments upon TSH stimulation.

(A) The Ep1 construct consists of a YFP/CFP FRET pair and a cAMP binding domain (CBD). We incorporated an N-Radixin segment to target the sensor to the EPAC-Radixin-PKA compartment. (B) The targeted FRET sensor, N-Rx-Ep1, co-localizes with Radixin. (C-D) TSH (1 mU/mL) stimulation in PCCL3 cells produces higher cAMP levels near the targeted sensor, N-Rx-Ep1, compared to cytoplasmic sensor, Ep1. Inhibition of PDE activity, via IBMX (250 μ M), promotes a sustained cAMP signal and confirms the TSH peak is not due to probe saturation.

2.3.2 N-Radixin Localized cAMP Production Stimulates Mitogenesis

Our model of the EPAC-Radixin-PKA compartment suggests that a co-localized cAMP pool is necessary for TSH/cAMP-mediated mitogenesis. Hence, spatio-temporal regulation of cAMP dynamics near this complex may be necessary for maintaining pathway specificity. We hypothesized local stimulation of cAMP production near the EPAC-PKA effector compartment will promote mitogenesis. There are a limited number of cAMP modulating tools with spatial and temporal accuracy, however the growing field of optogenetics offers unique opportunities for refined regulation of protein activity (185). The photoactivated adenylyl cyclase from *Beggiatoa* (bPAC) produces cAMP upon 435-455 nm light exposure within milliseconds, providing distinct temporal control (186). We modified this cytoplasmic protein to include an N-Rx sequence to target the protein to the EPAC-PKA effector compartment (Fig. 5A-B), thus adding spatial regulation. bPAC-mCherry exhibits localization throughout the cytosol and nucleus. N-Rx-bPAC-mCherry co-localized with Radixin-GFP, suggesting it was effectively localized to Radixin-associated sub-membrane domains. Basal activity of the cytosolic and N-Rx bPAC constructs increased BrdU incorporation under dark conditions. Despite the high basal level of activity, stimulation with light increased the population of cells entering the S phase in both compartments compared to the dsRed control group.

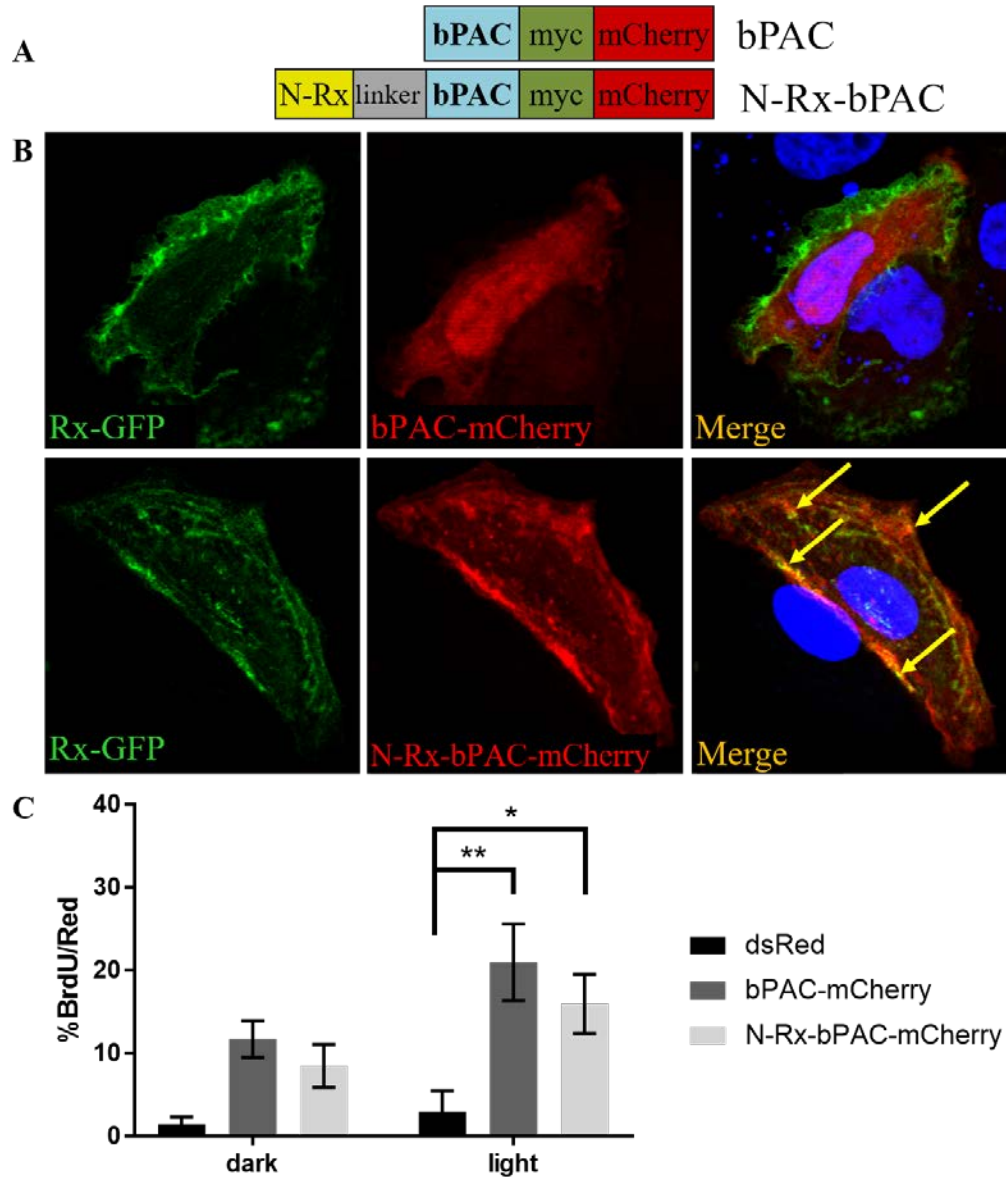


Figure 5. Cytosolic and N-Rx-localized bPAC stimulates mitogenesis.

(A) The N-terminal of Radixin (1-318) was added to the photoactivated adenylyl cyclase from *Beggiatoa* (bPAC) containing a myc tag and mCherry fluorescent marker. (B) This sequence sufficiently localizes the protein in the same submembrane compartment as Radixin and is thus positioned near EPAC-Radixin-PKA signalosomes. (C) PCCL3 cells starved of TSH were stimulated with 450 nm light from and LED in pulses of 500 ms every 15 min over 24 hr or kept in the dark (37°C, 5% CO₂). BrdU incorporation marks cells entering the S phase. While cytosolic bPAC had higher expression levels, both constructs could induce proliferation (Mean +/- S of n=3-4, >500 cells per sample, Two-way ANOVA, * = $P < 0.05$, ** = $P < 0.005$).

2.4 DISCUSSION

Here, we have identified a sub-membrane cAMP compartment associated with Radixin. The ERM family of cytoskeletal scaffolding proteins has become increasingly relevant in understanding AKAP-mediated cAMP signalosomes (187,188). N-Rx represents a unique motif to explore Radixin-localized sub-membrane domains as it does not appear to interfere with Radixin or EPAC localization at the membrane (79). Furthermore, we demonstrate increased cAMP levels in this compartment compared to the bulk cytosol, consistent with the two-compartment model of compartmentalization (111). More work is needed to verify the existence of the Radixin cAMP compartment although we already have some functional evidence that cAMP generated here is sufficient to trigger mitogenesis. The majority of N-Rx targeted FRET sensor appears in the sub-membrane region; however, there may be non-membrane populations and membrane populations which are not proximal to the EPAC-Radixin-PKA signalosome. Still, this method indicates Radixin-localized regions experience different cAMP dynamics compared to the bulk cytosol upon TSH-stimulation. It would be interesting to compare this to a more general membrane-localized FRET sensor to test whether Radixin cAMP dynamics are distinguishable from other membrane regions. Some studies have found distinct cAMP dynamics in different sub-membrane compartments (141,148); however, others have found it difficult to measure cAMP with localized FRET sensors alone. Our results support evidence for differential cAMP signaling between the membrane and bulk cytosol. While we are uncertain which mechanisms restrict cAMP or maintain this gradient, we have evidence that PKA-sensitive PDE4 is the major player responsible. Inhibition of PKA with H89 or inhibition of PDE4 with rolipram converts the transient TSH-stimulated cAMP signal into a sustained signal (unpublished data).

Hence the transient signature is likely maintained by a negative feedback loop of cAMP activation of PKA, PKA activating phosphorylation of PDE4, and PDE4 degradation of cAMP.

Radixin-localized and cytosolic cAMP production using bPAC promoted mitogenesis. Despite high basal activity, we were still able to see increased proliferative levels by stimulating with pulses of blue light over 24 hr. Consistent with our hypothesis, Radixin-localized cAMP was able to stimulate mitogenesis. Interestingly, cytosolic cAMP production also stimulated mitogenesis. There are a few potential possibilities to explain why both constructs stimulated this effect. Since cells were transiently transfected for these experiments, bPAC was overexpressed and may have saturated the regulatory machinery such that cAMP could access both compartments. Alternatively, these results could suggest both membrane and cytosolic compartments play a role in TSH/cAMP mitogenesis. The role of transmembrane ACs in thyroid cell proliferation is well documented; however, the role of sAC is not known. We have found sAC is expressed in PCCL3 cells in the sub-membrane regions, cytosol, and nucleus. Furthermore, inhibition of sAC with KH7 was able to block TSH-mediated proliferation, suggesting a role for a secondary pool of cAMP activity. While other possible explanations exist may explain our results, key experimental changes must be made.

To reduced basal levels of activity, we have since worked to reduce extraneous light exposure and lower protein expression. Long-term solutions to this problem, such as changing the promotor region or creating an inducible system, are described in chapter 3. Furthermore, to effectively compare compartments, future work will include altering the duration and intensity of light to create a dose-response curve. Comparing the potency between groups will more accurately compare responses, rather than relying on one stimulating condition. Overall, the results for a sub-membrane Radixin-localized pool of cAMP, the necessity for EPAC-Radixin-

PKA complex formation and activity, and pro-mitogenic effect of Radixin-localized cAMP production support our model for the Radixin-cAMP compartment. More work is required to dissect location-biased cAMP signaling in thyroid cells; however, there are few tools which can alter cAMP dynamics with sufficient spatial and temporal resolution. Hence, the next section describes our work to address this gap in the field by creating a bPAC-based toolset with greater temporal regulation.

3.0 LUMINESCENCE-ACTIVATED CYCLASE ALLOWS DUAL PHOTO AND CHEMICAL ACTIVATION OF cAMP SYNTHESIS

3.1 INTRODUCTION

3.1.1 Current Methods for Measuring and Modulating cAMP

The cAMP compartmentalization model has become a prominent explanation for how cAMP activates specific pathways. Although the hypothesis of cAMP compartmentalization was proposed 40 years ago, we are finally gaining mechanistic data including more direct measurements of cAMP diffusion and the identification of specific compartments. This section reviews current methods for monitoring cAMP and interfering with localized signaling. Additionally, we outline the gap in available methods used for synthetically modulating local cAMP production and introduce a novel toolset for answering said problem.

3.1.2 Fluorescence Resonance Energy Transfer Biosensors

cAMP production and degradation occur on the seconds to minutes timescale. Historically, antibody-based detection in cell lysates was unable to achieve refined measurements with much temporal accuracy let alone spatial accuracy. CNGs could be used to monitor cAMP signaling with great temporal accuracy, however it was only possible to measure membrane cAMP

dynamics. FRET-based technology has emerged as the primary means of detecting cAMP in live cells with exquisite spatio-temporal specificity. FRET takes advantage of a phenomenon that occurs between two fluorophores in close proximity. If the emission spectrum of one fluorophore sufficiently overlaps the excitation spectrum of another, then the excited donor fluorophore can transfer energy to the acceptor fluorophore through non-radiative dipole-dipole coupling. This results in increased acceptor fluorophore emission and quenching of donor fluorescence. FRET occurs only when the two fluorophores have sufficient spectral overlap (Fig. 6B), are in close proximity (1-10 nm), have parallel transition dipole orientations, and when the donor has a sufficient fluorescence lifetime for FRET (189,190). FRET sensors designed to monitor cAMP usually contain a CBD derived from PKA or EPAC which, when bound to cAMP, undergoes a conformational shift that alters the distance between fluorophores. For example, in the previous section we used Epac1-cAMPs which uses an ECFP and EYFP FRET pair with a connected CBD domain from EPAC1 (Fig. 6A). When unbound, the two fluorophores are in close proximity and FRET occurs upon excitation of ECFP. Once bound to cAMP, the fluorophores are separated and there is a loss of FRET signal. Typically, measurements are expressed as a ratio of acceptor fluorescence over donor fluorescence with additional corrections for background fluorescence, direct activation of the acceptor fluorophore, and photobleaching. To more easily communicate the data, we express it as a ratio of donor over acceptor fluorescence so that an increase in cAMP corresponds to an increase in FRET ratio (Fig. 6C).

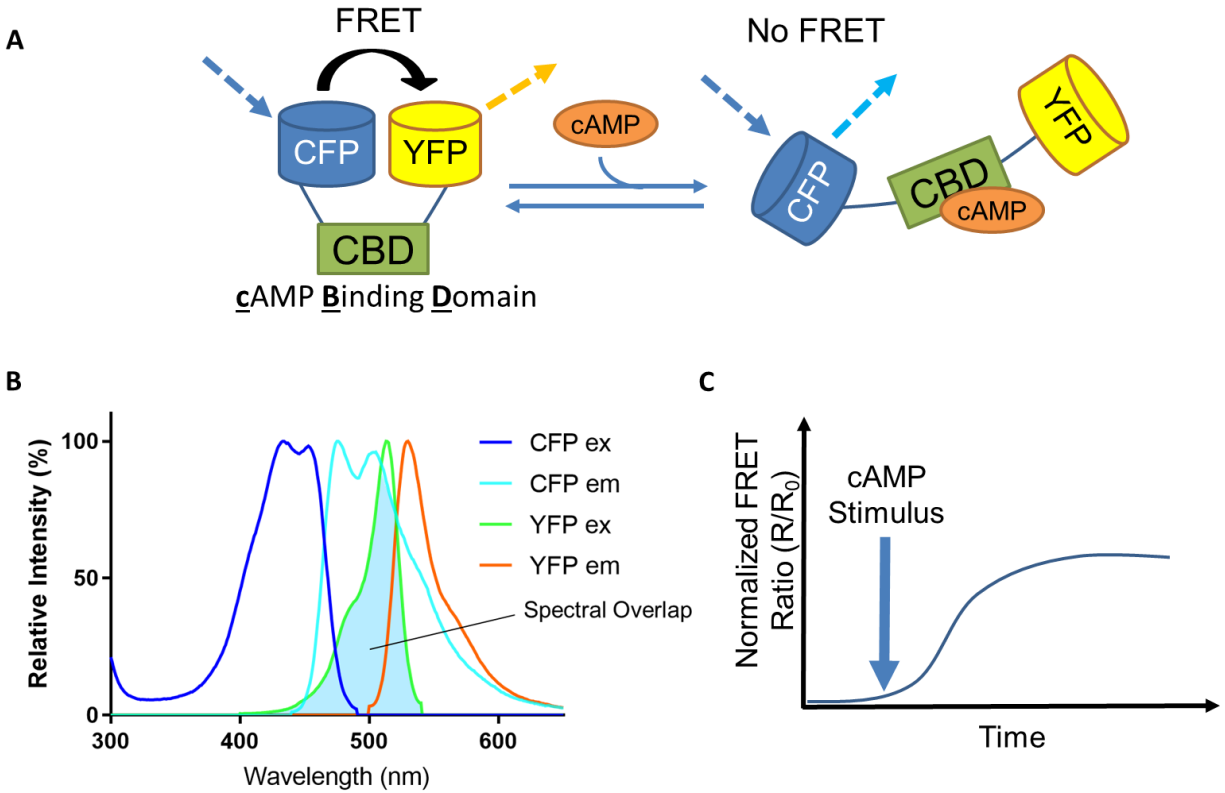


Figure 6. Fluorescence resonance energy transfer biosensors.

(A) The cAMP FRET sensor Epac1-cAMPs consists of an ECFP and EYFP FRET pair with a connecting CBD derived from EPAC1. FRET occurs in the absence of cAMP; upon binding it undergoes a conformational shift that decreases FRET efficiency. (B) FRET occurs between fluorophores with sufficient spectral overlap, i.e. the emission of the donor fluorophore overlaps with the excitation spectrum of the acceptor fluorophore (Data adapted from ThermoFisher Scientific Fluorescence SpectraViewer). (C) The change in fluorescence is expressed as the normalized ratio of YFP FRET emission over CFP emission such that an increase in cAMP will appear as an increase in FRET ratio.

The first visualization of cAMP compartmentalization used the FICRhR sensor which was introduced by Tsien and colleagues (191). It consisted of fluorescein-labeled PKA catalytic subunits and rhodamine-labeled regulatory units where cAMP induced dissociation of the subunits which led to a loss of FRET. While this was unprecedented at the time, several caveats

prevented widespread adoption of the technique. It required isolation of the protein, microinjection into individual cells, and retained endogenous PKA activity (192). Zaccolo and colleagues improved this approach by introducing a genetically encoded sensor with a GFP-labeled catalytic PKA subunit and blue GFP variant (EBFP) PKA regulatory RII subunit (89). The fluorophores were later changed to a CFP and YFP FRET pair which are more resistant to photobleaching (132). cAMP FRET sensors derived from PKA are commonly used (192), however many still retain endogenous PKA activity and localization. Buffering by PKA can also play a large role in interfering with measurements (193). This was used to Hofer and colleagues' advantage where they designed a 'cAMP sponge' from the RII β subunit of PKA to reduce cAMP levels (194); however, it illustrates a major drawback of PKA-based FRET sensors. Additionally, the slow kinetics of PKA dissociation and reassociation limit the temporal resolution. Unimolecular probes are more advantageous because they guarantee a one to one ratio of acceptor and donor fluorophores, thereby reducing additional controls needed. Hence, one of the most recently developed PKA-based FRET sensors is a unimolecular probe, Ri α #7. This sensor exhibits high cAMP affinity (~33 nM) and has been used to measure low extracellular levels of cAMP. It consists of a R1 α subunit sandwiched between circularly permuted Venus and CFP fluorophores (195). Circular permutation of fluorophores is a method which reorients fluorophores for more efficient energy transfer; the N and C termini of the fluorophore are joined while new termini are made at permissive sites (195,196).

After EPAC was discovered (75,76) several unimolecular cAMP FRET sensors were derived from this sequence. The EPAC class of sensors demonstrated higher FRET efficiency and more rapid kinetics compared to PKA sensors (88,192). The first EPAC-based FRET sensors were published in 2004 from three different research groups, each with a unique variant

(88,136,197). Researchers found removing the DEP domain of EPAC and introducing mutations in key catalytic residues prevented endogenous localization and activity (198,199). Some sensors, like Epac1-camps which is used in the previous section, only contain the minimal CBD domain from EPAC (amino acids 157-316) and still exhibit excellent kinetic properties (EC_{50} $2.35 \pm 0.42 \mu\text{M}$) (88). The most recent iterations of the sensor harbor high affinity mutations and circularly permuted fluorophores (200,201). In general, EPAC-based sensors are the most prominently used for their high FRET efficiency, unimolecular structure, fast kinetics, and ease of localizing to various compartments (196).

In addition to FRET sensors, genetically encoded cAMP biosensors have also been made from single wavelength fluorophores. Dimerization-dependent sensors from Campbell and colleagues consist of two fluorophores which fluoresce only when forming a heterodimer (202). For example, one iteration created the Red Dimerization Dependent cAMP sensor which when bound to cAMP exhibits a loss of fluorescence. The new Pink Flamingo sensor (Pink Fluorescent cAMP indicator) uses a single red fluorophore with an EPAC1 CBD inserted in the middle of the fluorophore by two linking regions (203). Pink Flamingo exhibits a 4.2-fold increase in fluorescence intensity upon cAMP binding with an affinity of $7.2 \mu\text{M}$. Ohta et. al. took a similar approach but strove to obtain a higher cAMP affinity using a PKA CBD and circularly permuted red fluorophore (204). They created R-Flnca (Red Fluorescent indicator for cAMP) which had a high affinity ($K_d = 0.3 \mu\text{M}$) and expanded dynamic range (8.6-fold increase at pH 7.2) (204). These single wavelength, red-shifted fluorophores are advantageous because they allow multi-color imaging whereas the range of compatible fluorophores with a FRET sensor are limited. Furthermore, they can be combined with optogenetic strategies that require blue-shifted excitation.

3.1.3 Localized Phosphodiesterase Activity

Uncovering the functional effects of localized signaling can be achieved by interfering with cAMP accumulation. Uneven distribution of PDEs is well documented (87,205-209). Additionally, computational models predict the K_m of the PDE isoform affects the steepness of a cAMP gradient (113). Lohse et. al. found cAMP proximal to PDE4A1 ($K_m \sim 2.4 \mu\text{M}$) was $<100 \text{ nM}$, suggesting clusters of PDEs could form cAMP sinks but only in areas of restricted cAMP diffusion ($\sim 10 \mu\text{m}^2/\text{s}$) (114). Hence interfering with PDE activity or localization can help assess downstream signaling from compartments. Fortunately, there are a multitude of pharmacologic agents which target specific PDE isoforms (86,210). Genetic knockdown approaches have shown the role of specific isoforms in membrane and cytosolic compartmentalization (137). Furthermore, overexpressing dominant negatives PDE4 which displaces endogenous anchored PDE4 increased cAMP levels (137,211). Disrupting localization is a key strategy in studying compartmentalization since the endogenous activity of the protein is preserved.

3.1.4 Signalosome Disruption

Interfering with cAMP compartment signaling can also be achieved by disrupting the associated signalosome. PKA inhibition can be achieved through pharmacological (H89) and genetic approaches; however, it can have undesired effects since PKA is part of multiple signalosomes. To alter PKA localization, AKAP deletion, siRNA knockdown, and mutations of the PKA binding α -helix can be used to target specific PKA and AKAP isoforms and interfere with compartmentalization. Another approach uses interfering peptides that mimic the AKAP α -helix and thus prevent PKA-AKAP interactions (67). Scott and colleagues were the first to develop

this peptide, Ht31, which globally disrupts PKA-AKAP binding. While Ht31 is still the most commonly used, newer versions have been designed to interfere with PKA regulatory subunits RI and RII. AKAP-in silico (AKAP-IS), Super AKAP-IS, and stapled anchoring disrupters 2/3 (STAD-2/3) all specifically interfere with PKA-II/AKAP interactions (212-214), whereas PV38, RIAD, and RI-STAD-1/2 were designed to interfere with PKA-RI/AKAP interactions (215-217). Recently, peptide-based approaches exhibit improved cell permeability by using stearaminated peptides, TAT protein fusions, or ‘stapled’ peptides that are locked in α -helical formations (151,218-220). These approaches allow more specific disruption of compartmentalized PKA isoforms without affecting activity of the protein itself.

Fewer methods exist for altering EPAC activity in signalosomes. Genetic knockdown methods have been useful for identifying EPAC function. The recently developed pharmacologic agent, ESI-05, specifically inhibits EPAC2 (221). EPAC1/2 inhibitors ESI-09 and HJC0197 have also been characterized; although, it was later found they have general protein denaturing properties rather than specific action on EPAC (222-224). Our lab was the first to use the N-terminus of EPAC as a dominant negative for interfering with localization. We have further developed a peptide inhibitor, similar to the concept of Ht31, which interferes with EPAC-Radixin interaction (unpublished data).

3.1.5 Localized Adenylyl Cyclases

To identify *bone fide* compartments and define their functional consequences, research would greatly benefit from synthetic localized cAMP production. Currently there are very few tools available that exhibit the temporal control needed to mimic cAMP signaling. Activation of specific adenylyl cyclase isoforms can be achieved using GPCR-mediated signaling; however,

the concomitant activation of several other pathways can mask cAMP-dependent effects. Soluble adenylyl cyclase (sAC) variants like the sACI/II chimera (225) and truncated but catalytically active form of sAC (135) have been used to study the effects of membrane, cytosolic, and nuclear cAMP signaling. However, activation of these cyclases requires forskolin (sACI/II) or bicarbonate (sAC truncated) which both activate endogenous cyclases and require wash-out to end the stimulus. This slow temporal regulation can interfere with kinetic studies.

Optogenetic light-activated cyclases are a powerful tool for rapid temporal regulation of cAMP synthesis. Photoactivated cyclases (PACs) are often derived from bacterial origins as cAMP signaling is a highly conserved evolutionary mechanism. For example, the first PAC discovered was from *Euglena gracilis* (euPAC). It consists of four subunits, each containing BLUF (sensor of blue light using flavin adenine dinucleotide)-type photoreceptor domains, two binding flavin adenine dinucleotides (FADs), and four catalytic domains (226). In response to blue light, it increases cAMP levels 80-fold (226). However, its large size (~412 kDa tetramer) and high dark activity makes it less than ideal for compartmentalization studies (186,227).

The recently characterized PAC from *Beggiatoa* (bPAC) is gaining popularity as a blue light-activated cyclase capable of producing a 300-fold increase in cAMP upon stimulation (186,228). Compared to euPAC, bPAC is much smaller (~77 kDa dimer) and has a lower dark activity (33 ± 5 pmol/min/mg of protein) (186). Each monomer contains a BLUF-domain and a Type III adenylyl cyclase. Light activation occurs within milliseconds, inducing a conformational shift opening the catalytic pocket of the cyclase; it returns to its dark-state quickly ($\tau_{\text{off}}=12$ sec) although residual cAMP accumulation is reported ($\tau=23 \pm 2$ sec) (186,229). Von Zastrow and colleagues were the first to use bPAC for spatial control over cAMP synthesis (36). By targeting bPAC to membrane and endosomal compartments, they discovered transcriptional differences

indicating endosomal cAMP signaling has functional consequences (36). Additionally, Averaimo et. al. targeted bPAC to lipid raft and non-raft membrane regions finding distinct physiological effects from raft domain signaling (148). Several have further engineered novel optogenetic cyclases to expand the range of activation and catalytic characteristics. Since blue light penetrates tissue poorly in *in vivo* applications (230), Gomelsky and colleagues designed an infrared light activated cyclase (Iiac) by fusing the phytochrome domain of *Rhodobacter sphaeroides* with an AC from *Nostoc sp* (231). To design a PAC with faster off-rates than bPAC, Sheib et. al. developed a chimeric protein using rhodopsin's millisecond on/off-kinetics and a mutated guanylyl cyclase domain which converts ATP to cAMP (232).

While optogenetic approaches are a powerful strategy that offer succinct control over cAMP production, it has not become a widely adopted technique. It is difficult to find commercially available light sources with tunable intensity and appropriate temporal regulation, cumbersome to mitigate external light when using typical lab techniques (ie: cell culture), and invasive for *in vivo* studies. Hochgeschwender and colleagues developed the luminopsins to circumvent these issues (233-235). By fusing the light-sensitive channelrhodopsin ion channel to *Gaussia* luciferase (GLuc) they created a new class of proteins with both optogenetic and chemical regulation of activation (233). GLuc is a small luciferase (19.9 kDa) that is activated by the substrate coelenterazine. GLuc emits 470 nm luminescence which overlaps with the excitation spectrum of channelrhodopsin, and thus it could potentially activate channelrhodopsin through non-radiative energy transfer. Genetic fusion of GLuc and channelrhodopsin adds an additional layer of control by chemical stimulation of light that bypasses the need for an external light source. Hochgeschwender's group and others has further expanded the family of

luminopsins by using different luciferases or using halorhodopsin to create an inhibitory luminopsin (235,236).

Using a similar strategy as the luminopsin protein, we have created a unique construct for regulating cAMP production in different subcellular compartments. We demonstrate that the fusion of bPAC and NanoLuciferase (nLuc) allows dual photo and chemical regulation of cAMP. Additionally, we have added a layer of spatial regulation using various targeting motifs to different subcellular compartments. The temporal and spatial flexibility of this construct make it widely adaptable for *in vitro* and *in vivo* applications.

3.2 METHODS

3.2.1 Cell Culture and Transfection

The rat hepatoma clonal cell line HC1 (237) was grown in DMEM supplemented with 10% FBS, Penicillin (100 IU/L) and Streptomycin (100 mg/L). PCCL3 were grown as described in the previous section. Cells were grown to ~90% confluency before passaging every 2-4 days at 37°C in 5% CO₂, 95% humidified air. For transient transfections, cells were transfected 24 hours after plating using Xtremegene HP (Roche) for HC1 cells, or Lipofectamine 3000 (Thermo Fischer Scientific) for PCCL3 cells. Cells were cultured for 24 hr and given fresh media.

3.2.2 Plasmid Preparation

Humanized bPAC with myc, nLuc, and several targeting sequences were generated and subcloned in a pcDNA3.1+ backbone (Genescript), including bPAC-nLuc (unmodified), N-Rx-bPAC-nLuc (amino acids 1-318 of N-Radixin), ER-bPAC-nLuc-AKDEL (endoplasmic reticulum, 18 amino acid BiP signal sequence + AKDEL), bPAC-nLuc-CAAX (plasma membrane, KRas4B-CVIM), NLS-bPAC-nLuc (nuclear localization sequence, PKKKRKVEDA), NES-bPAC-nLuc (nuclear export sequence LQLPPLERLTL), and MYR/Palm-bPAC-nLuc (myristolated/palmytolated, 17 amino acids N-terminus of Yes). All bPAC-nLuc sequences were subcloned into a pCDH-puro-cmyc vector (Addgene) and used to generate high-titer lentiviral suspensions (Cyagen Biosciences).

3.2.3 Lentiviral Infection and Stable Cell Line Generation

To optimize lentiviral infection conditions in PCCL3, 1×10^4 cells/well were seeded on a gelatin-coated 96-well dish. The next day different concentrations of polybrene and pLV[Exp]-EGFP:T2A:puro-EF1<mCherry lentiviral particles (1.2 TU/mL, Cyagen Biosciences) were mixed with complete Coon's media and incubated with cells for 24 hr. Approximate multiplicity of infection (MOI) was calculated assuming cells had doubled in number. A MOI of 80 and concentration of 5 $\mu\text{g/mL}$ polybrene was selected as the optimal infection conditions after imaging GFP fluorescence 48 hr after infection (Fig. 7). Stable cell lines were generated via puromycin selection at 1 $\mu\text{g/mL}$ for 4 days and maintained under selective pressure at 0.5 $\mu\text{g/mL}$.

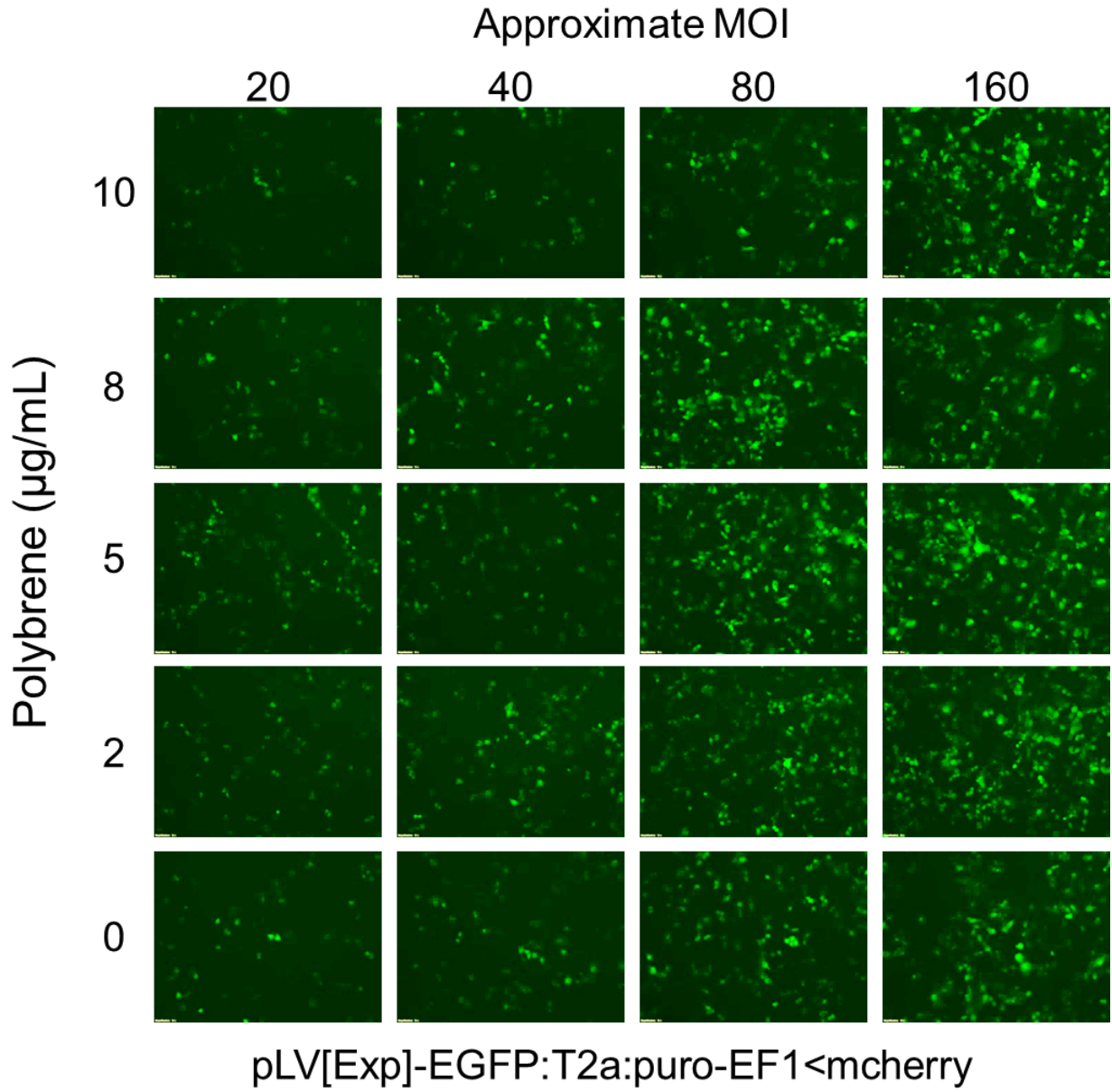


Figure 7. Lentiviral infection of PCCL3 cells.

PCCL3 infected with high titer EGFP lentiviral particles at varying MOIs and concentrations of polybrene show ample expression of the construct 48 hr after infection.

3.2.4 Luminescence Assays

8,000 HC1 cells were seeded in opaque 96well dishes (Corning) and transfected 24 hr later. 24 hr after transfection, cells were washed with phosphate-buffered saline (PBS) and incubated with OptiMEM lacking phenol red. Cells were stimulated with h-coelenterazine (h-CTZ, stock diluted in NanoFuel, NanoLight Technology) or NanoGlo® Luciferase Substrate (furimazine, Fz, Promega). Similarly, 5×10^4 cells/well of stable PCCL3 expressing bPAC-nLuc were seeded and stimulated 48 hr later with furimazine, Nano-Glo Endurazine Live Cell Substrate (furimazine-4377, Fz-4377, Promega), Furimazine-5455 (Fz-5455, Promega), or NanoGlo® Live Cell Substrate (Furimazine-Live Cell, Fz-LC, Promega). Luminescence was quantified using a TecanSpark 20M plate reader (SparkControl V1.2 software) or using a SpectraMax Paradigm plate reader (SoftMax Pro 6.2.2 Software) when measuring specific wavelengths.

3.2.5 Real Time cAMP Imaging – Red Dimerization Dependent Sensor

1.5×10^6 PCCL3 cells were seeded on 0.1% gelatin-coated 25 mm glass coverslips for 24 hr, transfected with the Red Dimerization Dependent Sensor (Montana Molecular), and given fresh media the next day. Cells were hormone starved for 3 hr prior to imaging in Coon's media with 1% FBS and lacking TSH, Insulin, and hydrocortisone (Starvation Coon's media). Cells were washed twice with PBS and imaged in imaged in OptiMEM lacking phenol red on an Olympus IX70 microscope equipped with a Till Poly V monochromator. Images were acquired every 10 s with a 60x/1.4 NA oil objective, 8x8 binning and a Hamamatsu CCD camera using 570 nm excitation (20% monochromator intensity, 15 nm bandpass) with emission filter 620/52 nm and dichroic 560 nm. Cells were stimulated with light at $4.41 \pm 0.301 \mu\text{W}/\text{mm}^2$ LED (450 nm) in

pulses varying in duration and 100 μM IBMX was added at the end to show the saturation point of the sensor.

3.2.6 Optogenetic Stimulation

Cell culture and experiments were performed in a dark environment using a red safelight lamp (Kodak GBX-2 Safelight Filter) with a 13 W amber compact fluorescence bulb (Low Blue Lights, Photonic Developments LLC) to prevent light exposure from wavelengths <500 nm. Light activation was achieved using a custom-built, Arduino-controlled system capable of regulating the duration, frequency, and intensity of light exposure. The illuminating high-power LED (royal blue CREE XTE Tri-Star LED, LED Supply) was mounted on a stage, keeping a distance of 18 cm from the sample to ensure a near-homogenous spread of light (Fig. 8A). For experiments performed inside an incubator, samples were placed atop the stage and cells were illuminated from below. The stage was inverted for real-time imaging experiments, such that samples were illuminated from above. The light intensity used for these experiments was $4.41 \pm 0.30 \mu\text{W}/\text{mm}^2$ as measured by a laser power meter (ThorLabs PM1100D, detector S130C). The program allows for pulses of light from milliseconds to minutes in duration. Additionally, intensity range spanned from $4.41 \pm 0.30 - 14.85 \pm 1.00 \mu\text{W}/\text{mm}^2$ when measuring irradiance at 18 cm distance from the LED through the bottom of a 6-well dish (Falcon, Corning) (Fig. 8B). The Arduino program allowed for pulses of light from milliseconds to minutes in duration. (See Appendix A for more details on the LED illumination system, Fig. 21-22, Table 1).

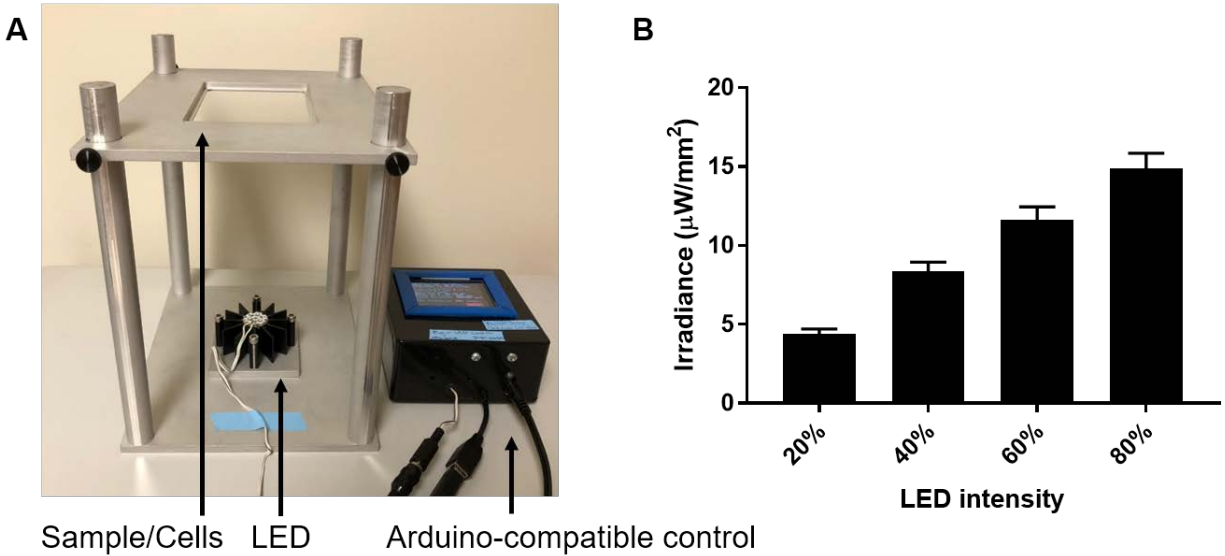


Figure 8. Arduino-compatible LED system and stage.

A royal blue LED mounted on a heat sink is attached to a stage 18 cm from sample. The LED connects to the power source and Arduino-controlled system. The intensity and pulsatile manner of LED exposure is controlled using Arduino v1.6.8 software providing an irradiance range from 4-15 $\mu\text{W}/\text{mm}^2$ when measured at an 18 cm distance through the bottom of a 6-well dish.

3.2.7 ELISA

1.5×10^5 HC1 cells were seeded in a 6-well dish, transfected, washed in PBS, lysed in 0.1 M HCl, and frozen at 80°C . Thawed lysates were diluted in Neutralizing Reagent to be within linear range and analyzed using the Monoclonal Anti-cAMP Antibody Based Direct cAMP ELISA Kit (non-acetylated, NewEast Biosciences). Briefly, the assay is a competitive immunoassay with goat-anti-mouse serum-coated plates and fixed concentrations of anti-cAMP antibody and cAMP-conjugated horse-radish peroxidase. Optical density was measured at 450 nm on a SpectraMax Paradigm reader and concentrations were calculated based on a standard curve.

Values were normalized to the amount of protein in lysates determined using the Pierce™ BCA Protein Assay Kit following manufacturer's instructions.

3.2.8 Immunocytochemistry

PCCL3 cells were seeded in a 6-well dish on 25 mm glass coverslips and transfected the next day. 24 hr later, cells were washed with PBS, fixed for 10 min in 4% paraformaldehyde, and permeabilized for 10 min 0.5% Triton X-100. Cells were washed and stained with anti-myc (1:500, 9E10, Covance), washed with 0.05% Tween-20 in PBS, and stained with DAPI and Donkey anti-mouse Alexa Fluor 594 (Jackson ImmunoResearch). Images were acquired using an upright Olympus Fluoview FV1000 confocal imaging system with a 60x/1.45 NA oil immersion objective using 405 and 559 nm excitation with the appropriate filters.

3.3 RESULTS

3.3.1 Luminescence-Activated Cyclase Allows Dual Photo and Chemical Activation of cAMP Production

To create a tool for cAMP synthesis with broad tunability, we fused *Beggiatoa* photoactivated adenylyl cyclase (bPAC) to NanoLuciferase (nLuc). bPAC is a blue-light sensitive cyclase with succinct on/off kinetics and high rate of synthesis (186). nLuc is a small (19 kDa) luciferase that emits blue-shifted luminescence in response to the luciferins furimazine (Fz) and h-coelenterazine (h-CTZ) (238). A myc-tag was included between the two moieties to aid

identification and visualization. The resulting bPAC-myc-nLuc fusion protein can be activated by blue light or chemical stimulation of luminescence (Fig. 9A).

To test whether the nLuc moiety retains activity in the fusion construct, we used the rat hepatoma cell line HC1 that has low basal levels of cAMP (8,237). Transiently transfected cells were stimulated with h-coelenterazine (h-CTZ) and furimazine (Fz). Cells luminesced in the blue light range (440-460 nm, 455 nm max) in a dose dependent manner (Fig. 9B-E). h-CTZ was used primarily for these experiments due to its commercial availability and ability to produce sufficient luminescence for activation. h-CTZ stimulated luminescence for ~1 hr (Fig. 9F), whereas furimazine induced luminescence was still detectable 2 hr later (Fig. 9G). New furimazine derivatives, endurazine (Fz-4377) and furimazine-5455 (Fz-5455), have been developed to provide long-lasting luminescence and lower toxicity. For example, endurazine contains a protecting group which requires esterase hydrolysis for activity, resulting in low but stable luminescence for >6 hr (Fig. 9G). Together, the different coelenterazine and furimazine derivatives can produce a broad range of temporal activation.

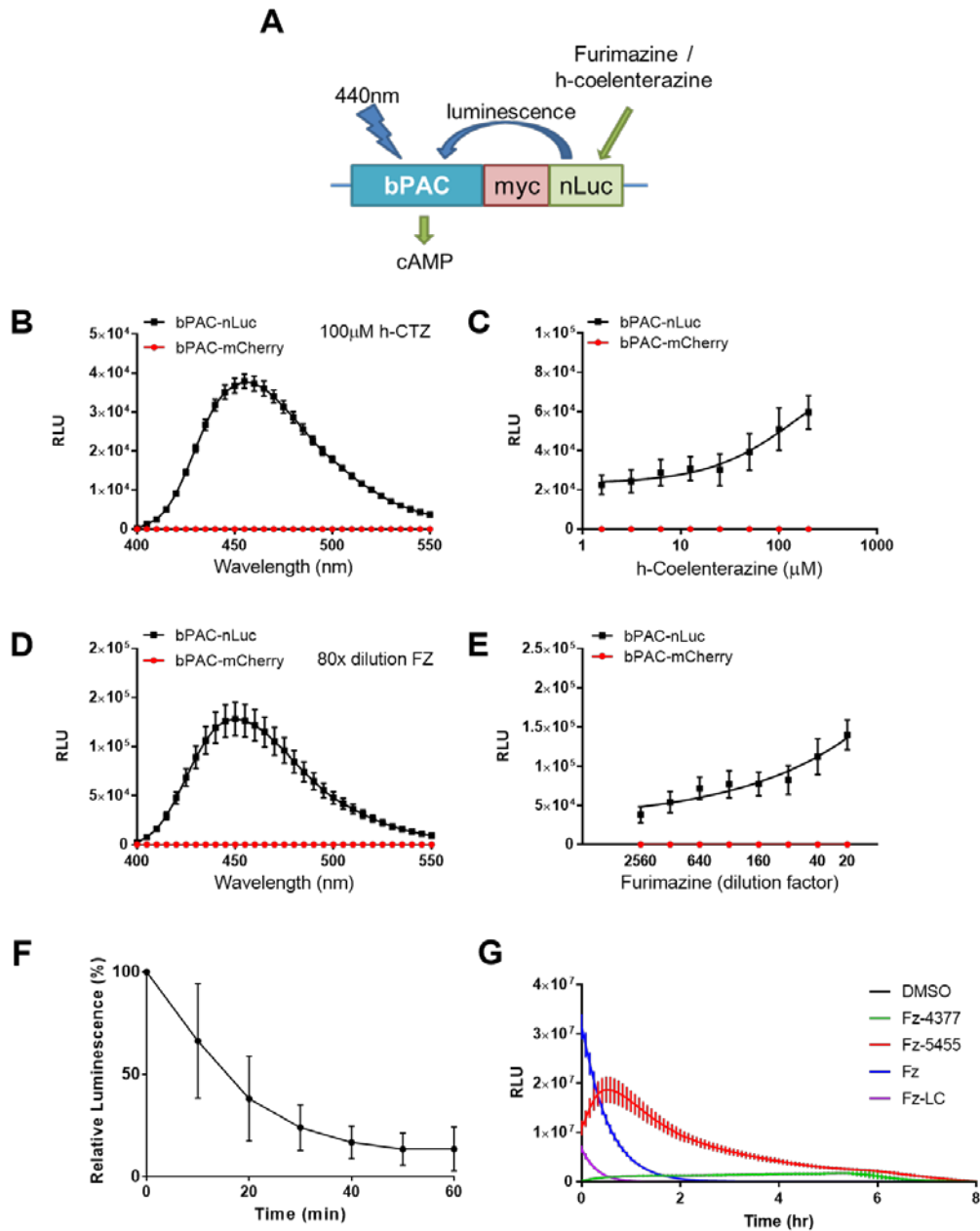


Figure 9. Luminescent characteristics of bPAC-nLuc fusion protein.

(A) To allow dual photo and chemical activation of cAMP production, we have created a fusion protein containing *beggiatoa* photoactivated cyclase (bPAC) and NanoLuciferase (nLuc). (B) Transiently transfected HC1 cells expressing bPAC-nLuc luminesce at a maximum of 455 nm (within the excitation range of the bPAC) when treated with 100 μM h-CTZ (mean ± SEM of n=4). (C) This effect occurs in a dose-dependent manner (mean ± SEM of n=4). (D-E) Similar luminescent properties were found with Fz which elicits higher max luminescence (mean ± SEM of n=4). (F) Treatment with 100 μM h-CTZ luminesces for up to 1 hr, with most of the reaction occurring in

the first 30 min (mean \pm SD of n=4). (G) Furimazine and newly developed derivatives furimazine-live cell (Fz-LC), Furimazine-4377, and Furimazine-5455 elicit different luminescent kinetic signatures in lentiviral-infected stable PCCL3 cells expressing bPAC-nLuc (1:1000 dilutions, mean \pm SD of n=4).

bPAC-nLuc retained its optogenetic properties as shown in PCCL3 rat thyroid cells co-expressing a red cAMP dimerization dependent sensor. Activation with 450 nm light occurred in milliseconds with cAMP levels returning to baseline levels quickly, demonstrating tight temporal regulation of activity with light (Fig. 10A). Furthermore, chemical stimulation of nLuc luminescence sufficiently activates light-sensitive bPAC. Stimulation with h-CTZ in the presence of IBMX induced up to >100-fold increase in cAMP accumulation in HC1 cells within 10 minutes, as shown by cAMP ELISA analysis (Fig. 10B). Single-cell analysis of PCCL3 expressing the red dimerization dependent sensor reveals h-CTZ stimulates sustained cAMP production for ~30 min (Fig. 10C-D). We found the duration and amplitude of cAMP levels were easily tuned by altering the light intensity and duration or the luciferin concentration and duration of exposure.

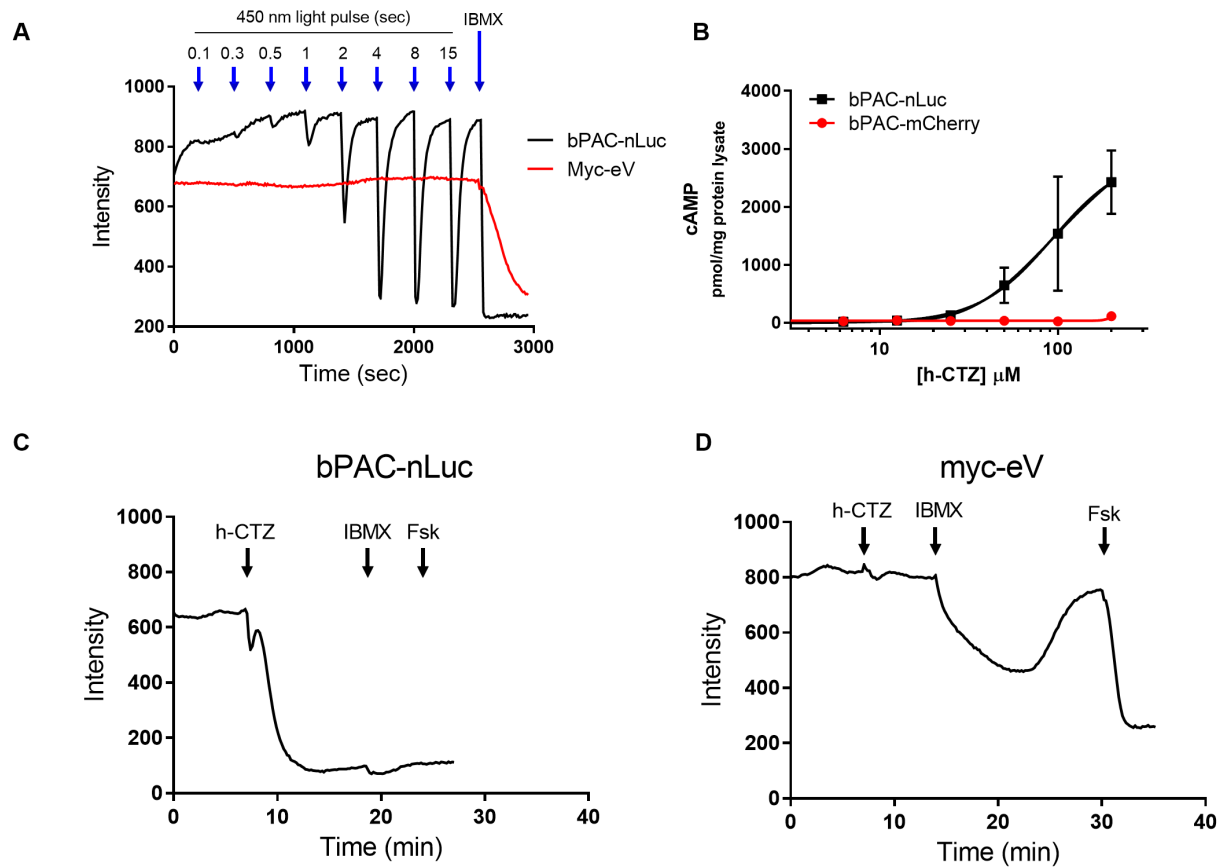


Figure 10. Photo and chemical stimulation activates bPAC-nLuc.

(A) The bPAC moiety responds to 450 nm light within milliseconds ($4.41 \pm 0.30 \mu\text{W}/\text{mm}^2$) with longer pulses of light inducing higher levels of cAMP. (B) h-CTZ specifically increases cAMP in HC1 cells expressing bPAC-nLuc in a dose dependent manner in the presence of 100 μM IBMX (mean \pm SEM of $n=4$). ELISA analysis shows a max stimulation >100-fold increase from basal levels. (C-D) 25 μM h-CTZ increases cAMP within minutes using PCCL3 cells co-transfected with a Red cAMP Dimerization Dependent Sensor which decreases in fluorescence when bound to cAMP. Myc-empty vector (myc-eV) transfected cells show h-CTZ does not affect sensor readings (representative single cell traces shown, 100 μM IBMX and 10 μM forskolin (Fsk) show saturation of sensor).

3.3.2 Luminescence-Activated Cyclase Can Be Localized to Distinct Subcellular Compartments

bPAC and nLuc were initially selected for their small size, resulting in a final ~60 kDa fusion protein. This size is at the upper limit for passively diffusing through nuclear pores (239), and the construct was distributed evenly throughout the cytosol and nucleus (Fig. 11). To improve spatial resolution of bPAC-nLuc, we targeted this construct to distinct subcellular regions using different targeting motifs. By modifying the N and/or C termini with targeting motifs, bPAC-nLuc localization could be re-distributed to specific sub-cellular regions. In PCCL3 cells, constructs localized to the nucleus (NLS), cytosol (NES), endoplasmic reticulum (ER), Radixin-localized submembrane domains (N-Rx), and plasma membrane (CAAX, MYR).

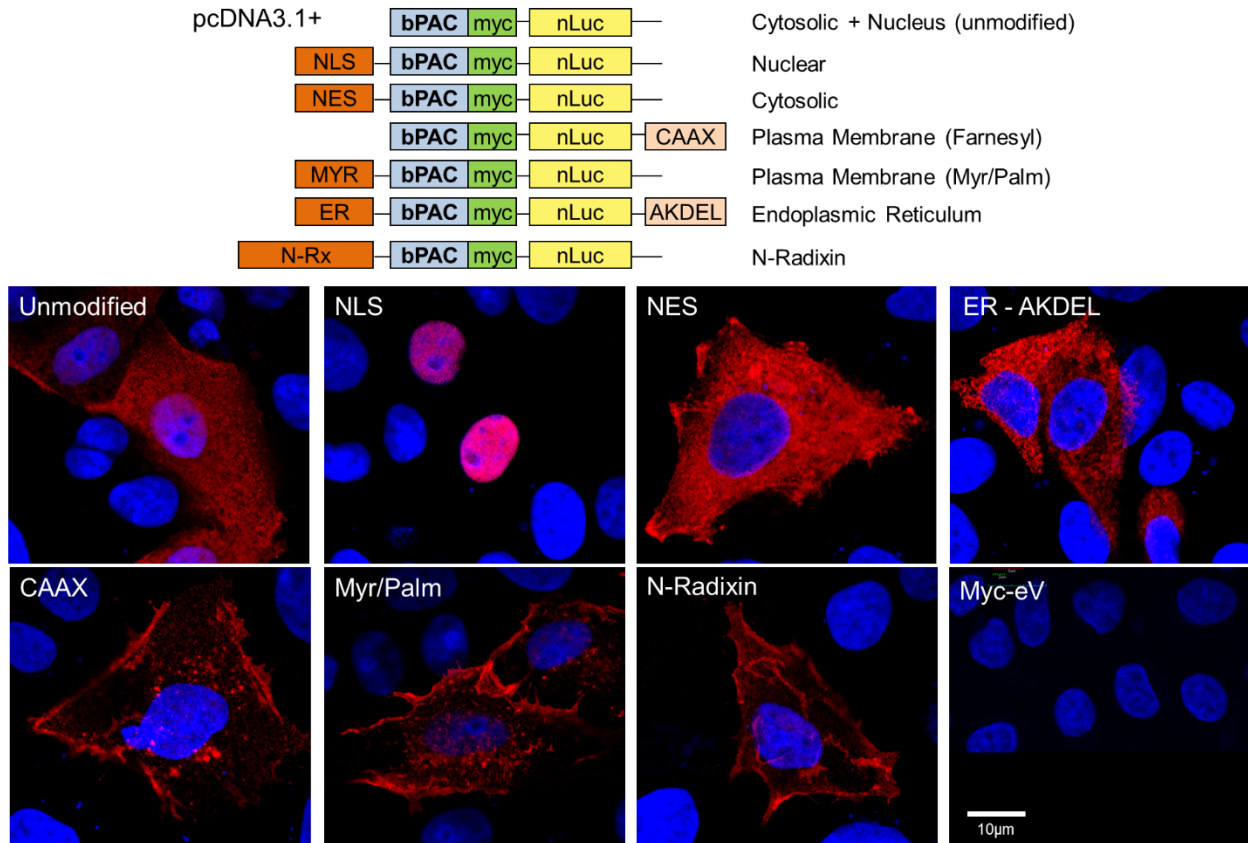


Figure 11. Luminescence-activated cyclase can be targeted to different sub-cellular regions.

Transiently transfected PCCL3 cells stained with anti-myc (red) and DAPI (blue) demonstrate differential localization of pcDNA3.1+bPAC-nLuc constructs throughout the cell (unmodified), nucleus NLS (PKKKRKVEDA), cytosol NES (LQLPPLERLTL), endoplasmic reticulum ER (BiP signal sequence 18aa, AKDEL), and plasma membrane using farnesylation CAAX (KRas4B-CVIM) and myristoylation/palmytolation (N-term Yes 17aa). Representative images shown with 10 µm scale bar (bottom, right) with myc-empty vector (myc-eV) negative control.

Since lipid-based transfection of PCCL3 yields low efficiency, we subcloned the bPAC-nLuc constructs into a pCDH-puro-myc lentiviral backbone to create lentivirus and increase the population of cells expressing our constructs. Stable cell lines were made from both the pcDNA3.1+ transfections and pCDH lentiviral infections; however, despite selective pressure, expression was lost after a few passages. This was true for heterogeneous and clonal populations.

The loss of expression may be due to selective pressure from cytotoxic effects, reduced proliferation, or silencing of the CMV promoter. Interestingly, HEK293 cells successfully formed stable lines from pcDNA3.1+ constructs and retain expression well after several passages. This suggests that any potential cytotoxic effects of bPAC-nLuc do not affect certain cell models.

PCCL3 experiments were done using bulk populations of cells since clonal populations lost expression before reaching necessary quantities. In stable PCCL3 expressing lentiviral pCDH bPAC-nLuc, furimazine treatment stimulates luminescence immediately, suggesting that furimazine enters intracellular compartments like the nucleus and endoplasmic reticulum within a similar timeframe (Fig. 12). Furthermore, luminescence is detectable up to two hours for all constructs even in cells with low expression.

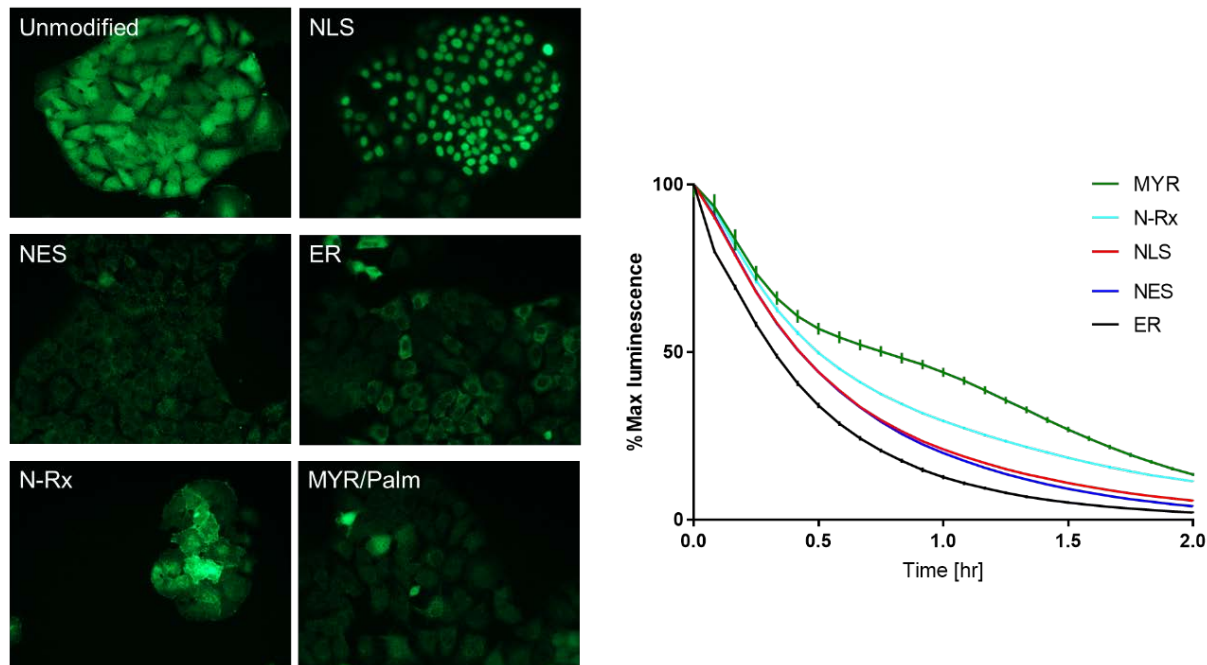


Figure 12. Stable lentiviral-infected PCCL3 expression and luminescence.

PCCL3 infected with lentiviral bPAC-nLuc constructs were selected in puromycin to form stable cell lines. Cells were stained with anti-myc (green) and imaged to ensure constructs effectively localize to their appropriate subcellular locations. Stimulus with Furimazine induces immediate expression in all compartments, including the nucleus and endoplasmic reticulum lumen. Decay kinetics of furimazine-induced luminescence show the highest activity in the first hour with lower, but still prominent luminescence at 2 hr (mean \pm SD of n=2).

3.4 DISCUSSION

The cAMP compartmentalization field has quickly expanded over the last two decades. A growing number of AKAP signalosome disruptors have been created to study compartment function. The field still notably lacks tools to mimic cAMP signaling with sufficient spatial and temporal resolution. Here, we have created a luminescence-activated cyclase that offers exquisite spatio-temporal control over cAMP synthesis. We show both the enzymatic activities of bPAC

and nLuc are preserved in the fusion protein. h-CTZ or Fz stimulated luminescence is sufficient to induce a high level of cAMP production. We found cAMP production was easily tunable by altering the duration and intensity of light, or the duration and concentration of luciferin stimulation. New time-released Fz analogs are being developed to extend that duration of luminescence, providing multiple kinetic signatures to stimulate bPAC-nLuc. As bPAC-nLuc is a relatively small construct (~60 kDa), it was readily redistributed to specific subcellular location when modified with a localization sequence. Importantly, furimazine stimulated immediate luminescence in all compartments, suggesting furimazine permeability is not an issue. Hence, bPAC-nLuc can serve as a unique tool for mimicking location-biased cAMP signaling.

Compared to other tools in its class, such as the sACI/II chimera (225) and truncated sAC (135), bPAC-nLuc does not require a chemical stimulus that could activate endogenous cyclases. Compared to bPAC alone (36,148), the bPAC-nLuc fusion provides more flexibility for *in vitro* studies when a light source is not available or when chronic signaling is needed. Our approach circumvents the individual obstacles of chemical activation and optogenetics, creating a versatile tool that can easily be adopted by labs entering the optogenetics field. Furthermore, it has great potential for *in vivo* applications where light sources would be highly invasive. Potential applications for bPAC-nLuc will be discussed in depth in the next chapter.

Working with bPAC-nLuc requires a specific work environment. Standard fluorescent lighting used in most labs emits blue light at 2-3 $\mu\text{W}/\text{mm}^2$ which activates bPAC. All light below 500 nm should be blocked from the room while in use. Incidental light exposure throughout cell culture may induce undesired effects in cAMP-sensitive systems. We found with our best effort to minimize light exposure, basal levels of cAMP were relatively low in our ELISA experiments

and only slightly above non-transfected controls. However, in cAMP-sensitive systems like PCCL3 cells, a small increase in basal cAMP levels can have significant functional effects.

When designing experiments, the stimulus must be carefully calibrated. bPAC has a very high maximal activity that may not correspond to endogenous cAMP signaling. Thus, tuning the duration and amplitude of light or chemical stimulus should be compared with endogenous signaling mechanisms such as GPCR-stimulated cAMP production. Using high concentrations of h-CTZ or furimazine can have cytotoxic and off-target effects from oxidation of the compound. Additionally, oxidative stress and activation of endogenous flavins from blue light exposure may be a concern in some systems (240).

There are several possible ways to reduce basal and maximal cAMP levels if needed. To lower maximum cAMP levels, we found reducing the amount of DNA during transfection lowers basal activity. The CMV promoter in our constructs yielded high expression, but this could be replaced with a low expression promoter to ensure the system does not oversaturate. Furthermore, the CMV promoter may have been silenced in our stable cell lines. Hence a different promoter or a vector which couples bPAC-nLuc and antibiotic resistance gene transcription would help ensure expressing cells maintain a growth advantage (e.g. pIRES, BD Biosciences) (241). One could also use an inducible system such as the Degradation Domain (DD)/Shield-1 system (Clontech) which destabilizes the protein until the ligand shield-1 is added (Fig. 25). Future work in our lab will include using a tetracycline-inducible promoter to prevent protein expression during routine cell culture. Another approach to altering bPAC-nluc basal activity would be to modify bPAC itself. Recently, structural characterization of bPAC identified the point mutation S27A which reduced basal dark activity by 40% but did not reduce maximal light-activated activity (242). The maximal absorbance was also red-shifted 15 nm (from 441 nm

to 456 nm) which should favor activation by nLuc. These variations of the bPAC-nLuc constructs could potentially tune expression and activity to fit the needs of the model organism.

4.0 POTENTIAL APPLICATIONS FOR LUMINESCENCE-ACTIVATED CYCLASE

4.1 INTRODUCTION

Dual photo and chemical activation of bPAC-nLuc circumnavigates the individual limitations of optogenetic and drug-induced cAMP production. These characteristics make bPAC-nLuc broadly adaptable and finely controlled for cAMP synthesis. Here we explore four potential applications of this tool to investigate spatial effects of cAMP signaling thyroid mitogenesis, mimic different temporal patterns of cAMP signaling, address the role of cAMP in a mouse melanoma metastasis model, and explore direct lentiviral injections of bPAC-nLuc in mouse thyroids.

4.1.1 Spatial Regulation of cAMP Synthesis in Thyroid Mitogenesis

As discussed in the previous chapters, our group identified a potential cAMP compartment involved in TSH-stimulated mitogenesis. We hypothesized Radixin positioned cAMP effectors EPAC and PKA near a site of high cAMP concentration. Using the N-terminus of Radixin, we show Radixin-localized sub-membrane regions exhibit increased cAMP levels immediately after TSH stimulus (Fig. 4). Hence, we wanted to expand our studies using N-Rx-bPAC-mCherry (Fig. 5) to include bPAC-nLuc constructs for expanded regulation. Our goal was to test if N-Rx localized cAMP production was necessary and sufficient for stimulating mitogenesis. While

transmembrane AC activation is known to promote proliferation, there is evidence that cAMP signaling is spatially encoded. Sustained cAMP signaling after receptor internalization suggests a source of cAMP production beyond the sub-membrane region can stimulate specific functions. Furthermore, a second layer of cAMP signaling could also come from intracellular sAC. Transmembrane cyclases have been shown to activate sAC through EPAC/PLC/Ca²⁺-mediated signaling (47). Since the role of sAC has not been determined in thyroid function, studying cAMP compartments which trigger functional effects could help identify functional sAC pools. Hence, we tested whether luminescence-activated cyclase could stimulate thyroid mitogenesis and began to test the effects of localized cAMP signaling.

4.1.2 Temporal Regulation of cAMP in GPCR Signaling

The dual stimulation of cAMP production by bPAC-nLuc represents two signaling modalities: transient pulses of cAMP production by light, and sustained cAMP production by luciferin stimulation. It is now well established that many GPCRs stimulate a transient peak of cAMP production from the plasma membrane and a following sustained phase of cAMP production during receptor endocytosis and redistribution in endosomes (32,33,92,94,243). Furthermore, multiple studies found oscillating patterns of cAMP regulate downstream functions (100-105). To test whether bPAC-nLuc could mimic these patterns of cAMP signaling, we transiently expressed bPAC-nLuc in HEK293 cells. We observed the same luminescent characteristics as detected in HC1 cells. h-CTZ and Fz stimulation generated blue luminescence with a maximum of 455 nm in a dose-dependent manner (Fig. 15A-D). High expression made luminescence visible to the naked eye and could be imaged using long exposures times (Fig. 15E).

Using HEK293 cells, we transiently expressed the high-affinity cAMP FRET-based sensor, YFP-EPAC-Q270E-mScarletI (H208) (Fig. 16A). Cells expressing MYR/Palm-bPAC-nLuc generated transient spikes of cAMP accumulation in response to pulses of blue light between 1 and 100 sec at $4.4 \mu\text{W}/\text{mm}^2$ (Fig. 16B). Stimulation with furimazine induced a significantly longer signal, lasting well-beyond 30 min (Fig. 16C). Together, these two methods of stimulation can potentially tease out the individual effects of the transient, sustained, and oscillating temporal patterns of cAMP signaling.

4.1.3 *In Vivo* Effects of cAMP in B16-F10 Mouse Melanoma Metastasis Model

To test the potential applications for bPAC-nLuc *in vivo*, we used the B16-F10 mouse melanoma metastasis model to conduct a proof-of-principal experiment. This model provided easy means to deliver the bPAC-nLuc constructs, had a relatively short experimental time line, and provided a cAMP-sensitive model in an organ which would be difficult to reach with light. The model was developed after the B16 cell line was cultured from a spontaneous skin tumor from a C57BL/6J mouse (244). B16 cells are injected intravenously (i.v) into syngenic C57BL/6 mice and these mice develop metastatic colonies in their lungs 2-3 weeks later. By resecting these pulmonary tumors and growing them in culture, this process can be repeated several times to create cell lines with increasing metastatic potential. This was repeated 10 times to create the B16-F10 cell line which is highly metastatic and less genetically stable (245,246). When B16-F10 are injected into the tail veins of mice, they colonize the lungs forming black tumors due to high melanin production. This metastatic event has been shown to be regulated by cAMP, however studies are limited.

Early studies hypothesized cAMP activity promoted metastasis. Gorelik and colleagues found growing B16-F10-BL6, a variant of the cell line found to penetrate the bladder wall, in DMEM media as opposed to RPMI increases basal cAMP levels, reduces proliferation, promotes differentiation, and increases pulmonary tumor metastases (247). Similarly, B16-F10 cells treated with cAMP-elevating N-MSH ((4-norleucine-7-D-phenylalanine)- α -melanocyte-stimulating hormone) and sodium bicarbonate to induce differentiation exhibit increased metastasis (248). There is a correlation in cAMP responsiveness in cells with more metastatic characteristics (249-252); however, more direct studies on the role of cAMP conclude increased cAMP reduces metastatic potential (253-255). All reported studies using the metastasis model stimulate cAMP production in B16-F10 cells prior to injection with forskolin, IBMX, or GPCR stimulation with α -MSH. This is hypothesized to induce differentiation which negatively correlates with metastatic potential. However, none of these reports address the role of cAMP after colonizing the lung. One group tried to systemically increase cAMP by administering forskolin prior to injecting cells (256). They found reduced melanoma-induced platelet aggregation and lung colonization, but this approach lacks specificity in identifying which cell response is linked to the physiologic endpoint. A discrepancy remains whether cAMP inhibits or promotes proliferation of B16-F10 *in vitro* and there is little evidence of its effects *in vivo* (253,255,257). bPAC-nLuc expressing cells have the potential to test the effects of cAMP pre- and post-injection through luminescence-based activation. Here we injected bPAC-nLuc expressing B16-F10 cells and administered furimazine i.v. daily throughout the course of the experiment.

4.1.4 Direct Lentiviral Thyroid Injection with Ultrasound Guided Microinjection

We selected another mouse model for our *in vivo* proof-of-concept experiments. To prevent artifacts from bPAC overexpression in cell lines and study cells in their native environment, we used ultrasound guided (USG) microinjection of bPAC-nLuc lentiviruses in mouse thyroids. USG microinjection is excellent to identify and inject thyroid glands in mice (258,259). Compared to surgical procedures it is far less invasive and leads to longer survival times (258). Direct lentivirus injection is ideal over other forms of genetic manipulation because it can infect non-dividing cells (unlike retroviruses) and requires less time to generate a model compared to creating transgenic mouse lines (260,261). The purpose of our study was to test whether luminescence-activated cyclase could stimulate thyroid cell proliferation two weeks after viral injections with daily furimazine treatment. Similar to previous studies in our lab administering goitrogen to induce cAMP-mediated proliferation in mice. Although the studies are not complete at the time of this dissertation, we show initial adaptation of this model for our lab.

4.2 METHODS

4.2.1 PCCL3 EdU Incorporation Assay

Similar to the BrdU incorporation assays used for transiently expressing cells (Chapter 2), Edu incorporation assays were used on stably expressing cells for increased throughput. PCCL3 stable cell lines expressing pCDH-bPAC-nLuc constructs were cultured as described in the previous section. 2×10^5 cells/well were seeded in a 96-well dish (Perkin Elmer, black walled,

clear bottom). Approximately 24 hr later, cells were hormone starved in Starvation Coon's media with 5% FBS for 16 hr. Media was replaced with fresh starvation Coon's media (5% FBS) containing Nano-Glo Endurazine Live Cell Substrate (Fz-4377) or DMSO. 8 hr after stimulation, 10 μ M EdU was added using a small volume and incubated an additional 16 hr. Then cells were washed in PBS, fixed for 10 min in 4% PFA, and permeabilized 10min in 0.5% TritonX-100. Cells were stained for EdU using a cocktail of 100 mM Tris buffer (pH 7.6), 4 mM CuSO₄ (Fisher Sci), 8 μ M 5'-6-FAM (Lumiprobe), and 100 mM Sodium Ascorbate (Sigma) added in this order. Cells were incubated 30 min at room temperature, protected from light. Finally, cells were washed thoroughly in PBS, stained 10 min with DAPI, and washed thoroughly in PBS again. Plates were imaged using a Nikon Eclipse Ti equipped with a 10x objective with help from Dr. Watkins. Images were analyzed as %EdU positive nuclei/total DAPI stained nuclei using NIS Elements Bright Spot Counting software.

4.2.2 HEK293 Cell Culture and Luminescence

HEK293 were grown in DMEM supplemented with 10% FBS, Penicillin (100 IU/L) and Streptomycin (100 mg/L). Cells were passaged at 80-90% confluence ever 2-3 days and transfected using Xtremegene HP (Roche) for luminescence assays. Cells were seeded in poly-D-lysine coated opaque 96-well dishes (Corning) and transfected 24 hr later. 24 hr after transfection, cells were washed with PBS and incubate with OptiMEM lacking phenol red. Cells were stimulated with h-coelenterazine (h-CTZ, stock diluted in NanoFuel, NanoLight Technology), NanoGlo[®] Luciferase Substrate (furimazine, Fz, Promega). Luminescence was measured and quantified as described in the previous chapter.

4.2.3 FRET Imaging

The cAMP FRET sensor H208, kindly provided to us before publication by Dr. Jalink, consists of a YFP and mScarletI (262) fluorescent pair flanking catalytically inactive Epac1 with a high affinity mutation (200) (YFP-EPAC-Q270E-mScarletI, H208) and exhibits a loss in FRET signal upon binding cAMP. Note that the Jalink lab does not recommend this sensor for general experimentation due to punctate speckles forming a few days after transfection. This was confirmed in our hands but did not hamper our experiments which were performed 2 days after transfection. Cells exhibited a relatively even cytosolic distribution of the sensor in the experiments shown here. For further details on the construct, please contact the Jalink lab. HEK293 cells were seeded on poly-D-lysine coated glass coverslips and transfected using Lipofectamine 3000 24 hr afterwards. When using MYR/Palm-bPAC-nLuc, we used a low amount of DNA (100 ng MYR/Palm-bPAC-nLuc + 900 ng H208) to avoid saturation of the cAMP sensor. 48 hr after transfection, cells were washed and imaged in a HEPES imaging buffer with 137 mM NaCl, 5.4 mM KCl, 2mM CaCl₂, 1 mM MgCl₂, 10 mM HEPES, pH 7.3. Images were acquired every 30 s with a 60x/1.4 NA oil objective, 4x4 binning using 500 nm excitation with emission filters 510/20 (Semrock) and 620/52 and a dichroic beam splitter 468/526/596 (BrightLine® Semrock). Data was collected using Slidebook software (Intelligent Imaging Innovations, Inc) and the ratio of Scarlet/YFP (donor over acceptor) fluorescence is normalized to maximum FRET response as determined by forskolin and IBMX stimulation. Cells were stimulated with 4.4 μW/mm² LED light and 1:1000 Fz.

4.2.4 B16-F10 Melanoma Cell Culture

B16-F10 cells were kindly provided by Dr. Storkus. Cells were maintained in RPMI supplemented with penicillin/streptomycin and 10%FBS. Cells were passaged every 2-3 days when ~80% confluent. Lentiviral constructs were used at a MOI of ~100 with 5 µg/mL polybrene (Vector Builder). Cell expression was selected with 4 days of 1.0 µg/mL puromycin treatment. 16 hr prior to harvesting for animal experiments, cells were maintained in puromycin-free media to ensure maximum cell viability.

4.2.5 Melanoma Metastasis Model

20 female C57/BL6 mice were obtained from Jackson Laboratories and used at 13 weeks of age. B16-F10 expressing bPAC-nLuc and GFP were harvested in their exponential phase of growth, diluted in PBS, and kept on ice prior to injection. Cell culture and mouse injections were performed in darkness under a red lamp. 3×10^5 cells/200 µL/mouse were injected i.v. in the tail vein on 'Day 0.' Additionally, 3×10^3 cells/100 µL/mouse were injected intradermally (i.d.) in the lower abdomen. Extra cells were seeded to measure luminescence and cAMP (ELISA, 5×10^5 cells/well) as described in the previous chapter. On Day 1-18, furimazine was injected into the tail veins of mice at a 1:40 dilution in 100 µL PBS (~5 µg, < 0.25 mg/kg, Stacer 2013), or PBS alone was injected as a control. On Day 19, mice were sacrificed and lungs and i.d. tumors were harvested. Prior to resection of one i.d. tumor, furimazine was injected directly into the tumor to test for bPAC-nLuc expression using a Nikon D7100 DSLR camera (ISO 1000-5000, exposure 1 min). All procedures were performed according to the University of Pittsburgh Institutional Animal Care Committee.

4.2.6 Ultrasound Guided Thyroid Microinjection

8-week-old FVB female mice were obtained from Charles River Laboratories. Mice were anesthetized using isoflurane/oxygen, hair was removed from the throat region, and mice were placed on a warming stage. Using the Vevo 770 system (VisualSonics, probe 704), we identified the thyroid lobes which reside on each side of the trachea and just above the carotid arteries. High titer lentiviral particles ($>10^9$) were injected in 9 μ L volumes mixed with 1 μ L T800-F (kindly provided by Dr. Choi) using an insulin syringe (BD Biosciences, 30 G, 12.7 mm length, Cat #328431). Mice were imaged using an *In Vivo* Imaging System (IVIS Lumina, Xenogen). All procedures were performed according to the University of Pittsburgh Institutional Animal Care Committee.

4.3 RESULTS

4.3.1 bPAC-nLuc Stimulates Thyroid Cell Mitogenesis

To test bPAC-nLuc functionality in thyroid cells, we transiently transfected the construct in PCCL3. After hormone starvation, cells were stimulated with 450 nm light over the course of 24 hr in 500 ms pulses every 15 min at 4.4 μ W/mm². We found expression alone significantly increased mitogenesis even when kept in darkness (Fig. 13A), likely due to high expression in this model. To avoid overexpression from transient transfections, stable PCCL3 cell lines were tested for luminescence-stimulated activation using endurazine (Fz-4377), a Fz derivative which requires esterase hydrolysis for activity, resulting in low but stable luminescence for >6 hr (Fig.

9G). In this model the dark activity of bPAC-nLuc was not significantly different from non-expressing PCCL3 (Fig. 13B). Light activation stimulated a clear increase in mitogenesis, showing our luminescence-activated cyclase is capable of inciting physiological cAMP-dependent events.

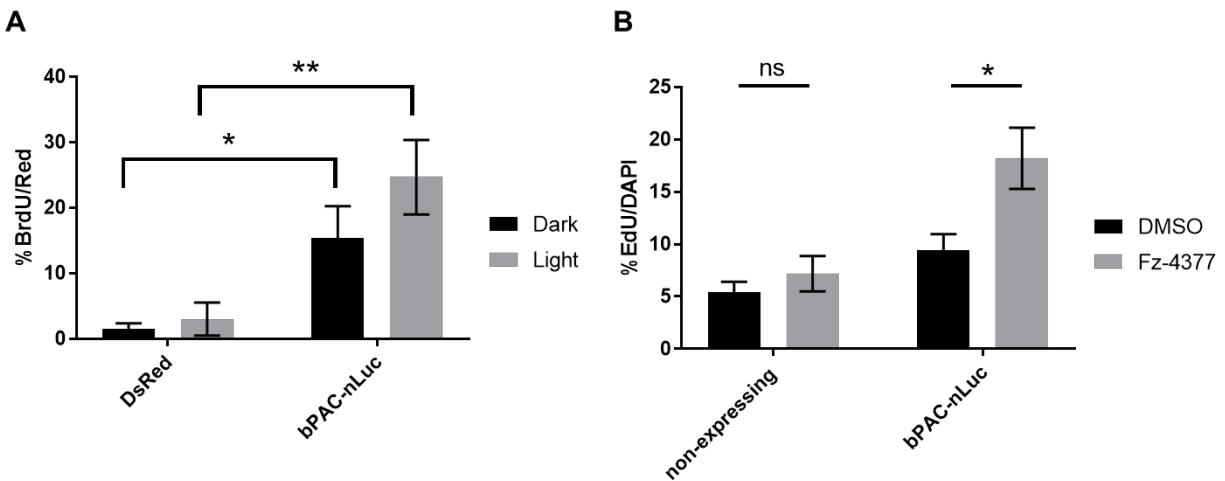


Figure 13. Light and luciferin-activated bPAC-nLuc stimulates mitogenesis.

(A) Transiently transfected PCCL3 were stimulated with 4.4 $\mu\text{W}/\text{mm}^2$ light for 500 ms/15 min/24 hr. Mitogenesis was measured as the percent of BrdU positive cells out of the total number transfected cells (red = dsRed fluorescence or anti-myc staining) (mean \pm SEM of $n=3-4$, each >500 cells). bPAC-nLuc expression alone significantly increased basal levels of mitogenesis. (B) Stable cell lines expressing bPAC-nLuc stimulated with long-lasting Fz-4377 (1:1000) exhibit higher levels of mitogenesis specifically. Mitogenesis was measured as the percent of EdU positive cells out of the total number of cells (mean \pm SEM of $n=5-6$, each $>6,000$ cells). Statistical analysis was performed using a 2-way ANOVA with Sidak's multiple comparisons test, * = $P<0.05$, ** = $P<0.005$.

Although technical difficulties in maintaining bPAC-nLuc expression in PCCL3 prevented full characterization of localized bPAC-nLuc constructs, our preliminary evidence

suggests cAMP synthesis exhibits location bias. Activation of nuclear, cytoplasmic, and myristoylated/palmitoylated bPAC-nLuc with Fz-4377 stimulated mitogenesis. Whereas farnesylated (CAAX), N-Rx, and luminal endoplasmic reticulum (ER) targeted bPAC-nLuc did not exhibit any changes in mitogenesis (Fig. 14). However, our stable cell lines lost expression throughout these experiments and this may have obfuscated these results. Only untargeted and MYR/Palm-bPAC-nLuc showed statistical significance over non-expressing cells with Fz-4377 stimulation. Further work (i.e., controlling for expression, testing changes in drug potency) is needed to draw any decisive conclusions, but these results show several of the targeted bPAC-nLuc constructs can stimulate cAMP-dependent functions.

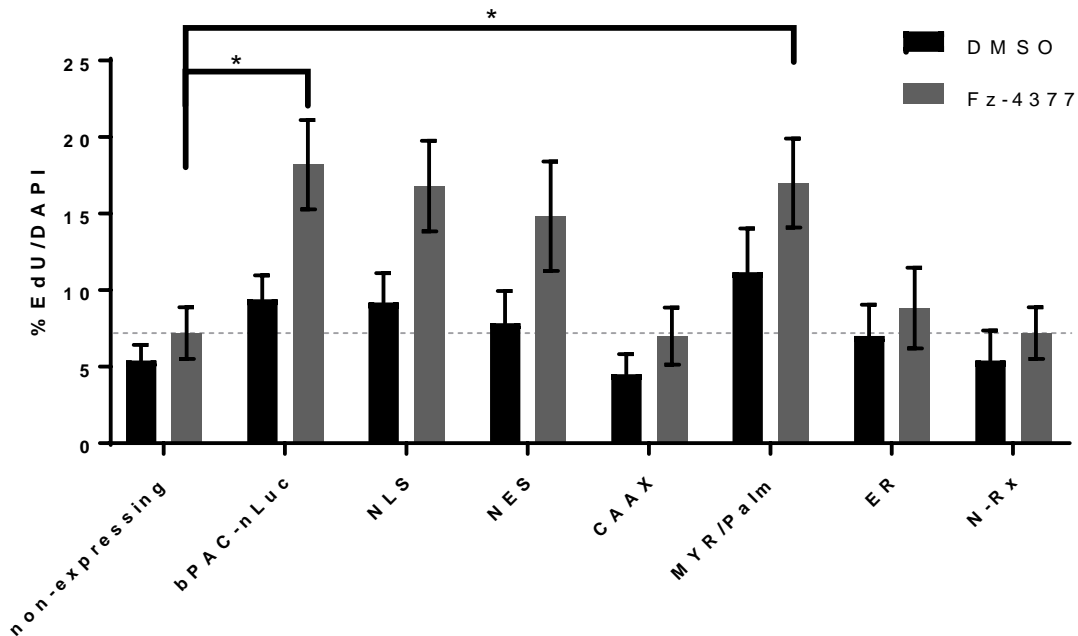


Figure 14. Localized bPAC-nLuc constructs stimulate proliferation.

Stable PCCL3 cell lines expressing targeted bPAC-nLuc constructs were treated with long-lasting Fz-4377. Several groups exhibited increased mitogenesis however further testing is needed to confirm differences between compartmentalized signaling. Compared to non-expressing PCCL3 (dotted line shown to facilitate comparison), cell lines expressing bPAC-nLuc (unmodified) and MYR/Palm-bPAC-nLuc exhibit increased mitogenesis in the presence of Fz-4377 (mean \pm SEM of $n=3-4$, 2-way ANOVA with Sidak's multiple comparison test, * = $P<0.05$).

4.3.2 *In Vitro* Sustained and Transient cAMP Signaling in HEK293

To test the temporal spectrum of bPAC-nLuc activity using light or chemical stimulation, we examined sustained and transient cAMP production in HEK193 cells. The dual regulation of bPAC-nLuc can be applied to studies on persistent cAMP signaling from endosomes since it can mimic both phases of cAMP signaling. Transiently transfected HEK293 expressing bPAC-nLuc exhibit the same luminescent characteristics described in the previous chapter. h-CTZ and Fz stimulation emits blue luminescence with a maximum at 455 nm in a dose-dependent manner

(Fig. 15A-D). High expression makes luminescence visible to the naked eye and can be imaged using long exposures times (Fig. 15E).

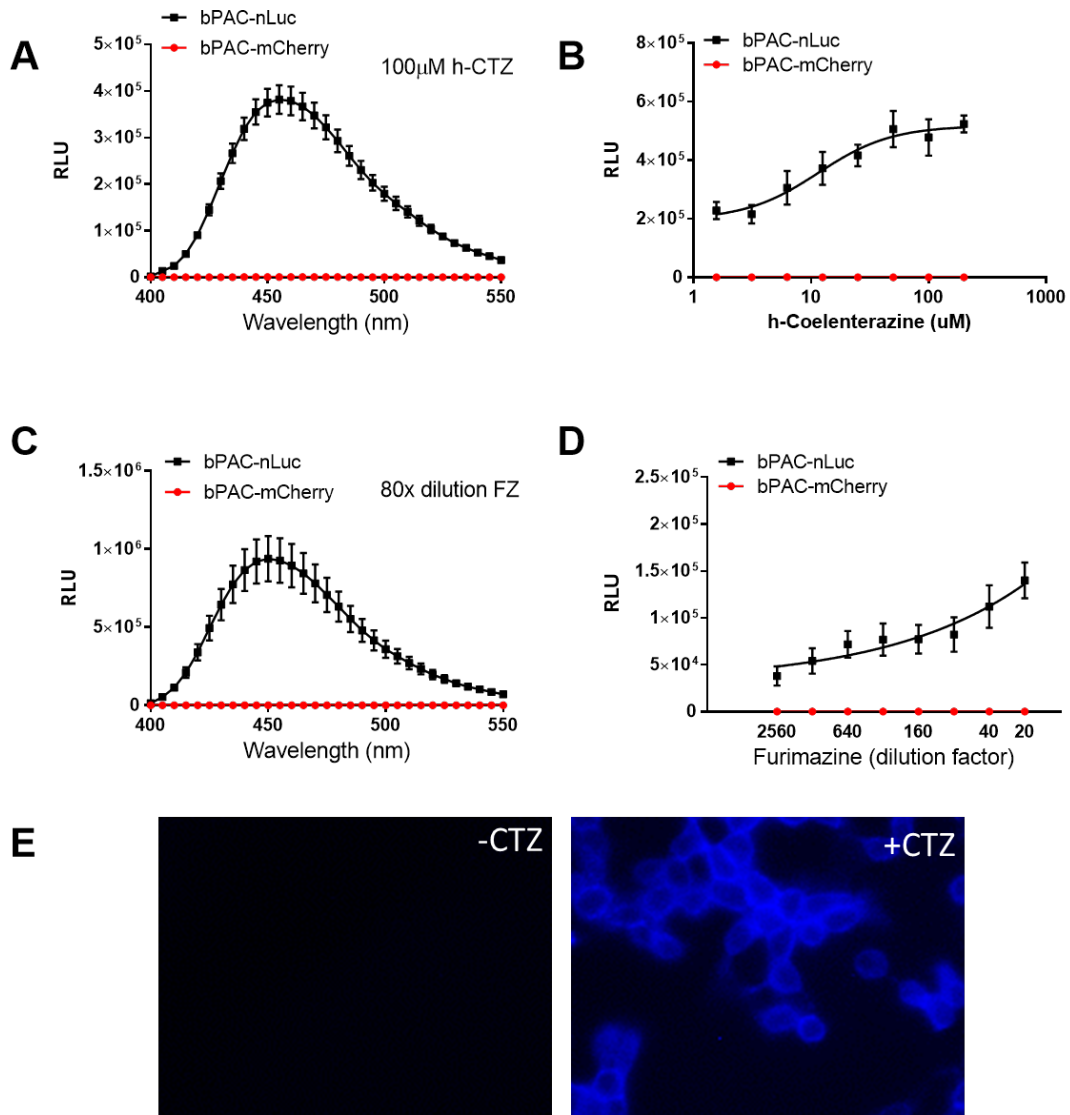


Figure 15. Luciferin-induced luminescence in HEK293.

(A-B) Transiently transfected HEK293 expressing bPAC-nLuc were treated with h-CTZ. Cells luminesce at a maximum of 455 nm and respond in a dose dependent manner. (C-D) Fz treatment causes similar trends in luminescence. (E) Long exposure images were taken before and after 100 μ M h-CTZ stimulation.

Using HEK293 cells, we transiently expressed the high-affinity cAMP FRET-based sensor, YFP-EPAC-Q270E-mScarletI (H208) (Fig. 16A). Cells expressing MYR/Palm-bPAC-nLuc generated transient spikes of cAMP accumulation in response to pulses of blue light between 1 and 100 sec at $4.4 \mu\text{W}/\text{mm}^2$ (Fig. 16B). Stimulation with furimazine induced a significantly longer signal, lasting well-beyond 30 min (Fig. 16C). Together, these two methods of stimulation can potentially tease out the individual effects of the transient, sustained, and oscillating temporal patterns of cAMP signaling.

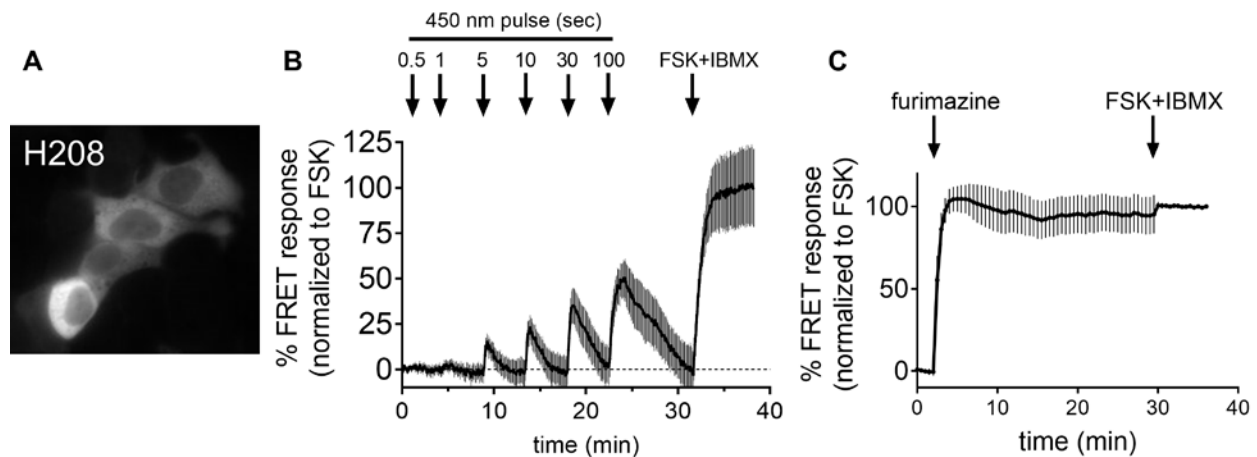


Figure 16. Light and chemical activation mimic cAMP production phases in PTH receptor signaling.

(A) Epifluorescence images of HEK293 cells expressing the cAMP sensor H208. (B) Accumulation of cytosolic cAMP in HEK293 cells expressing MYR/Palm-bPAC-nLuc with pulses of $4.4 \mu\text{W}/\text{mm}^2$ light (mean \pm SD of $n=8$ cells). (C) Stimulation with 1:1000 Fz promotes sustained cAMP production well over 30 min (mean \pm SD of $n=4$ cells).

4.3.3 *In Vivo* Application in Mouse Melanoma Metastasis Model

To test potential applications for bPAC-nLuc activity *in vivo*, we used the mouse melanoma metastasis model. bPAC-nLuc or GFP control lentiviruses were used to infect and create stable cell lines from B16-F10. We found with each subsequent passage bPAC-nLuc expression was reduced, suggesting either reduced proliferative rates, low cell viability, or silencing of the CMV promoter. To ensure the highest number of cells expressing the construct, B16-F10 were used the first passage after antibiotic selection. Additionally, the same cells which were prepared for animal injections were tested for expression and activity. GFP stable B16-F10 cell lines exhibit fluorescence in all cells compared to non-infected wild type (WT) cells (Fig. 17A). Expression of bPAC-nLuc was tested via luminescence, which we found to be very high compared to later passages of the cell line (Fig. 17B). Furthermore, Fz specifically stimulated cAMP production in the bPAC-nLuc expressing cells alone (Fig. 17C) demonstrating the cells used for the following experiment exhibited high levels of expression and activity.

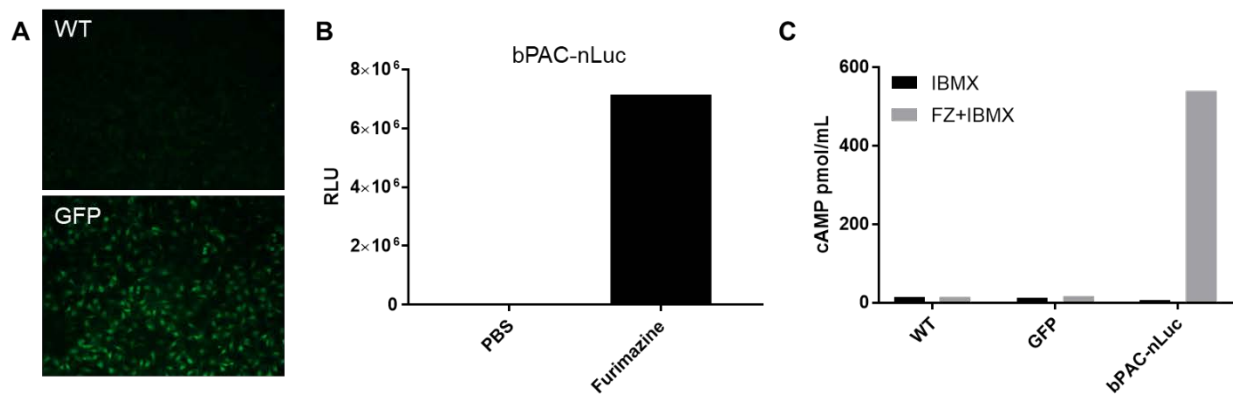


Figure 17. B16-F10 stable cells used for *in vivo* study express GFP and bPAC-nLuc.

cAMP activity and expression were tested in cells prepared for mouse injections. (A) GFP stable B16-F10 cells exhibit fluorescence compared to WT cells. (B) bPAC-nLuc expression was confirmed via luminescence where 1:200 Fz stimulated a >900,000-fold change in luminescence. (C) B16-F10 stable cells were treated with 100 μ L IBMX \pm 1:100 Fz for 10 min and measured using an ELISA assay. Fz stimulated a >80-fold change in cAMP concentration specifically in bPAC-nLuc expressing cells.

Stable B16-F10 cells were injected into syngenic C57/BL6 mice (Day 0) and treated daily with 100 μ L of a 1:40 dilution of furimazine i.v. for Days 1-18. Mice were sacrificed on Day 19 and their lungs were harvested. Typically, B16-F10 cells have been reported to form black colonies in the lung due to their high melanin production. We found WT (not shown), GFP, and bPAC-nLuc cell lines formed white and black colonies. There were no significant differences between the number of white and black colonies in any individual group, hence the total number of foci should also reflect any biological differences between treatments. We found GFP expressing cells formed many foci regardless of treatment with PBS or Fz. Expression of bPAC-nLuc alone significantly reduced metastatic foci formation. Fz treatment did not further change this effect (Fig. 18). We suspect incidental light exposure before or during injections may explain why PBS treated mice still had a large effect on metastasis.

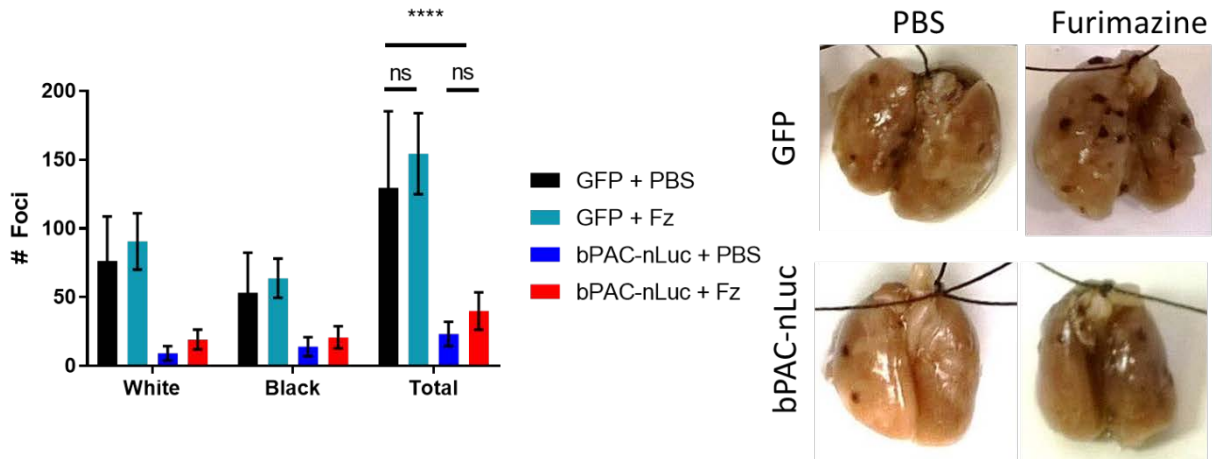


Figure 18. bPAC-nLuc use in the mouse melanoma metastasis model.

C57/BL6 mice were injected with B16-F10 cells stably expression GFP or bPAC-nLuc. Mice were treated with PBS or 1:40 Fz (100 μ L) daily. One day 19, mice were sacrificed and lungs were harvested to count the number of lung foci. White and black tumors show no statistical difference in individual groups. The total number of colonies was significantly reduced in bPAC-nLuc injected mice regardless of drug treatment (mean \pm SD of n=5, 2-way ANOVA with Tukey's multiple comparison test).

In tandem, we injected cells i.d. in the lower abdomen. There were no significant differences in tumor volume between groups when resected on Day 19. Tumors formed in all groups; however, only one formed in the bPAC-nLuc + Fz group (Fig. 19A). The large variation in these groups may be due to the difficulty of performing these injections in low/red lighting conditions. We were also concerned about whether bPAC-nLuc expression was still present by the end of these tests since cell lines successively lost expression over time. By directly injecting furimazine into an i.d. tumor, we found luminescence could still be detected (Fig. 19B). This suggests the selective pressures *in vitro* differ from *in vivo* pressures and that bPAC-nLuc was still present at Day 19.

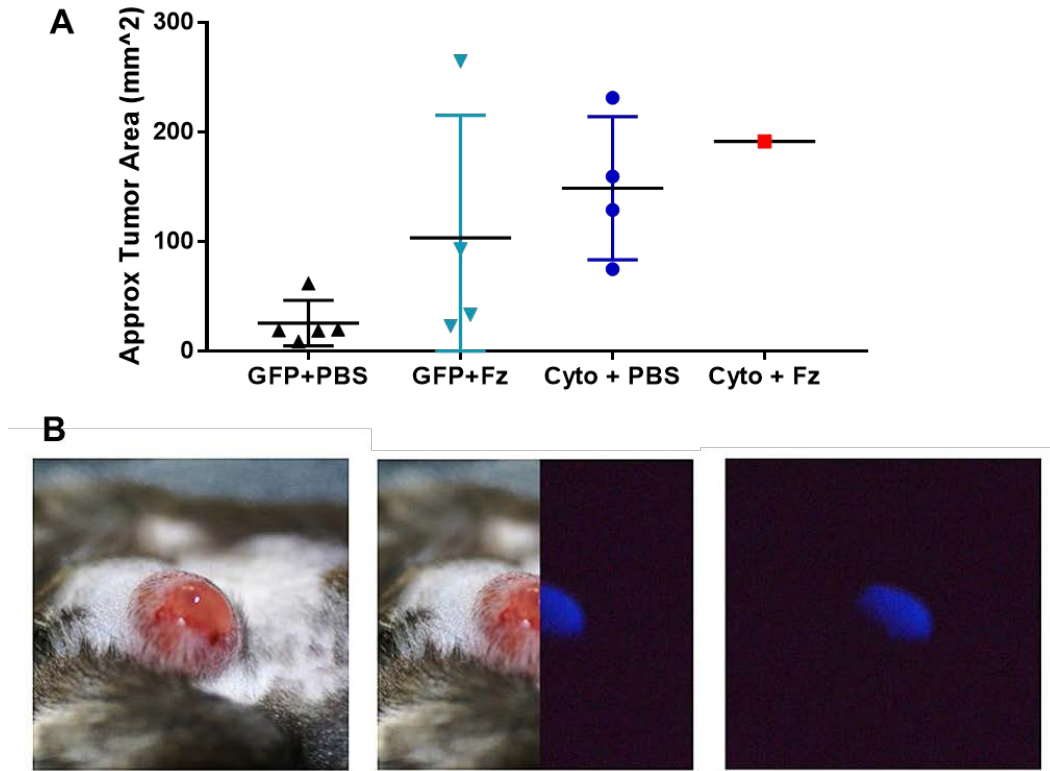


Figure 19. Intradermal tumor formation of bPAC-nLuc expressing B16-F10.

C57/BL6 mice injected i.d. with GFP and bPAC-nLuc stable B16-F10 cells were treated with PBS or 1:40 Fz (100 μ L) daily. On Day 19, tumors were resected and measured. **(A)** Tumor volumes did not significantly differ between groups, however only one bPAC-nLuc + Fz mouse formed a tumor (mean \pm SD of n=5, One-way ANOVA with Tukey's multiple comparison test). **(B)** An i.d. tumor formed from bPAC-nLuc expressing B16-F10 was injected with Fz. A long-exposure image of the tumor shows luminescence restricted to the area of liquid.

4.3.4 Ultrasound Guided Lentiviral Injection in Thyroid Lobes

To examine bPAC-nLuc function *in vivo* we sought to inject lentiviral particles into the thyroid directly. Unlike our previous experiments which injected cells expressing the construct, this approach avoids potential light activation during injections. It also allows studies to occur in normal cells in their native environment and has a shorter experimental timeline than creating

transgenic mice. Using high resolution ultrasound imaging system, we identified FVB mouse thyroid glands (Fig. 20A-B). To optimize the lentiviral injection conditions, we co-injected a high titer GFP lentivirus with T800-F, a near-infrared halogenated fluorophore which is specifically absorbed into thyroid and parathyroid glands (263,264) (Fig. 20C-E). 30 min after injection, T800-F accumulation in the thyroid is visible (Fig. 20F). 72 hr post injection, the mouse thyroid still retains the fluorophore even after dissection, showing high specificity (Fig. 20G-H). GFP expression was not detectable at this timepoint using IVIS imaging. Thyroid glands were removed and processed for imaging; however, no GFP was detected at this time.

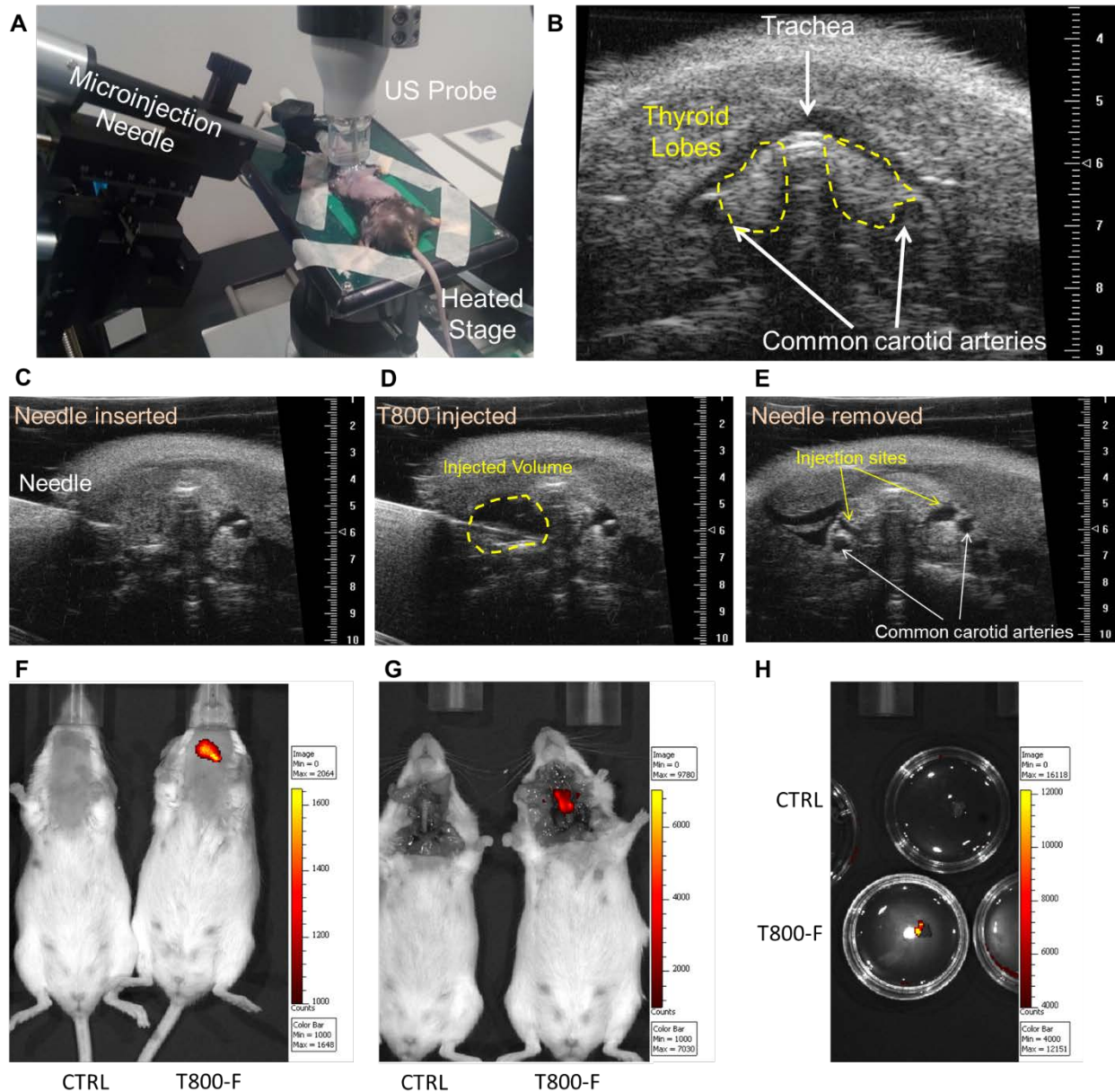


Figure 20. Ultrasound guided thyroid lobe injection.

(A) Anesthetized mice are held on a warming platform with an ultrasound (US) probe positioned at the throat. A microinjection needle is inserted at a 20° angle using a micromanipulator or freehand. (B) Ultrasound images at 40MHz shows both thyroid lobes flanking the trachea. Identification is guided by the carotid arteries below the lobes. (C-E) For injection of T800-F and lentiviruses, the needle is inserted above the carotid artery, a 10 μ L volume is injecting creating a ‘hole’ in the image, and after the needle is removed the injection sites are still visible but with relatively little tissue damage. (F) T800-F/GFP lentivirus and PBS (CTRL) injected FVB mice were imaged 30min

after injection on an IVIS (710-760 nm ex / 810-875 nm em) showing thyroid localization. **(G-H)** 72 hr later, T800-F is still visible in the dissected thyroid. GFP fluorescence was not visible. Ultrasound image scale bars are in mm.

4.4 DISCUSSION

4.4.1 Luminescence-Activated Cyclase Stimulation of Thyroid Mitogenesis

Understanding the role of cAMP in thyroid disease is clinically imperative. Several key observations suggest spatial and temporal regulation is necessary for normal function and represents an unexplored therapeutic intervention. Normal TSH stimulus of the thyroid occurs in a pulsatile manner while several disease models show constitutive cAMP signaling via mutation in the TSHR pathway promotes hyperproliferation (159-163). In intact thyroid follicles, the TSHR receptor has been shown to internalize upon stimulation and promote sustained cAMP production (32). Although, TSHR endocytosis-independent sustained cAMP signaling has been reported (265). Hence, teasing out the effects of transient pulses of cAMP and sustained or chronic cAMP signaling can positively impact clinical understanding. Furthermore, recently it has been shown that transmembrane ACs can indirectly activate sAC, creating a second mechanism for sustained cAMP signaling (47). These studies found corticotropin-releasing hormone receptor 1-stimulated cAMP requires sAC activity for full endocytic-dependent cAMP production (94). The role of transmembrane and soluble ACs in disease initiation and progression is poorly understood, illustrating or lack of understanding spatial cues. Our lab has recently found sAC is expressed in PCCL3 cells in nuclear, cytosolic, and submembrane compartments. Furthermore, we have found inhibition using the KH7 inhibitor blocks TSH-

mediated mitogenesis (data not shown). To our knowledge, this is the first evidence of sAC function in TSH signaling. We plan to use our targeted bPAC-nLuc constructs in the future to determine the role of sAC and explore whether signaling is compartmentalized.

Here we present a construct capable of testing both spatial and temporal regulation of cAMP signaling. In PCCL3 thyroid epithelial cells, we found bPAC-nLuc expression in stable cell lines induced mitogenesis when stimulated with Fz-4377 (endurazine). Fz-4377 yields very low levels of luminescence, however it has a very long and stable signal. Interestingly, overexpression of bPAC-nLuc by transient transfection lead to high levels of basal mitogenesis, but we still found and increase upon stimulus. These data suggest the expression and activation of bPAC-nLuc must be carefully tuned to each system. Furthermore, dose-responses are necessary for comparing between different constructs. Approaches for lowering expression and activation are discussed in the previous chapter.

Further experimentation is required to confirm our findings regarding the effect of local cAMP production on mitogenesis. To ensure proper comparison between compartments, differences in expression and activity can significantly impact interpretations of the data. Yet, it is interesting that stimulation of bPAC-nLuc in the cytosol and nucleus triggered thyroid mitogenesis. While this may seem contradictory to the known membrane production of cAMP and our hypothesis of compartmentalization, it potentially highlights the role of sAC in thyroid cell proliferation. Alternatively, this may indicate the location of cAMP production is less important compared to other factors such as timing or concentration. Expression of bPAC-nLuc throughout these cell lines was significantly different, hence different maximal cAMP concentrations are likely. The highest expressing lines were ER, unmodified bPAC-nLuc, NES, and NLS, followed by CAAX, MYR, and N-Rx as determined by luminescence. Interestingly, no

significant increase was found from ER, CAAX, and N-Rx targeted constructs. We anticipated cAMP production in the endoplasmic reticulum lumen would not trigger mitogenesis since cAMP is membrane-impermeable (266,267). In this model, N-Rx-bPAC-nLuc did not trigger mitogenesis even though N-Rx-bPAC-mCherry shows a trend towards increased mitogenesis. Our hypothesis of a Radixin-associated cAMP compartment may be incorrect, but this could also be attributed to differences in expression or activity of the construct. These results must further be explored to verify the findings shown here. Since expression in these cell lines steadily decreased over time, we were not able to characterize full dose responses of light or furimazine to control for differences in expression and activity. For future studies, combining this approach with methods like flow cytometry would be a simple way to ensure even levels of expression are compared.

4.4.2 *In Vitro* Sustained and Temporal Signaling of bPAC-nLuc

The two modes of bPAC-nLuc activation can be manipulated to evoke multiple kinetic signatures for cAMP accumulation. Pulses of light can promote cAMP synthesis for seconds to minutes and luciferin stimulation can potentially produce cAMP for hours. Using different luciferin derivatives can create a broad range of activation. For example, h-CTZ luminescence lasts ~1 hr while the newly developed furimazine derivative provides luminescence for >6 hours. In HEK293, PTH-stimulated cAMP production triggers an immediate increase in cAMP production followed by sustained cAMP. We found this could be mimicked using bPAC-nLuc by stimulating with blue pulses to immediately induce high levels of cAMP or with furimazine to stimulate a longer, steady levels of cAMP accumulation. This approach could be useful for dissecting the functional effects of transient and sustained cAMP signaling using a single

construct. Previous approaches include inhibition of endocytosis or using biased agonists, such as PTHrP, which only stimulates transient cAMP signaling and does not induce receptor internalization (33). However, not all GPCR models have established agonists which can exploit that approach. Additionally, studies examining the effects of endosomal bPAC activation use a maximum stimulation period of 5 min to stimulate high levels of cAMP (36). Compared to hormone-stimulated sustained cAMP signals which can last >1 hr, using targeted bPAC alone mainly compares spatial regulation rather than temporal regulation. Using bPAC alone also means researchers are limited by the lighting equipment available. Hence, the maximum duration of exposure is determined by how much the lighting system can tolerate, especially when using high-powered LEDs where overheating can be a problem. Luminescence-based stimulation of bPAC circumvents these issues and stimulates a cAMP signature which more closely resembles physiologic sustained cAMP signaling.

4.4.3 *In Vivo* Applications of bPAC-nLuc

Luminescence activation of bPAC has several advantageous properties. In addition to the convenience of using chemical reagents and specificity of activation, bPAC-nLuc can be used *in vivo* to study internal organs that would be difficult to reach with light. As a proof-of-concept, we initially used the melanoma mouse metastasis model. In this study, we administered ~5 µg of furimazine daily for almost 3 weeks and did not note any changes in health. No long-term treatment regimens were reported prior to these experiments and our approach currently remains longest regimen reported. After these experiments were conducted, a group studying furimazine toxicity reported daily intraperitoneal administration of 20-60 µg for 1 week caused hydropic dystrophy of hepatocytes (20 µg having minimal damage); however, dividing the dose into 3

daily injections of 7 μg caused almost no liver damage (268). Thus, we believe our treatment regimen was within reason for minimizing toxicity.

bPAC-nLuc expression in B16-F10 significantly reduced colony formation compared to GFP expressing controls. Since this also occurred in the absence of drug, we hypothesize this may be due to: 1) incidental light exposure during mouse injections, 2) incidental light exposure during routine cell culture, or 3) expression may be toxic to cells. Our *in vitro* cAMP ELISA assays suggest our cell culture conditions have minimal effects on cAMP induction and proliferation. Since previous studies found cAMP stimulation promoted cell differentiation, either high expression of bPAC-nLuc or light exposure may have triggered this response. We noticed over time bPAC-nLuc expressing B16-F10 cells in culture exhibit a more spread morphology and appear darker in color. This increased cell spreading and potentially melanin production are markers of differentiation in melanoma cells. More differentiated cells are reported to reduce lung colonization. Hence, the effect of furimazine in our study may be masked due to bPAC-nLuc saturating cAMP effects during or prior to injections.

Although we minimized exposure to blue light as best as possible, most animal facilities are not designed to work under said conditions and the injections present a high technical hurdle. A better alternative for *in vivo* work may be direct injections of lentiviral constructs. This approach prevents incidental light exposure during injections and has no complications of altering cell characteristics prior to treatment. We are currently working to use this technique in our lab. We anticipate expression of bPAC-nLuc in thyroid glands will stimulate follicular cell mitogenesis upon treatment with furimazine. If successful, this work will serve as a proof-of-concept for *in vivo* application of bPAC-nLuc.

4.4.4 Closing Remarks

Over the last two decades, particularly from the beginning of this dissertation work, the number of articles studying cAMP compartmentalization has exploded. Since the year 2000, over 35 unique cAMP biosensors have been developed (196). With these tools, long standing observations now have mechanistic explanations (14,134). Interestingly, the concept of restricted diffusion was used in many models even though more direct measurements of cAMP diffusion were only published two years ago (121,122). The cAMP compartmentalization model has gained broad acceptance throughout the field. Now, concepts from the cAMP compartmentalization model are being investigated through a clinical lens (150-152). Here we began to examine the role of cAMP compartmentalization in thyroid cell mitogenesis and develop a novel tool to dissect spatial and temporal regulation of cAMP synthesis. The luminescence-activated cyclase has the ability to examine the distinct roles of transmembrane and soluble cyclases, compare transient and sustained signaling paradigms, and potentially address these concepts *in vivo*. At this time, no other constructs available are as adaptable for different experimental needs, as refined in temporal control, or specific enough to minimize off-target activation of endogenous cyclases. As the cAMP compartmentalization field expands, being able to artificially regulate localized cAMP signaling will be crucial to test whether this model will stand the test of time or if new components need to be considered.

APPENDIX A

ARDUINO-CONTROLLED LED SYSTEM

The LED illumination system was created keeping user-friendliness and adaptability in mind, such that it can be duplicated with basic working knowledge of electronics and programming. A photo of the complete system from the outside shows the stage that holds the LED below samples, and the Arduino-based control system (Fig. 8A). The stage can be placed inside a standard-sized incubator. A wiring diagram of the components clarifies how the system was designed (Fig. 21) from a parts list of components shown in Table 1 (screws, wires, etc. not listed). Overall cost was US \$200-250 in 2015. Other parts can be substituted for the LED, microcontroller, touch screen, etc.; but any changes to hardware may require further changes to both hardware and software to ensure proper working of the system. For example, the Redboard (Sparkfun) was chosen as the Arduino-compatible microcontroller board. The system has not been tested with other microcontroller boards, but there is no foreseeable reason that other Arduino-compatible boards would not work with possible changes to the board connections.

LED Control Electronics

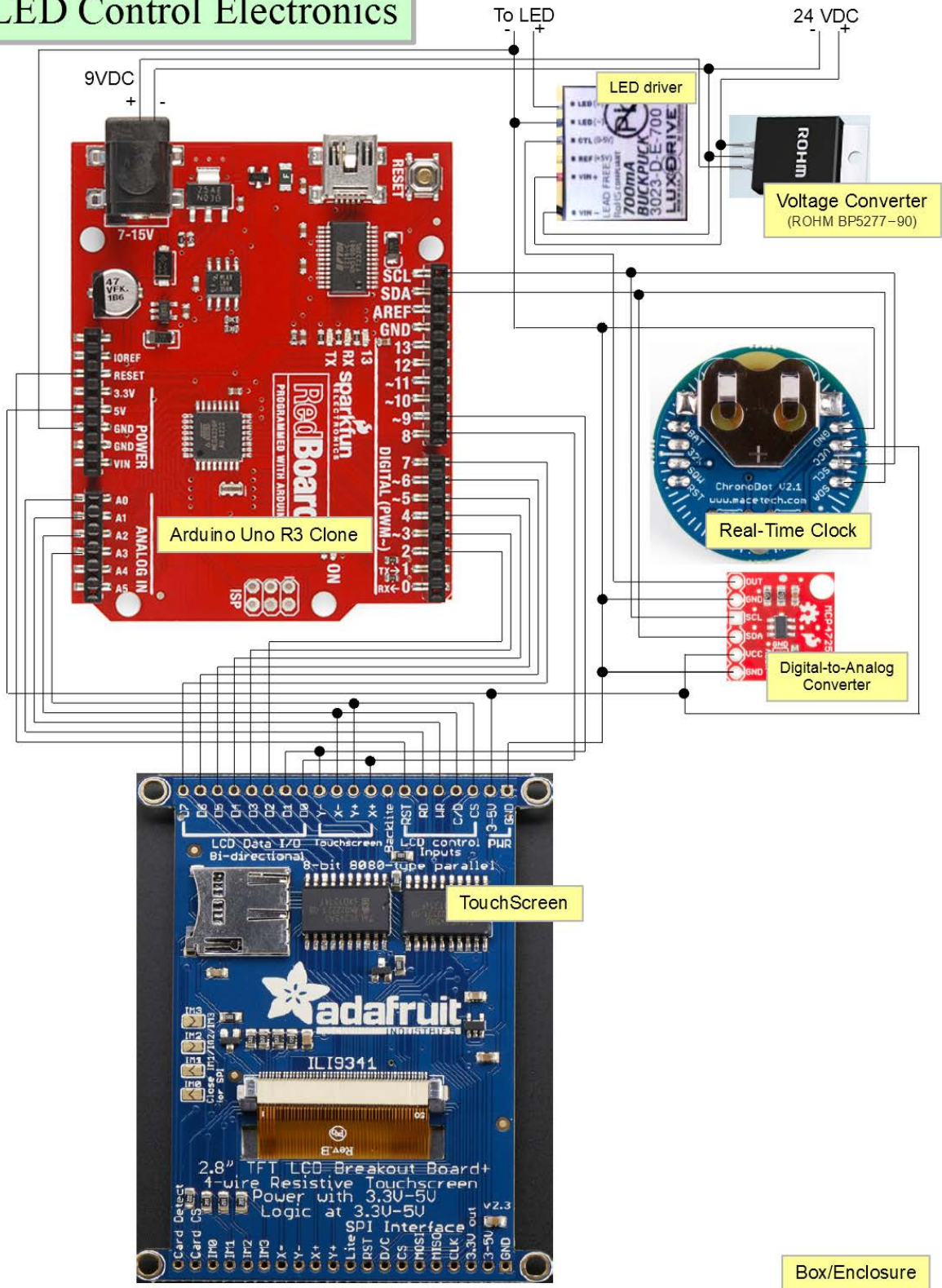


Figure 21. Diagram of Arduino-controlled LED system.

Subsystem	Description	Comment	Qty	Vendor	part#
LED	Cree XTE - Indus Star 3-Up Royal-Blue High Power LED	Notice the 3 LEDs are pre-soldered in series	1	ledsupply.com	CREEXTE- ROY-3
LED	Wired BuckPuck - 700mA Constant Current LED Driver with Dimming	Outputs voltage to LED; takes input from DAC controlled by Arduino	1	ledsupply.com	03023-D-E- 700
LED	10509 Carclo Lens - 3-Up Frosted Wide Spot LED Optic	Attaches directly to LED to widen beam just enough for the SDS plate	1	ledsupply.com	10509
LED	Arctic Silver - Premium Silver Thermal Epoxy Heat Sink –	For gluing the LED to the heat sink	1	ledsupply.com	ASTA-7G
LED	Wakefield 882- 100AB BOX ABS	LED is mounted to this	1	digikey.com	345-1105- ND
Box & Power	4.72X4.72X2.32" BLACK	the "project box"	1	digikey.com	HM123-ND
Box & Power	PWR SUPPLY EXT 24V 1.67A 40W; XP Power VEH40US24	Main power supply for everything; LED driver requires higher voltage than other electronics	1	digikey.com	1470-2320- ND
Box & Power	Power CABLE IEC TO NEMA 6'; Tripp Lite P006-006	typical power cable; used with main power supply	1	digikey.com	TL415-ND
Box & Power	CON PWR JCK 2.5 X 6.4MM HIGH CUR; CUI PJ-038BH	connector on the box for the power supply	1	digikey.com	CP-038BH- ND
Box & Power	IC BUCK DC-DC CONVERTER MOD 9.0V SIP3; Rohm BP5277-90	Steps voltage down for digital electronics; inside the box, the first thing power feeds into USB	1	digikey.com	BP5277-90- ND
Box & Power	CBL USB B RCPT- MNI B PLUG 100MM; Tensility 10- 00660	adaptor/connector for the box, so the connector on the board doesn't wear out	1	digikey.com	839-1116- ND
Digital Electronics	RedBoard - Programmed with Arduino Retail	The brain- microcontroller; similar to Arduino Uno, but useful differences	1	sparkfun.com	RTL-11804
Digital Electronics	Arduino Stackable Header Kit - R3		2	sparkfun.com	PRT-11417
Digital	Header - 2x3 (Male,		1	sparkfun.com	PRT-12807

Electronics	0.1")				
Digital Electronics	Arduino ProtoShield - Bare PCB		1	sparkfun.com	DEV-11665
Digital Electronics	Breakout Board for MCP4725 I2C DAC		1	sparkfun.com	BOB-08736
Digital Electronics	2.8" TFT LCD with Touchscreen Breakout Board w/MicroSD Socket	Touchscreen utilized only for display, but could potentially be used for parameter input instead of USB connection	1	adafruit.com	1770
Digital Electronics	ChronoDot - Ultra-precise Real Time Clock - v2.1 Premium	CR1632 battery not included! (but necessary to set clock)	1	adafruit.com	255
Digital Electronics	Female/Male 'Extension' Jumper Wires - 40 x 3" (75mm)		1	adafruit.com	826
Digital Electronics	Half-size breadboard	Used as a wire junction point between electronic components	1	adafruit.com	64
Digital Electronics	Breadboarding wire bundle		1	adafruit.com	153

Table 1. List of Arduino-controlled LED system components.

A photo of the interior of the control box is shown (Fig. 22). Except for the LED and the power supply, all the electronics components were mounted inside the plastic control box, with holes made for the power supply connector, a USB port (used as a USB adapter for the Redboard USB port), and wires to the LED. The LED wires out of the box were short and had standard RCA-style plugs on them for quick connections.

The Arduino program (“sketch”) used to control the LED contained detailed notes explaining the organization and function of the code. The segment of the code is shown here in text form (Fig. 23). Currently, the code is set for manual input of parameters through the Arduino program rather than the touchscreen included. This requires manual connection of the control

box to the USB port of a computer running the Arduino IDE software, and uploading the updated code to the Redboard. The timing paradigm for the experiment typically consists of one or more periodic flashes of the LED, with the train of flashes starting at a user-determined time, anywhere from the present (i.e., shortly after loading the new code, up to a few days from the present). Each flash is of the same duration, falling in the range of 10 msec to several minutes. Controlling LED illumination intensity requires verification and calibration for each individual system to ensure the emitted light intensity of the LED is accurate and consistent as in Fig. 8B. We recommend for consistent intensity during experiments that only the main power supply be connected, rather than connecting both the power supply and computer USB which can also serve as a power source.

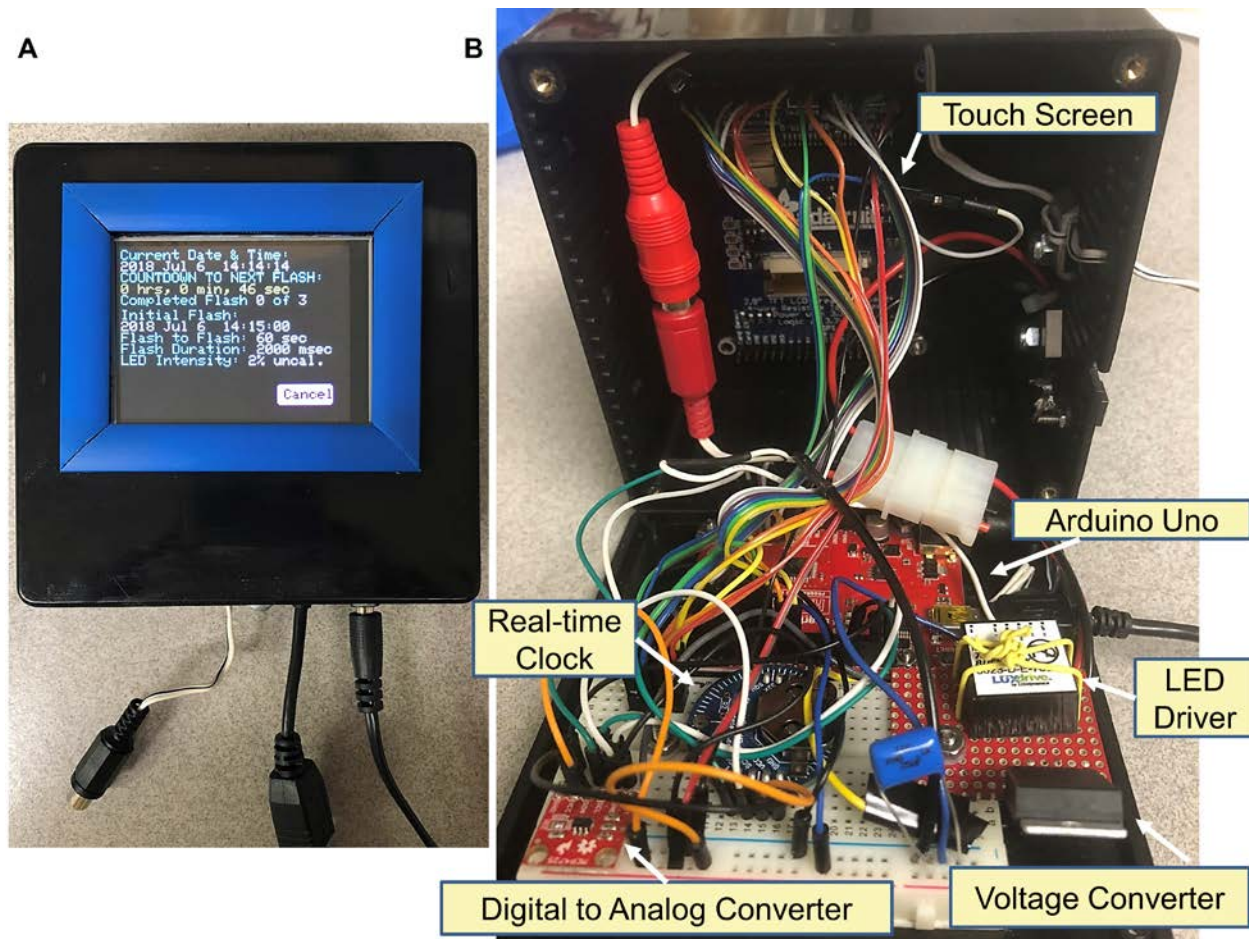


Figure 22. Arduino-controlled system.

(A) An image of the outer box shows a LED touchscreen with the current date and time, countdown to the initial flash, frequency, duration, and intensity of the flash. (B) An image of the inner circuitry and overall design.

```

// This program was working with:
//   - Arduino 1.6.8
//   - Sparkfun Redboard RTL-11804
//   - ChronoDot v2.1
//   - SparkFun MCP4725 I2C DAC Breakout (pn# B0B-08736)
//   - adafruit 1770 - 2.8" TFT LCD with Touchscreen

// Authors: Jeff M Reece, with Nyla Naim making modifications as needed.

// SUMMARY:      This program provides timing and intensity
// control of one or more high-power LEDs, as would be used for a
// typical optogenetics experiment in a research lab.
// The current version of this program is based on an Arduino Uno-compatible
// board, the Sparkfun Redboard. Using a different type of Arduino board
// would require changing some of the pin connections, at the least.

// LED INTENSITY CONTROL: ...is managed through a 12-bit DAC which is slave
// to the Arduino, using the I2C protocol. The output of the DAC is
// typically 0-5V, connected to a BuckPuck LED driver.
// This code uses a MCP4725 breakout DAC with a library taken from Adafruit.

// The user chooses a value between 0-100%, but this value is not calibrated!
// Explanation: The conversion from input voltage to output current in the BuckPuck
// happens in "reverse", meaning that 0V to the BuckPuck will produce maximum
// current, and 5V produces zero current. It is also not a simple straight
// line relationship, so that there is essentially no decrease in output
// current until the input reaches ~1.5V (which for the time being is called
// "100%"); and zero output current is essentially
// reached when the input hits ~4.3V (which we call "0%").
// Both ends are asymptotic with a pretty much inverse linear range from ~2-4V.

// In addition, the output of the LED is not linear with respect to the
// current that the BuckPuck provides it, with a minimum threshold current
// for stable output-- although it is a positive, monotonic relationship
// from that minimum to its maximum, rated value.

// Thus, although the output of the DAC
// would have 4095 addressable intensity levels, in reality not all those
// values are usable; and some calibration is necessary by the user.
// The calibration currently implemented is very, very roughly linear.

// TIMING:      The timing paradigm for the experiment typically consists
// of one or more periodic flashes of

```



```

// the LED, with the train of flashes starting at a user-determined time,
// from the present up to a few days from the present.
// Each flash is of the same duration, conceivably falling in the range
// of 10msec to several minutes.
// The flashes in the train can be no faster than 1 second apart
// as the program is currently written, but this is an arbitrarily
// established safe limit given the hardware; undoubtedly the code could be
// be changed and the true lower limit of the hardware be determined.
// The upper limit is currently 32000 secs.
// The duration of the flash is defined in msec, but the real practical limit
// will most likely be determined by the hardware outside of the Arduino.

// The timing of the events is controlled in two ways, running in parallel.
// First, the generic Arduino Time library, with resolution in seconds,
// is used for convenience to handle the setting of the
// clock and interfacing with the user.
// For this clock functionality, it is desirable to have a true RTC
// (real time clock) with battery backup,
// so a ChronoDot v2.1 was chosen for this function, but any RTC compatible
// with DS1307 should work with this code. The ChronoDot is on the same I2C
// interface with the DAC, but having a different address.

// However, for speed and resolution,
// calls to the internal Arduino millis function are used for the actual
// control of the LED timing. The program performs bookkeeping to make sure that
// the time held by the clock is aligned with the millis function.

// PARAMETER ENTRY: Until the touch screen on the TFT is used for input,
// it will be necessary to use Arduino through the USB port to manually
// enter timing parameters, directly in the next section of the program below,

// INCLUDE SECTION for libraries that are used ....
// Some of these libraries must be manually downloaded, separate from the
// Arduino software...

#include <Wire.h>
#include <DS1307RTC.h>
#include <Time.h>
#include <Adafruit_MCP4725.h>
#include <Adafruit_GFX.h>
#include <Adafruit_TFTLCD.h>
#include <pin_magic.h>
#include <registers.h>
#include <TouchScreen.h>

// ***** MANUAL ENTRY OF PARAMETERS, UNTIL GUI IS DEVELOPED *****
// ***** only change the numbers after the equals signs *****

```



```

// ***** and only in the following section *****

// If you want to set experiment parameters manually rather than through the
// touchscreen, then set this value to true, otherwise false
boolean SetParamsManually = true; // NOT YET IMPLEMENTED, SO KEEP "true"
// if true, then doublecheck the following values before you upload
// to the Arduino

// ***** SET DAY AND TIME OF FIRST LED EXPOSURE *****
// ***** ONLY CHANGE THE NUMBERS before the semi colon ';' *****
// ***** CHECK VALUES! no error checking in program!! *****
// ***** TRIM OFF ALL LEADING ZEROS !!! *****
const int InitExp_Year = 2016; // range is 2014-up
const int InitExp_Month = 8; // range is 1-12
const int InitExp_Day = 20; // range is 1-31, depending on month
const int InitExp_Hour = 17; // range is 0-23 (military style)
const int InitExp_Minute = 0; // range is 0-59
const int InitExp_Second = 0; // range is 0-59

// Set how many exposures (number of cycles) :
unsigned long TotalFlashes = 96;
// What is the time interval from exposure to exposure (in seconds)? :
unsigned long FlashTimeInterval = 900; // in sec
// Set duration of exposure in each cycle (in millisec) :
unsigned long FlashDurationEachCycle = 500; // in msec
// Set the intensity of LED during each exposure (in %, 1-100) :
unsigned long FlashIntensity = 20; // in %, but this is uncalibrated, VERY rough

```

Figure 23. Portion of Arduino code for LED illumination.

Arduino coding for the initial pulse time and date, number of pulses, duration of pulse, interval, and intensity.

APPENDIX B

SUPPORTING FIGURES

We prepared N-Rx targeted cAMP FRET sensors from the mTurquoise Δ -Epac(CD, Δ DEP)-cp¹⁷³Venus-Venus (H74, (198)). This FRET sensor has improved signal-noise-ratio and photostability compared to the Epac1-cAMPs sensor. We subcloned the N-Rx motif using HindIII cut sites upstream of the sensor. We found this modification effectively localized to the submembrane similar to N-Rx-Ep1 (Fig. 4). Using HEK293 lysates expressing H74 and N-Rx-74, we titrated in varying amounts of cAMP (Promega) and measured the FRET ratio using a SpectraMax Paradigm plate reader. We found no significant differences in cAMP binding affinity in terms of EC₅₀ and Hill coefficient (Fig. 24). We conducted similar studies comparing Ep1 and N-Rx-Ep1, however its stability in solution and lower fluorescence limited our ability to measure changes in FRET ratio. Still, these data suggest N-Rx is useful for targeting different FRET sensors and does not impact cAMP activity.

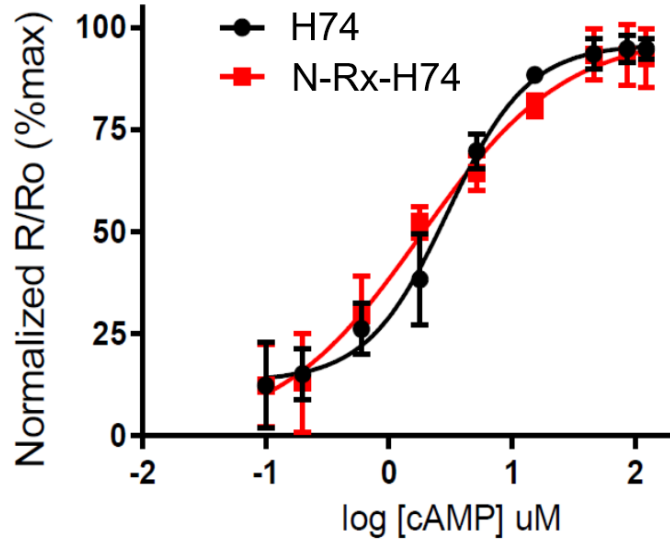
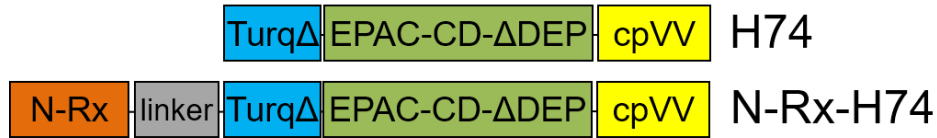


Figure 24. N-Rx targeting motif does not alter cAMP affinity.

The H74 cAMP FRET sensor consists of a mTurquoise fluorophore lacking the last 11 C-terminal amino acids (TurqΔ) and a tandem of circularly permuted (cp173) Venus with Venus fluorophore (cpVV). The Epac1-derived cAMP binding motif is catalytically dead (T781A and F782A) and lacks the N-terminal DEP domain. The addition of the N-Rx targeting motif did not significantly alter cAMP binding affinity (EC_{50} or Hill coefficient) as shown by the normalized FRET ratio (mean \pm SD of $n=2$).

To reduce basal activity of bPAC-mCherry, we knew reducing the level of expression reduced basal proliferation by reducing the amount of DNA used in transfections (data not shown). Hence, we made an inducible system using the degradation domain (DD)/shield-1 system (Clontech). By subcloning the DD sequence upstream of bPAC-mCherry, basal expression was undetectable by western blot analysis. The addition of 1 μ M shield-1 peptide which binds and stabilizes the DD prevented proteasomal degradation and lead to increased expression within 2 hr (Fig. 25).

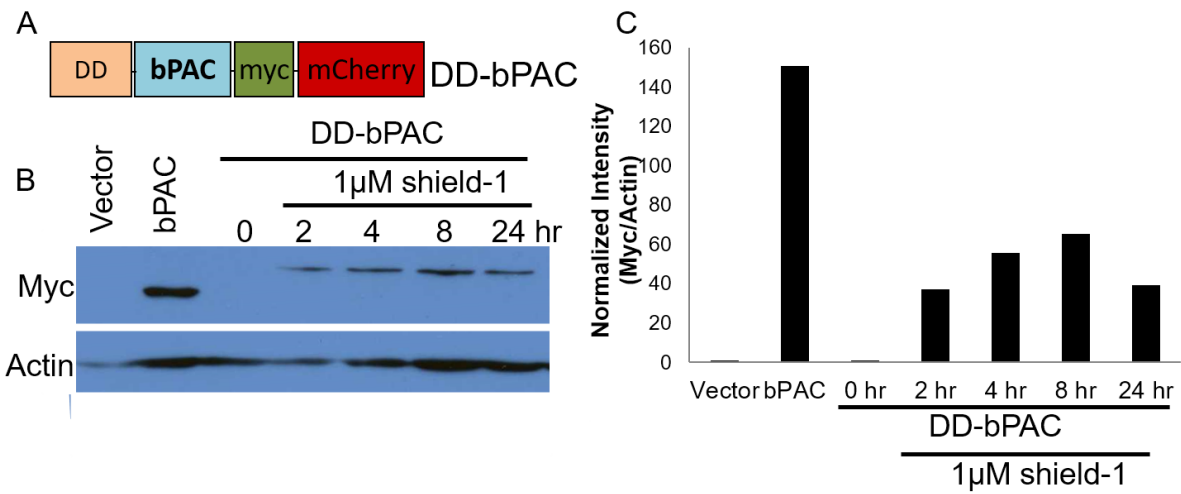


Figure 25. bPAC expression can be controlled using the DD/shield-1 inducible system.

(A) The bPAC construct was modified to include a destabilization domain (DD) which targets a tagged protein for proteasomal degradation. (B-C) The addition of shield-1 ligand stabilizes the protein which prevents its degradation and increases protein expression levels. A representative western blot analysis indicates increased bPAC expression after 2 hr of incubation with shield-1.

BIBLIOGRAPHY

1. Sutherland, E. W., and Rall, T. W. (1958) Fractionation and characterization of a cyclic adenine ribonucleotide formed by tissue particles. *J Biol Chem* **232**, 1077-1091
2. Walsh, D. A., Perkins, J. P., and Krebs, E. G. (1968) An adenosine 3',5'-monophosphate-dependant protein kinase from rabbit skeletal muscle. *J Biol Chem* **243**, 3763-3765
3. Smith, F. D., and Scott, J. D. (2006) Anchored cAMP signaling: onward and upward - a short history of compartmentalized cAMP signal transduction. *European journal of cell biology* **85**, 585-592
4. Benovic, J. L., Strasser, R. H., Caron, M. G., and Lefkowitz, R. J. (1986) Beta-adrenergic receptor kinase: identification of a novel protein kinase that phosphorylates the agonist-occupied form of the receptor. *Proc Natl Acad Sci U S A* **83**, 2797-2801
5. Lohse, M. J., Benovic, J. L., Caron, M. G., and Lefkowitz, R. J. (1990) Multiple pathways of rapid beta 2-adrenergic receptor desensitization. Delineation with specific inhibitors. *J Biol Chem* **265**, 3202-3211
6. Rodbell, M., Birnbaumer, L., and Pohl, S. L. (1971) Characteristics of glucagon action on the hepatic adenylate cyclase system. *The Biochemical journal* **125**, 58p-59p
7. Rodbell, M., Birnbaumer, L., Pohl, S. L., and Sundby, F. (1971) The reaction of glucagon with its receptor: evidence for discrete regions of activity and binding in the glucagon molecule. *Proc Natl Acad Sci U S A* **68**, 909-913
8. Ross, E. M., and Gilman, A. G. (1977) Resolution of some components of adenylate cyclase necessary for catalytic activity. *J Biol Chem* **252**, 6966-6969
9. Ross, E. M., and Gilman, A. G. (1977) Reconstitution of catecholamine-sensitive adenylate cyclase activity: interactions of solubilized components with receptor-replete membranes. *Proc Natl Acad Sci U S A* **74**, 3715-3719

10. Otten, J., Johnson, G. S., and Pastan, I. (1971) Cyclic AMP levels in fibroblasts: relationship to growth rate and contact inhibition of growth. *Biochem Biophys Res Commun* **44**, 1192-1198
11. Abell, C. W., and Monahan, T. M. (1973) The role of adenosine 3',5'-cyclic monophosphate in the regulation of mammalian cell division. *The Journal of cell biology* **59**, 549-558
12. Macmanus, J. P., and Whitfield, J. F. (1970) Inhibition by thyrocalcitonin of the mitogenic actions of parathyroid hormone and cyclic adenosine=3',5'-monophosphate on rat thymocytes. *Endocrinology* **86**, 934-939
13. Hirschhorn, R., Grossman, J., and Weissmann, G. (1970) Effect of cyclic 3',5'-adenosine monophosphate and theophylline on lymphocyte transformation. *Proceedings of the Society for Experimental Biology and Medicine. Society for Experimental Biology and Medicine (New York, N.Y.)* **133**, 1361-1365
14. Buxton, I. L., and Brunton, L. L. (1983) Compartments of cyclic AMP and protein kinase in mammalian cardiomyocytes. *The Journal of biological chemistry* **258**, 10233-10239
15. Hayes, J. S., Brunton, L. L., Brown, J. H., Reese, J. B., and Mayer, S. E. (1979) Hormonally specific expression of cardiac protein kinase activity. *Proceedings of the National Academy of Sciences of the United States of America* **76**, 1570-1574
16. Vegesna, R. V., and Diamond, J. (1986) Effects of prostaglandin E1, isoproterenol and forskolin on cyclic AMP levels and tension in rabbit aortic rings. *Life sciences* **39**, 303-311
17. Borland, G., Smith, B. O., and Yarwood, S. J. (2009) EPAC proteins transduce diverse cellular actions of cAMP. *Br J Pharmacol* **158**, 70-86
18. Corcoran, M. L., and Stetler-Stevenson, W. G. (1995) Tissue inhibitor of metalloproteinase-2 stimulates fibroblast proliferation via a cAMP-dependent mechanism. *J Biol Chem* **270**, 13453-13459
19. Hecquet, C., Lefevre, G., Valtink, M., Engelmann, K., and Mascarelli, F. (2002) cAMP inhibits the proliferation of retinal pigmented epithelial cells through the inhibition of ERK1/2 in a PKA-independent manner. *Oncogene* **21**, 6101-6112
20. Indolfi, C., Di Lorenzo, E., Rapacciuolo, A., Stingone, A. M., Stabile, E., Leccia, A., Torella, D., Caputo, R., Ciardiello, F., Tortora, G., and Chiariello, M. (2000) 8-chloro-cAMP inhibits smooth muscle cell proliferation in vitro and neointima formation induced by balloon injury in vivo. *Journal of the American College of Cardiology* **36**, 288-293

21. Yamaguchi, T., Pelling, J. C., Ramaswamy, N. T., Eppler, J. W., Wallace, D. P., Nagao, S., Rome, L. A., Sullivan, L. P., and Grantham, J. J. (2000) cAMP stimulates the in vitro proliferation of renal cyst epithelial cells by activating the extracellular signal-regulated kinase pathway. *Kidney international* **57**, 1460-1471
22. Rocha, A. S., Paternot, S., Coulonval, K., Dumont, J. E., Soares, P., and Roger, P. P. (2008) Cyclic AMP inhibits the proliferation of thyroid carcinoma cell lines through regulation of CDK4 phosphorylation. *Mol Biol Cell* **19**, 4814-4825
23. Hilger, D., Masureel, M., and Kobilka, B. K. (2018) Structure and dynamics of GPCR signaling complexes. *Nature Structural & Molecular Biology* **25**, 4-12
24. Luttrell, L. M. (2008) Reviews in Molecular Biology and Biotechnology: Transmembrane Signaling by G Protein-Coupled Receptors. *Molecular Biotechnology* **39**, 239-264
25. Walther, C., and Ferguson, S. S. G. (2015) Minireview: Role of Intracellular Scaffolding Proteins in the Regulation of Endocrine G Protein-Coupled Receptor Signaling. *Molecular Endocrinology* **29**, 814-830
26. Brand, C. S., Sadana, R., Malik, S., Smrcka, A. V., and Dessauer, C. W. (2015) Adenylyl Cyclase 5 Regulation by G $\beta\gamma$ Involves Isoform-Specific Use of Multiple Interaction Sites. *Molecular Pharmacology* **88**, 758-767
27. van Koppen, C. J., and Jakobs, K. H. (2004) Arrestin-independent internalization of G protein-coupled receptors. *Mol Pharmacol* **66**, 365-367
28. Krupinski, J., Coussen, F., Bakalyar, H. A., Tang, W. J., Feinstein, P. G., Orth, K., Slaughter, C., Reed, R. R., and Gilman, A. G. (1989) Adenylyl cyclase amino acid sequence: possible channel- or transporter-like structure. *Science* **244**, 1558-1564
29. Tang, W. J., and Hurley, J. H. (1998) Catalytic mechanism and regulation of mammalian adenylyl cyclases. *Mol Pharmacol* **54**, 231-240
30. Tesmer, J. J., Sunahara, R. K., Gilman, A. G., and Sprang, S. R. (1997) Crystal structure of the catalytic domains of adenylyl cyclase in a complex with G α .GTP γ S. *Science* **278**, 1907-1916
31. Sadana, R., and Dessauer, C. W. (2009) Physiological Roles for G-Protein Regulated Adenylyl Cyclase Isoforms: Insights from Knockout and Overexpression Studies. *Neuro-Signals* **17**, 5-22

32. Calebiro, D., Nikolaev, V. O., Gagliani, M. C., de Filippis, T., Dees, C., Tacchetti, C., Persani, L., and Lohse, M. J. (2009) Persistent cAMP-signals triggered by internalized G-protein-coupled receptors. *PLoS Biol* **7**, e1000172
33. Ferrandon, S., Feinstein, T. N., Castro, M., Wang, B., Bouley, R., Potts, J. T., Gardella, T. J., and Vilardaga, J.-P. (2009) Sustained cyclic AMP production by parathyroid hormone receptor endocytosis. *Nature chemical biology* **5**, 734-742
34. Kotowski, S. J., Hopf, F. W., Seif, T., Bonci, A., and von Zastrow, M. (2011) Endocytosis promotes rapid dopaminergic signaling. *Neuron* **71**, 278-290
35. Irannejad, R., Tomshine, J. C., Tomshine, J. R., Chevalier, M., Mahoney, J. P., Steyaert, J., Rasmussen, S. G., Sunahara, R. K., El-Samad, H., Huang, B., and von Zastrow, M. (2013) Conformational biosensors reveal GPCR signalling from endosomes. *Nature* **495**, 534-538
36. Tsvetanova, N. G., and von Zastrow, M. (2014) Spatial encoding of cyclic AMP signaling specificity by GPCR endocytosis. *Nature chemical biology* **10**, 1061-1065
37. Buck, J., Sinclair, M. L., Schapal, L., Cann, M. J., and Levin, L. R. (1999) Cytosolic adenylyl cyclase defines a unique signaling molecule in mammals. *Proc Natl Acad Sci U S A* **96**, 79-84
38. Litvin, T. N., Kamenetsky, M., Zarifyan, A., Buck, J., and Levin, L. R. (2003) Kinetic properties of "soluble" adenylyl cyclase. Synergism between calcium and bicarbonate. *J Biol Chem* **278**, 15922-15926
39. Zippin, J. H., Chen, Y., Nahirney, P., Kamenetsky, M., Wuttke, M. S., Fischman, D. A., Levin, L. R., and Buck, J. (2003) Compartmentalization of bicarbonate-sensitive adenylyl cyclase in distinct signaling microdomains. *Faseb j* **17**, 82-84
40. Zippin, J. H., Farrell, J., Huron, D., Kamenetsky, M., Hess, K. C., Fischman, D. A., Levin, L. R., and Buck, J. (2004) Bicarbonate-responsive "soluble" adenylyl cyclase defines a nuclear cAMP microdomain. *J Cell Biol* **164**, 527-534
41. Zippin, J. H., Chadwick, P. A., Levin, L. R., Buck, J., and Magro, C. M. (2010) Soluble adenylyl cyclase defines a nuclear cAMP microdomain in keratinocyte hyperproliferative skin diseases. *The Journal of investigative dermatology* **130**, 1279-1287
42. Feng, Q., Zhang, Y., Li, Y., Liu, Z., Zuo, J., and Fang, F. (2006) Two domains are critical for the nuclear localization of soluble adenylyl cyclase. *Biochimie* **88**, 319-328

43. Acin-Perez, R., Salazar, E., Brosel, S., Yang, H., Schon, E. A., and Manfredi, G. (2009) Modulation of mitochondrial protein phosphorylation by soluble adenylyl cyclase ameliorates cytochrome oxidase defects. *EMBO molecular medicine* **1**, 392-406
44. Acin-Perez, R., Salazar, E., Kamenetsky, M., Buck, J., Levin, L. R., and Manfredi, G. (2009) Cyclic AMP produced inside mitochondria regulates oxidative phosphorylation. *Cell metabolism* **9**, 265-276
45. Kumar, S., Kostin, S., Flacke, J. P., Reusch, H. P., and Ladilov, Y. (2009) Soluble adenylyl cyclase controls mitochondria-dependent apoptosis in coronary endothelial cells. *J Biol Chem* **284**, 14760-14768
46. Watson, R. L., Buck, J., Levin, L. R., Winger, R. C., Wang, J., Arase, H., and Muller, W. A. (2015) Endothelial CD99 signals through soluble adenylyl cyclase and PKA to regulate leukocyte transendothelial migration. *The Journal of experimental medicine* **212**, 1021-1041
47. Ivonnet, P., Salathe, M., and Conner, G. E. (2015) Hydrogen peroxide stimulation of CFTR reveals an Epac-mediated, soluble AC-dependent cAMP amplification pathway common to GPCR signalling. *Br J Pharmacol* **172**, 173-184
48. Wang, H., Pineda, V. V., Chan, G. C., Wong, S. T., Muglia, L. J., and Storm, D. R. (2003) Type 8 adenylyl cyclase is targeted to excitatory synapses and required for mossy fiber long-term potentiation. *The Journal of neuroscience : the official journal of the Society for Neuroscience* **23**, 9710-9718
49. Storm, D. R., Hansel, C., Hacker, B., Parent, A., and Linden, D. J. (1998) Impaired cerebellar long-term potentiation in type I adenylyl cyclase mutant mice. *Neuron* **20**, 1199-1210
50. Wu, Z. L., Thomas, S. A., Villacres, E. C., Xia, Z., Simmons, M. L., Chavkin, C., Palmiter, R. D., and Storm, D. R. (1995) Altered behavior and long-term potentiation in type I adenylyl cyclase mutant mice. *Proc Natl Acad Sci U S A* **92**, 220-224
51. Villacres, E. C., Wu, Z., Hua, W., Nielsen, M. D., Watters, J. J., Yan, C., Beavo, J., and Storm, D. R. (1995) Developmentally expressed Ca(2+)-sensitive adenylyl cyclase activity is disrupted in the brains of type I adenylyl cyclase mutant mice. *J Biol Chem* **270**, 14352-14357
52. Ishikawa, Y., Iwatsubo, K., Tsunematsu, T., and Okumura, S. (2005) Genetic manipulation and functional analysis of cAMP signalling in cardiac muscle: implications for a new target of pharmacotherapy. *Biochemical Society transactions* **33**, 1337-1340

53. Wong, S. T., Trinh, K., Hacker, B., Chan, G. C., Lowe, G., Gaggar, A., Xia, Z., Gold, G. H., and Storm, D. R. (2000) Disruption of the type III adenylyl cyclase gene leads to peripheral and behavioral anosmia in transgenic mice. *Neuron* **27**, 487-497
54. Kamenetsky, M., Middelhaufe, S., Bank, E. M., Levin, L. R., Buck, J., and Steegborn, C. (2006) Molecular Details of cAMP Generation in Mammalian Cells: A Tale of Two Systems. *Journal of molecular biology* **362**, 623-639
55. Head, B. P., Patel, H. H., Roth, D. M., Murray, F., Swaney, J. S., Niesman, I. R., Farquhar, M. G., and Insel, P. A. (2006) Microtubules and actin microfilaments regulate lipid raft/caveolae localization of adenylyl cyclase signaling components. *J Biol Chem* **281**, 26391-26399
56. Pagano, M., Clynes, M. A., Masada, N., Ciruela, A., Ayling, L.-J., Wachten, S., and Cooper, D. M. F. (2009) Insights into the residence in lipid rafts of adenylyl cyclase AC8 and its regulation by capacitative calcium entry. *American Journal of Physiology - Cell Physiology* **296**, C607-C619
57. Ostrom, R. S., Gregorian, C., Drenan, R. M., Xiang, Y., Regan, J. W., and Insel, P. A. (2001) Receptor number and caveolar co-localization determine receptor coupling efficiency to adenylyl cyclase. *J Biol Chem* **276**, 42063-42069
58. Rybin, V. O., Xu, X., Lisanti, M. P., and Steinberg, S. F. (2000) Differential targeting of beta -adrenergic receptor subtypes and adenylyl cyclase to cardiomyocyte caveolae. A mechanism to functionally regulate the cAMP signaling pathway. *J Biol Chem* **275**, 41447-41457
59. Weigand, I., Ronchi, C. L., Rizk-Rabin, M., Dalmazi, G. D., Wild, V., Bathon, K., Rubin, B., Calebiro, D., Beuschlein, F., Bertherat, J., Fassnacht, M., and Sbiera, S. (2017) Differential expression of the protein kinase A subunits in normal adrenal glands and adrenocortical adenomas. *Scientific Reports* **7**, 49
60. Skalhegg, B. S., and Tasken, K. (2000) Specificity in the cAMP/PKA signaling pathway. Differential expression, regulation, and subcellular localization of subunits of PKA. *Frontiers in bioscience : a journal and virtual library* **5**, D678-693
61. Isobe, K., Jung, H. J., Yang, C. R., Claxton, J., Sandoval, P., Burg, M. B., Raghuram, V., and Knepper, M. A. (2017) Systems-level identification of PKA-dependent signaling in epithelial cells. *Proc Natl Acad Sci U S A* **114**, E8875-e8884
62. Corbin, J. D., Sugden, P. H., Lincoln, T. M., and Keely, S. L. (1977) Compartmentalization of adenosine 3':5'-monophosphate and adenosine 3':5'-monophosphate-dependent protein kinase in heart tissue. *J Biol Chem* **252**, 3854-3861

63. Brunton, L. L., Hayes, J. S., and Mayer, S. E. (1979) Hormonally specific phosphorylation of cardiac troponin I and activation of glycogen phosphorylase. *Nature* **280**, 78-80
64. Brunton, L. L., Hayes, J. S., and Mayer, S. E. (1981) Functional compartmentation of cyclic AMP and protein kinase in heart. *Advances in cyclic nucleotide research* **14**, 391-397
65. Hayes, J. S., Brunton, L. L., and Mayer, S. E. (1980) Selective activation of particulate cAMP-dependent protein kinase by isoproterenol and prostaglandin E1. *J Biol Chem* **255**, 5113-5119
66. Carr, D. W., Stofko-Hahn, R. E., Fraser, I. D., Bishop, S. M., Acott, T. S., Brennan, R. G., and Scott, J. D. (1991) Interaction of the regulatory subunit (RII) of cAMP-dependent protein kinase with RII-anchoring proteins occurs through an amphipathic helix binding motif. *J Biol Chem* **266**, 14188-14192
67. Carr, D. W., Hausken, Z. E., Fraser, I. D., Stofko-Hahn, R. E., and Scott, J. D. (1992) Association of the type II cAMP-dependent protein kinase with a human thyroid RII-anchoring protein. Cloning and characterization of the RII-binding domain. *J Biol Chem* **267**, 13376-13382
68. Dodge-Kafka, K. L., Soughayer, J., Pare, G. C., Carlisle Michel, J. J., Langeberg, L. K., Kapiloff, M. S., and Scott, J. D. (2005) The protein kinase A anchoring protein mAKAP co-ordinates two integrated cAMP effector pathways. *Nature* **437**, 574-578
69. Viswanatha, R., Wayt, J., Ohouo, P. Y., Smolka, M. B., and Bretscher, A. (2013) Interactome analysis reveals ezrin can adopt multiple conformational states. *J Biol Chem* **288**, 35437-35451
70. Luconi, M., Cantini, G., Baldi, E., and Forti, G. (2011) Role of a-kinase anchoring proteins (AKAPs) in reproduction. *Frontiers in bioscience (Landmark edition)* **16**, 1315-1330
71. Greenwald, E. C., and Saucerman, J. J. (2011) Bigger, better, faster: principles and models of AKAP signaling. *Journal of cardiovascular pharmacology* **58**, 462-469
72. Fraser, I. D., Cong, M., Kim, J., Rollins, E. N., Daaka, Y., Lefkowitz, R. J., and Scott, J. D. (2000) Assembly of an A kinase-anchoring protein-beta(2)-adrenergic receptor complex facilitates receptor phosphorylation and signaling. *Current biology : CB* **10**, 409-412

73. Cong, M., Perry, S. J., Lin, F. T., Fraser, I. D., Hu, L. A., Chen, W., Pitcher, J. A., Scott, J. D., and Lefkowitz, R. J. (2001) Regulation of membrane targeting of the G protein-coupled receptor kinase 2 by protein kinase A and its anchoring protein AKAP79. *J Biol Chem* **276**, 15192-15199
74. Bauman, A. L., Soughayer, J., Nguyen, B. T., Willoughby, D., Carnegie, G. K., Wong, W., Hoshi, N., Langeberg, L. K., Cooper, D. M., Dessauer, C. W., and Scott, J. D. (2006) Dynamic regulation of cAMP synthesis through anchored PKA-adenylyl cyclase V/VI complexes. *Mol Cell* **23**, 925-931
75. de Rooij, J., Zwartkruis, F. J., Verheijen, M. H., Cool, R. H., Nijman, S. M., Wittinghofer, A., and Bos, J. L. (1998) Epac is a Rap1 guanine-nucleotide-exchange factor directly activated by cyclic AMP. *Nature* **396**, 474-477
76. Kawasaki, H., Springett, G. M., Toki, S., Canales, J. J., Harlan, P., Blumenstiel, J. P., Chen, E. J., Bany, I. A., Mochizuki, N., Ashbacher, A., Matsuda, M., Housman, D. E., and Graybiel, A. M. (1998) A Rap guanine nucleotide exchange factor enriched highly in the basal ganglia. *Proceedings of the National Academy of Sciences of the United States of America* **95**, 13278-13283
77. Li, Y., Asuri, S., Rebhun, J. F., Castro, A. F., Parnavitana, N. C., and Quilliam, L. A. (2006) The RAP1 guanine nucleotide exchange factor Epac2 couples cyclic AMP and Ras signals at the plasma membrane. *J Biol Chem* **281**, 2506-2514
78. Schmidt, M., Dekker, F. J., and Maarsingh, H. (2013) Exchange protein directly activated by cAMP (epac): a multidomain cAMP mediator in the regulation of diverse biological functions. *Pharmacol Rev* **65**, 670-709
79. Hochbaum, D., Barila, G., Ribeiro-Neto, F., and Altschuler, D. L. (2011) Radixin assembles cAMP effectors Epac and PKA into a functional cAMP compartment: role in cAMP-dependent cell proliferation. *J Biol Chem* **286**, 859-866
80. Roscioni, S. S., Elzinga, C. R., and Schmidt, M. (2008) Epac: effectors and biological functions. *Naunyn Schmiedebergs Arch Pharmacol* **377**, 345-357
81. Grandoch, M., Roscioni, S. S., and Schmidt, M. (2010) The role of Epac proteins, novel cAMP mediators, in the regulation of immune, lung and neuronal function. *British Journal of Pharmacology* **159**, 265-284
82. Consonni, S. V., Gloerich, M., Spanjaard, E., and Bos, J. L. (2012) cAMP regulates DEP domain-mediated binding of the guanine nucleotide exchange factor Epac1 to phosphatidic acid at the plasma membrane. *Proceedings of the National Academy of Sciences of the United States of America* **109**, 3814-3819

83. Gloerich, M., Ponsioen, B., Vliem, M. J., Zhang, Z., Zhao, J., Kooistra, M. R., Price, L. S., Ritsma, L., Zwartkruis, F. J., Rehmann, H., Jalink, K., and Bos, J. L. (2010) Spatial regulation of cyclic AMP-Epac1 signaling in cell adhesion by ERM proteins. *Mol Cell Biol* **30**, 5421-5431
84. Liu, C., Takahashi, M., Li, Y., Dillon, T. J., Kaech, S., and Stork, P. J. (2010) The interaction of Epac1 and Ran promotes Rap1 activation at the nuclear envelope. *Mol Cell Biol* **30**, 3956-3969
85. Banerjee, U., and Cheng, X. (2015) Exchange protein directly activated by cAMP encoded by the mammalian rapgef3 gene: Structure, function and therapeutics. *Gene* **570**, 157-167
86. Bender, A. T., and Beavo, J. A. (2006) Cyclic nucleotide phosphodiesterases: molecular regulation to clinical use. *Pharmacol Rev* **58**, 488-520
87. Conti, M., Mika, D., and Richter, W. (2014) Cyclic AMP compartments and signaling specificity: role of cyclic nucleotide phosphodiesterases. *J Gen Physiol* **143**, 29-38
88. Nikolaev, V. O., Bunemann, M., Hein, L., Hannawacker, A., and Lohse, M. J. (2004) Novel single chain cAMP sensors for receptor-induced signal propagation. *J Biol Chem* **279**, 37215-37218
89. Zaccolo, M., De Giorgi, F., Cho, C. Y., Feng, L., Knapp, T., Negulescu, P. A., Taylor, S. S., Tsien, R. Y., and Pozzan, T. (2000) A genetically encoded, fluorescent indicator for cyclic AMP in living cells. *Nat Cell Biol* **2**, 25-29
90. Cui, W., Smith, A., Darby-King, A., Harley, C. W., and McLean, J. H. (2007) A temporal-specific and transient cAMP increase characterizes odorant classical conditioning. *Learning & Memory* **14**, 126-133
91. Vedel, L., Brauner-Osborne, H., and Mathiesen, J. M. (2015) A cAMP Biosensor-Based High-Throughput Screening Assay for Identification of Gs-Coupled GPCR Ligands and Phosphodiesterase Inhibitors. *Journal of biomolecular screening* **20**, 849-857
92. Kuna, R. S., Girada, S. B., Asalla, S., Vallentyne, J., Maddika, S., Patterson, J. T., Smiley, D. L., DiMarchi, R. D., and Mitra, P. (2013) Glucagon-like peptide-1 receptor-mediated endosomal cAMP generation promotes glucose-stimulated insulin secretion in pancreatic β -cells. *American Journal of Physiology-Endocrinology and Metabolism* **305**, E161-E170
93. Merriam, L. A., Baran, C. N., Girard, B. M., Hardwick, J. C., May, V., and Parsons, R. L. (2013) Pituitary Adenylate Cyclase 1 Receptor Internalization and Endosomal Signaling

- Mediate the Pituitary Adenylate Cyclase Activating Polypeptide-Induced Increase in Guinea Pig Cardiac Neuron Excitability. *The Journal of Neuroscience* **33**, 4614-4622
94. Inda, C., Dos Santos Claro, P. A., Bonfiglio, J. J., Senin, S. A., Maccarrone, G., Turck, C. W., and Silberstein, S. (2016) Different cAMP sources are critically involved in G protein-coupled receptor CRHR1 signaling. *The Journal of cell biology* **214**, 181-195
 95. Pavlos, N. J., and Friedman, P. A. (2017) GPCR Signaling and Trafficking: The Long and Short of It. *Trends in endocrinology and metabolism: TEM* **28**, 213-226
 96. Persani, L., Lania, A., Alberti, L., Romoli, R., Mantovani, G., Filetti, S., Spada, A., and Conti, M. (2000) Induction of Specific Phosphodiesterase Isoforms by Constitutive Activation of the cAMP Pathway in Autonomous Thyroid Adenomas¹. *The Journal of Clinical Endocrinology & Metabolism* **85**, 2872-2878
 97. Weinstein, L. S., Shenker, A., Gejman, P. V., Merino, M. J., Friedman, E., and Spiegel, A. M. (1991) Activating mutations of the stimulatory G protein in the McCune-Albright syndrome. *The New England journal of medicine* **325**, 1688-1695
 98. Boot, A. M., Lumbroso, S., Verhoef-Post, M., Richter-Unruh, A., Looijenga, L. H. J., Funaro, A., Beishuizen, A., van Marle, A., Drop, S. L. S., and Themmen, A. P. N. (2011) Mutation Analysis of the LH Receptor Gene in Leydig Cell Adenoma and Hyperplasia and Functional and Biochemical Studies of Activating Mutations of the LH Receptor Gene. *The Journal of Clinical Endocrinology and Metabolism* **96**, E1197-E1205
 99. Min, K. S., Liu, X., Fabritz, J., Jaquette, J., Abell, A. N., and Ascoli, M. (1998) Mutations that induce constitutive activation and mutations that impair signal transduction modulate the basal and/or agonist-stimulated internalization of the Lutropin/Choriogonadotropin receptor. *J Biol Chem* **273**, 34911-34919
 100. Dyachok, O., Isakov, Y., Sagetorp, J., and Tengholm, A. (2006) Oscillations of cyclic AMP in hormone-stimulated insulin-secreting beta-cells. *Nature* **439**, 349-352
 101. Tian, G., Sagetorp, J., Xu, Y., Shuai, H., Degerman, E., and Tengholm, A. (2012) Role of phosphodiesterases in the shaping of sub-plasma-membrane cAMP oscillations and pulsatile insulin secretion. *J Cell Sci* **125**, 5084-5095
 102. Vitalis, E. A., Costantin, J. L., Tsai, P.-S., Sakakibara, H., Paruthiyil, S., Iiri, T., Martini, J.-F., Taga, M., Choi, A. L. H., Charles, A. C., and Weiner, R. I. (2000) Role of the cAMP signaling pathway in the regulation of gonadotropin-releasing hormone secretion in GT1 cells. *Proceedings of the National Academy of Sciences* **97**, 1861-1866

103. Nicol, X., Voyatzis, S., Muzerelle, A., Narboux-Neme, N., Sudhof, T. C., Miles, R., and Gaspar, P. (2007) cAMP oscillations and retinal activity are permissive for ephrin signaling during the establishment of the retinotopic map. *Nature neuroscience* **10**, 340-347
104. Haisenleder, D. J., Yasin, M., and Marshall, J. C. (1992) Enhanced effectiveness of pulsatile 3',5'-cyclic adenosine monophosphate in stimulating prolactin and alpha-subunit gene expression. *Endocrinology* **131**, 3027-3033
105. Brooker, G. (1973) Oscillation of Cyclic Adenosine Monophosphate Concentration during the Myocardial Contraction Cycle. *Science* **182**, 933-934
106. Lowe, G., and Gold, G. H. (1993) Nonlinear amplification by calcium-dependent chloride channels in olfactory receptor cells. *Nature* **366**, 283
107. Chen, C., Nakamura, T., and Koutalos, Y. (1999) Cyclic AMP diffusion coefficient in frog olfactory cilia. *Biophys J* **76**, 2861-2867
108. Bowen, W. J., and Martin, H. L. (1964) The diffusion of adenosine triphosphate through aqueous solutions. *Archives of Biochemistry and Biophysics* **107**, 30-36
109. Rich, T. C., Fagan, K. A., Nakata, H., Schaack, J., Cooper, D. M., and Karpen, J. W. (2000) Cyclic nucleotide-gated channels colocalize with adenylyl cyclase in regions of restricted cAMP diffusion. *J Gen Physiol* **116**, 147-161
110. Dessauer, C. W., and Gilman, A. G. (1997) The catalytic mechanism of mammalian adenylyl cyclase. Equilibrium binding and kinetic analysis of P-site inhibition. *J Biol Chem* **272**, 27787-27795
111. Rich, T. C., Fagan, K. A., Tse, T. E., Schaack, J., Cooper, D. M., and Karpen, J. W. (2001) A uniform extracellular stimulus triggers distinct cAMP signals in different compartments of a simple cell. *Proc Natl Acad Sci U S A* **98**, 13049-13054
112. Rehmann, H., Schwede, F., Doskeland, S. O., Wittinghofer, A., and Bos, J. L. (2003) Ligand-mediated activation of the cAMP-responsive guanine nucleotide exchange factor Epac. *The Journal of biological chemistry* **278**, 38548-38556
113. Feinstein, W. P., Zhu, B., Leavesley, S. J., Sayner, S. L., and Rich, T. C. (2012) Assessment of cellular mechanisms contributing to cAMP compartmentalization in pulmonary microvascular endothelial cells. *Am J Physiol Cell Physiol* **302**, C839-852

114. Lohse, C., Bock, A., Maiellaro, I., Hannawacker, A., Schad, L. R., Lohse, M. J., and Bauer, W. R. (2017) Experimental and mathematical analysis of cAMP nanodomains. *PLoS One* **12**, e0174856
115. Saucerman, J. J., Zhang, J., Martin, J. C., Peng, L. X., Stenbit, A. E., Tsien, R. Y., and McCulloch, A. D. (2006) Systems analysis of PKA-mediated phosphorylation gradients in live cardiac myocytes. *Proc Natl Acad Sci U S A* **103**, 12923-12928
116. Neves, S. R., Tsokas, P., Sarkar, A., Grace, E. A., Rangamani, P., Taubenfeld, S. M., Alberini, C. M., Schaff, J. C., Blitzer, R. D., Moraru, II, and Iyengar, R. (2008) Cell shape and negative links in regulatory motifs together control spatial information flow in signaling networks. *Cell* **133**, 666-680
117. Oliveira, R. F., Terrin, A., Di Benedetto, G., Cannon, R. C., Koh, W., Kim, M., Zaccolo, M., and Blackwell, K. T. (2010) The role of type 4 phosphodiesterases in generating microdomains of cAMP: large scale stochastic simulations. *PLoS One* **5**, e11725
118. Saucerman, J. J., Greenwald, E. C., and Polanowska-Grabowska, R. (2014) Mechanisms of cyclic AMP compartmentation revealed by computational models. *J Gen Physiol* **143**, 39-48
119. Dix, J. A., and Verkman, A. S. (2008) Crowding effects on diffusion in solutions and cells. *Annual review of biophysics* **37**, 247-263
120. Luby-Phelps, K. (2000) Cytoarchitecture and physical properties of cytoplasm: volume, viscosity, diffusion, intracellular surface area. *International review of cytology* **192**, 189-221
121. Agarwal, S. R., Clancy, C. E., and Harvey, R. D. (2016) Mechanisms Restricting Diffusion of Intracellular cAMP. *Sci Rep* **6**, 19577
122. Richards, M., Lomas, O., Jalink, K., Ford, K. L., Vaughan-Jones, R. D., Lefkimmatis, K., and Swietach, P. (2016) Intracellular tortuosity underlies slow cAMP diffusion in adult ventricular myocytes. *Cardiovascular research* **110**, 395-407
123. Zaccolo, M., Di Benedetto, G., Lissandron, V., Mancuso, L., Terrin, A., and Zamparo, I. (2006) Restricted diffusion of a freely diffusible second messenger: mechanisms underlying compartmentalized cAMP signalling. *Biochemical Society transactions* **34**, 495-497
124. McCormick, K., and Baillie, G. S. (2014) Compartmentalisation of second messenger signalling pathways. *Current opinion in genetics & development* **27**, 20-25

125. Monterisi, S., Favia, M., Guerra, L., Cardone, R. A., Marzulli, D., Reshkin, S. J., Casavola, V., and Zacco, M. (2012) CFTR regulation in human airway epithelial cells requires integrity of the actin cytoskeleton and compartmentalized cAMP and PKA activity. *Journal of cell science* **125**, 1106-1117
126. Iancu, R. V., Jones, S. W., and Harvey, R. D. (2007) Compartmentation of cAMP signaling in cardiac myocytes: a computational study. *Biophys J* **92**, 3317-3331
127. Surdo, N. C., Berrera, M., Koschinski, A., Brescia, M., Machado, M. R., Carr, C., Wright, P., Gorelik, J., Morotti, S., Grandi, E., Bers, D. M., Pantano, S., and Zacco, M. (2017) FRET biosensor uncovers cAMP nano-domains at beta-adrenergic targets that dictate precise tuning of cardiac contractility. *Nat Commun* **8**, 15031
128. Cheepala, S., Hulot, J.-S., Morgan, J. A., Sassi, Y., Zhang, W., Naren, A. P., and Schuetz, J. D. (2013) Cyclic Nucleotide Compartmentalization: Contributions of Phosphodiesterases and ATP-Binding Cassette Transporters. *Annual review of pharmacology and toxicology* **53**, 231-253
129. Sassi, Y., Abi-Gerges, A., Fauconnier, J., Mougenot, N., Reiken, S., Haghghi, K., Kranias, E. G., Marks, A. R., Lacampagne, A., Engelhardt, S., Hatem, S. N., Lompre, A.-M., and Hulot, J.-S. (2012) Regulation of cAMP homeostasis by the efflux protein MRP4 in cardiac myocytes. *The FASEB Journal* **26**, 1009-1017
130. Bacskai, B. J., Hochner, B., Mahaut-Smith, M., Adams, S. R., Kaang, B. K., Kandel, E. R., and Tsien, R. Y. (1993) Spatially resolved dynamics of cAMP and protein kinase A subunits in *Aplysia* sensory neurons. *Science* **260**, 222-226
131. Calebiro, D., and Maiellaro, I. (2014) cAMP signaling microdomains and their observation by optical methods. *Frontiers in cellular neuroscience* **8**, 350
132. Zacco, M., and Pozzan, T. (2002) Discrete microdomains with high concentration of cAMP in stimulated rat neonatal cardiac myocytes. *Science* **295**, 1711-1715
133. Schleicher, K., and Zacco, M. (2018) Using cAMP Sensors to Study Cardiac Nanodomains. *Journal of Cardiovascular Development and Disease* **5**, 17
134. Di Benedetto, G., Zoccarato, A., Lissandron, V., Terrin, A., Li, X., Houslay, M. D., Baillie, G. S., and Zacco, M. (2008) Protein kinase A type I and type II define distinct intracellular signaling compartments. *Circ Res* **103**, 836-844
135. Sample, V., DiPilato, L. M., Yang, J. H., Ni, Q., Saucerman, J. J., and Zhang, J. (2012) Regulation of nuclear PKA revealed by spatiotemporal manipulation of cyclic AMP. *Nature chemical biology* **8**, 375-382

136. DiPilato, L. M., Cheng, X., and Zhang, J. (2004) Fluorescent indicators of cAMP and Epac activation reveal differential dynamics of cAMP signaling within discrete subcellular compartments. *Proc Natl Acad Sci U S A* **101**, 16513-16518
137. Terrin, A., Di Benedetto, G., Pertegato, V., Cheung, Y. F., Baillie, G., Lynch, M. J., Elvassore, N., Prinz, A., Herberg, F. W., Houslay, M. D., and Zaccolo, M. (2006) PGE(1) stimulation of HEK293 cells generates multiple contiguous domains with different [cAMP]: role of compartmentalized phosphodiesterases. *The Journal of cell biology* **175**, 441-451
138. Harootunian, A. T., Adams, S. R., Wen, W., Meinkoth, J. L., Taylor, S. S., and Tsien, R. Y. (1993) Movement of the free catalytic subunit of cAMP-dependent protein kinase into and out of the nucleus can be explained by diffusion. *Mol Biol Cell* **4**, 993-1002
139. Hagiwara, M., Brindle, P., Harootunian, A., Armstrong, R., Rivier, J., Vale, W., Tsien, R., and Montminy, M. R. (1993) Coupling of hormonal stimulation and transcription via the cyclic AMP-responsive factor CREB is rate limited by nuclear entry of protein kinase A. *Mol Cell Biol* **13**, 4852-4859
140. Agarwal, S. R., Yang, P. C., Rice, M., Singer, C. A., Nikolaev, V. O., Lohse, M. J., Clancy, C. E., and Harvey, R. D. (2014) Role of membrane microdomains in compartmentation of cAMP signaling. *PloS one* **9**, e95835
141. Agarwal, S. R., Gratwohl, J., Cozad, M., Yang, P. C., Clancy, C. E., and Harvey, R. D. (2018) Compartmentalized cAMP Signaling Associated With Lipid Raft and Non-raft Membrane Domains in Adult Ventricular Myocytes. *Front Pharmacol* **9**, 332
142. Wachten, S., Masada, N., Ayling, L. J., Ciruela, A., Nikolaev, V. O., Lohse, M. J., and Cooper, D. M. (2010) Distinct pools of cAMP centre on different isoforms of adenylyl cyclase in pituitary-derived GH3B6 cells. *J Cell Sci* **123**, 95-106
143. Willoughby, D., Wong, W., Schaack, J., Scott, J. D., and Cooper, D. M. (2006) An anchored PKA and PDE4 complex regulates subplasmalemmal cAMP dynamics. *The EMBO journal* **25**, 2051-2061
144. Maiellaro, I., Lohse, M. J., Kittel, R. J., and Calebiro, D. (2016) cAMP Signals in Drosophila Motor Neurons Are Confined to Single Synaptic Boutons. *Cell reports* **17**, 1238-1246
145. Depry, C., Allen, M. D., and Zhang, J. (2011) Visualization of PKA activity in plasma membrane microdomains. *Mol Biosyst* **7**, 52-58

146. Agarwal, S. R., MacDougall, D. A., Tyser, R., Pugh, S. D., Calaghan, S. C., and Harvey, R. D. (2011) Effects of cholesterol depletion on compartmentalized cAMP responses in adult cardiac myocytes. *J Mol Cell Cardiol* **50**, 500-509
147. Agarwal, S. R., Miyashiro, K., Latt, H., Ostrom, R. S., and Harvey, R. D. (2017) Compartmentalized cAMP responses to prostaglandin EP2 receptor activation in human airway smooth muscle cells. *Br J Pharmacol* **174**, 2784-2796
148. Averaimo, S., Assali, A., Ros, O., Couvet, S., Zagar, Y., Genescu, I., Rebsam, A., and Nicol, X. (2016) A plasma membrane microdomain compartmentalizes ephrin-generated cAMP signals to prune developing retinal axon arbors. *Nat Commun* **7**, 12896
149. Kennedy, E. J., and Scott, J. D. (2015) Selective disruption of the AKAP signaling complexes. *Methods Mol Biol* **1294**, 137-150
150. Otero, C., Penaloza, J. P., Rodas, P. I., Fernandez-Ramires, R., Velasquez, L., and Jung, J. E. (2014) Temporal and spatial regulation of cAMP signaling in disease: role of cyclic nucleotide phosphodiesterases. *Fundamental & clinical pharmacology* **28**, 593-607
151. Poppinga, W. J., Munoz-Llancao, P., Gonzalez-Billault, C., and Schmidt, M. (2014) A-kinase anchoring proteins: cAMP compartmentalization in neurodegenerative and obstructive pulmonary diseases. *Br J Pharmacol* **171**, 5603-5623
152. Froese, A., and Nikolaev, V. O. (2015) Imaging alterations of cardiomyocyte cAMP microdomains in disease. *Frontiers in Pharmacology* **6**
153. Fisher, D. A. (1996) Physiological variations in thyroid hormones: physiological and pathophysiological considerations. *Clinical Chemistry* **42**, 135-139
154. Kopp, P. (2001) Human Genome and Diseases: Review¶The TSH receptor and its role in thyroid disease. *Cellular and Molecular Life Sciences CMLS* **58**, 1301-1322
155. Nicolau, G. Y., and Haus, E. (1992) Chronobiology of the Hypothalamic-Pituitary-Thyroid Axis. in *Biologic Rhythms in Clinical and Laboratory Medicine* (Touitou, Y., and Haus, E. eds.), Springer Berlin Heidelberg, Berlin, Heidelberg. pp 330-347
156. Pellegriti, G., Frasca, F., Regalbuto, C., Squatrito, S., and Vigneri, R. (2013) Worldwide increasing incidence of thyroid cancer: update on epidemiology and risk factors. *J Cancer Epidemiol* **2013**, 965212
157. Allgeier, A., Offermanns, S., Van Sande, J., Spicher, K., Schultz, G., and Dumont, J. E. (1994) The human thyrotropin receptor activates G-proteins Gs and Gq/11. *J Biol Chem* **269**, 13733-13735

158. Dumont, J. E., Lamy, F., Roger, P., and Maenhaut, C. (1992) Physiological and pathological regulation of thyroid cell proliferation and differentiation by thyrotropin and other factors. *Physiol Rev* **72**, 667-697
159. Ledent, C., Dumont, J. E., Vassart, G., and Parmentier, M. (1992) Thyroid expression of an A2 adenosine receptor transgene induces thyroid hyperplasia and hyperthyroidism. *The EMBO journal* **11**, 537-542
160. Michiels, F. M., Caillou, B., Talbot, M., Dessarps-Freichey, F., Maunoury, M. T., Schlumberger, M., Mercken, L., Monier, R., and Feunteun, J. (1994) Oncogenic potential of guanine nucleotide stimulatory factor alpha subunit in thyroid glands of transgenic mice. *Proc Natl Acad Sci U S A* **91**, 10488-10492
161. Zeiger, M. A., Saji, M., Gusev, Y., Westra, W. H., Takiyama, Y., Dooley, W. C., Kohn, L. D., and Levine, M. A. (1997) Thyroid-specific expression of cholera toxin A1 subunit causes thyroid hyperplasia and hyperthyroidism in transgenic mice. *Endocrinology* **138**, 3133-3140
162. Parma, J., Duprez, L., Sande, J. V., Cochaux, P., Gervy, C., Mockel, J., Dumont, J., and Vassart, G. (1993) Somatic mutations in the thyrotropin receptor gene cause hyperfunctioning thyroid adenomas. *Nature* **365**, 649
163. Kosugi, S., Shenker, A., and Mori, T. (1994) Constitutive activation of cyclic AMP but not phosphatidylinositol signaling caused by four mutations in the 6th transmembrane helix of the human thyrotropin receptor. *FEBS letters* **356**, 291-294
164. Leet, A. I., and Collins, M. T. (2007) Current approach to fibrous dysplasia of bone and McCune-Albright syndrome. *Journal of children's orthopaedics* **1**, 3-17
165. Brillante, B., Guthrie, L., and Van Ryzin, C. (2015) McCune-Albright Syndrome: An Overview of Clinical Features. *Journal of pediatric nursing* **30**, 815-817
166. Roger, P. P., Servais, P., and Dumont, J. E. (1983) Stimulation by thyrotropin and cyclic AMP of the proliferation of quiescent canine thyroid cells cultured in a defined medium containing insulin. *FEBS letters* **157**, 323-329
167. Deleu, S., Pirson, I., Coulonval, K., Drouin, A., Taton, M., Clermont, F., Roger, P. P., Nakamura, T., Dumont, J. E., and Maenhaut, C. (1999) IGF-1 or insulin, and the TSH cyclic AMP cascade separately control dog and human thyroid cell growth and DNA synthesis, and complement each other in inducing mitogenesis. *Mol Cell Endocrinol* **149**, 41-51

168. Kimura, T., Van Keymeulen, A., Golstein, J., Fusco, A., Dumont, J. E., and Roger, P. P. (2001) Regulation of thyroid cell proliferation by TSH and other factors: a critical evaluation of in vitro models. *Endocr Rev* **22**, 631-656
169. Depoortere, F., Van Keymeulen, A., Lukas, J., Costagliola, S., Bartkova, J., Dumont, J. E., Bartek, J., Roger, P. P., and Dremier, S. (1998) A requirement for cyclin D3-cyclin-dependent kinase (cdk)-4 assembly in the cyclic adenosine monophosphate-dependent proliferation of thyrocytes. *The Journal of cell biology* **140**, 1427-1439
170. Van Keymeulen, A., Bartek, J., Dumont, J. E., and Roger, P. P. (1999) Cyclin D3 accumulation and activity integrate and rank the comitogenic pathways of thyrotropin and insulin in thyrocytes in primary culture. *Oncogene* **18**, 7351-7359
171. Iacovelli, L., Capobianco, L., Salvatore, L., Sallese, M., D'Ancona, G. M., and De Blasi, A. (2001) Thyrotropin activates mitogen-activated protein kinase pathway in FRTL-5 by a cAMP-dependent protein kinase A-independent mechanism. *Mol Pharmacol* **60**, 924-933
172. Dremier, S., Pohl, V., Poteet-Smith, C., Roger, P. P., Corbin, J., Doskeland, S. O., Dumont, J. E., and Maenhaut, C. (1997) Activation of cyclic AMP-dependent kinase is required but may not be sufficient to mimic cyclic AMP-dependent DNA synthesis and thyroglobulin expression in dog thyroid cells. *Mol Cell Biol* **17**, 6717-6726
173. Kupperman, E., Wen, W., and Meinkoth, J. L. (1993) Inhibition of thyrotropin-stimulated DNA synthesis by microinjection of inhibitors of cellular Ras and cyclic AMP-dependent protein kinase. *Mol Cell Biol* **13**, 4477-4484
174. Dremier, S., Milenkovic, M., Blancquaert, S., Dumont, J. E., Døskeland, S. O., Maenhaut, C., and Roger, P. P. (2007) Cyclic Adenosine 3',5'-Monophosphate (cAMP)-Dependent Protein Kinases, But Not Exchange Proteins Directly Activated by cAMP (Epac), Mediate Thyrotropin/cAMP-Dependent Regulation of Thyroid Cells. *Endocrinology* **148**, 4612-4622
175. Huk, D., Ashtekar, A., Magner, A., La Perle, K., and Kirschner, L. S. (2018) Deletion of Rap1b, but not Rap1a or Epac1, reduces PKA-mediated thyroid cancer. *Thyroid*
176. Hochbaum, D., Hong, K., Barila, G., Ribeiro-Neto, F., and Altschuler, D. L. (2008) Epac, in synergy with cAMP-dependent protein kinase (PKA), is required for cAMP-mediated mitogenesis. *The Journal of biological chemistry* **283**, 4464-4468
177. Fusco, A., Berlingieri, M. T., Di Fiore, P. P., Portella, G., Grieco, M., and Vecchio, G. (1987) One- and two-step transformations of rat thyroid epithelial cells by retroviral oncogenes. *Molecular and Cellular Biology* **7**, 3365-3370

178. Enserink, J. M., Christensen, A. E., de Rooij, J., van Triest, M., Schwede, F., Genieser, H. G., Doskeland, S. O., Blank, J. L., and Bos, J. L. (2002) A novel Epac-specific cAMP analogue demonstrates independent regulation of Rap1 and ERK. *Nat Cell Biol* **4**, 901-906
179. Christensen, A. E., Selheim, F., de Rooij, J., Dremier, S., Schwede, F., Dao, K. K., Martinez, A., Maenhaut, C., Bos, J. L., Genieser, H. G., and Doskeland, S. O. (2003) cAMP analog mapping of Epac1 and cAMP kinase. Discriminating analogs demonstrate that Epac and cAMP kinase act synergistically to promote PC-12 cell neurite extension. *J Biol Chem* **278**, 35394-35402
180. Mangeat, P., Roy, C., and Martin, M. (1999) ERM proteins in cell adhesion and membrane dynamics. *Trends in Cell Biology* **9**, 187-192
181. Gary, R., and Bretscher, A. (1995) Ezrin self-association involves binding of an N-terminal domain to a normally masked C-terminal domain that includes the F-actin binding site. *Mol Biol Cell* **6**, 1061-1075
182. Pearson, M. A., Reczek, D., Bretscher, A., and Karplus, P. A. (2000) Structure of the ERM protein moesin reveals the FERM domain fold masked by an extended actin binding tail domain. *Cell* **101**, 259-270
183. Amieva, M. R., Litman, P., Huang, L., Ichimaru, E., and Furthmayr, H. (1999) Disruption of dynamic cell surface architecture of NIH3T3 fibroblasts by the N-terminal domains of moesin and ezrin: in vivo imaging with GFP fusion proteins. *J Cell Sci* **112** (Pt 1), 111-125
184. Vaiskunaite, R., Adarichev, V., Furthmayr, H., Kozasa, T., Gudkov, A., and Voynoyasenetskaya, T. A. (2000) Conformational activation of radixin by G13 protein alpha subunit. *J Biol Chem* **275**, 26206-26212
185. Rein, M. L., and Deussing, J. M. (2012) The optogenetic (r)evolution. *Mol Genet Genomics* **287**, 95-109
186. Stierl, M., Stumpf, P., Udvari, D., Gueta, R., Hagedorn, R., Losi, A., Gartner, W., Petereit, L., Efetova, M., Schwarzl, M., Oertner, T. G., Nagel, G., and Hegemann, P. (2011) Light modulation of cellular cAMP by a small bacterial photoactivated adenylyl cyclase, bPAC, of the soil bacterium *Beggiatoa*. *J Biol Chem* **286**, 1181-1188
187. Deming, P. B., Campbell, S. L., Stone, J. B., Rivard, R. L., Mercier, A. L., and Howe, A. K. (2015) Anchoring of protein kinase A by ERM (ezrin-radixin-moesin) proteins is required for proper netrin signaling through DCC (deleted in colorectal cancer). *J Biol Chem* **290**, 5783-5796

188. Ruppelt, A., Mosenden, R., Gronholm, M., Aandahl, E. M., Tobin, D., Carlson, C. R., Abrahamsen, H., Herberg, F. W., Carpen, O., and Tasken, K. (2007) Inhibition of T cell activation by cyclic adenosine 5'-monophosphate requires lipid raft targeting of protein kinase A type I by the A-kinase anchoring protein ezrin. *Journal of immunology (Baltimore, Md. : 1950)* **179**, 5159-5168
189. Newman, R. H., and Zhang, J. (2014) The design and application of genetically encodable biosensors based on fluorescent proteins. *Methods Mol Biol* **1071**, 1-16
190. Bajar, B. T., Wang, E. S., Zhang, S., Lin, M. Z., and Chu, J. (2016) A Guide to Fluorescent Protein FRET Pairs. *Sensors (Basel, Switzerland)* **16**, 1488
191. Adams, S. R., Harootunian, A. T., Buechler, Y. J., Taylor, S. S., and Tsien, R. Y. (1991) Fluorescence ratio imaging of cyclic AMP in single cells. *Nature* **349**, 694-697
192. Patel, N., and Gold, M. G. (2015) The genetically encoded tool set for investigating cAMP: more than the sum of its parts. *Front Pharmacol* **6**, 164
193. Paramonov, V. M., Mamaeva, V., Sahlgren, C., and Rivero-Müller, A. (2015) Genetically-encoded tools for cAMP probing and modulation in living systems. *Frontiers in Pharmacology* **6**, 196
194. Lefkimmatis, K., Moyer, M. P., Curci, S., and Hofer, A. M. (2009) "cAMP Sponge": A Buffer for Cyclic Adenosine 3', 5'-Monophosphate. *PLoS ONE* **4**, e7649
195. Ohta, Y., Kamagata, T., Mukai, A., Takada, S., Nagai, T., and Horikawa, K. (2016) Nontrivial Effect of the Color-Exchange of a Donor/Acceptor Pair in the Engineering of Förster Resonance Energy Transfer (FRET)-Based Indicators. *ACS Chem Biol* **11**, 1816-1822
196. Jiang, J. Y., Falcone, J. L., Curci, S., and Hofer, A. M. (2017) Interrogating cyclic AMP signaling using optical approaches. *Cell calcium* **64**, 47-56
197. Ponsioen, B., Zhao, J., Riedl, J., Zwartkruis, F., van der Krogt, G., Zaccolo, M., Moolenaar, W. H., Bos, J. L., and Jalink, K. (2004) Detecting cAMP-induced Epac activation by fluorescence resonance energy transfer: Epac as a novel cAMP indicator. *EMBO Reports* **5**, 1176-1180
198. Klarenbeek, J. B., Goedhart, J., Hink, M. A., Gadella, T. W., and Jalink, K. (2011) A mTurquoise-based cAMP sensor for both FLIM and ratiometric read-out has improved dynamic range. *PLoS One* **6**, e19170

199. van der Krogt, G. N., Ogink, J., Ponsioen, B., and Jalink, K. (2008) A comparison of donor-acceptor pairs for genetically encoded FRET sensors: application to the Epac cAMP sensor as an example. *PLoS One* **3**, e1916
200. Klarenbeek, J., Goedhart, J., van Batenburg, A., Groenewald, D., and Jalink, K. (2015) Fourth-generation epac-based FRET sensors for cAMP feature exceptional brightness, photostability and dynamic range: characterization of dedicated sensors for FLIM, for ratiometry and with high affinity. *PLoS One* **10**, e0122513
201. Castro, L. R. V., Gervasi, N., Guiot, E., Cavellini, L., Nikolaev, V. O., Paupardin-Tritsch, D., and Vincent, P. (2010) Type 4 Phosphodiesterase Plays Different Integrating Roles in Different Cellular Domains in Pyramidal Cortical Neurons. *The Journal of Neuroscience* **30**, 6143-6151
202. Alford, S. C., Ding, Y., Simmen, T., and Campbell, R. E. (2012) Dimerization-Dependent Green and Yellow Fluorescent Proteins. *ACS Synthetic Biology* **1**, 569-575
203. Harada, K., Ito, M., Wang, X., Tanaka, M., Wongso, D., Konno, A., Hirai, H., Hirase, H., Tsuboi, T., and Kitaguchi, T. (2017) Red fluorescent protein-based cAMP indicator applicable to optogenetics and in vivo imaging. *Sci Rep* **7**, 7351
204. Ohta, Y., Furuta, T., Nagai, T., and Horikawa, K. (2018) Red fluorescent cAMP indicator with increased affinity and expanded dynamic range. *Sci Rep* **8**, 1866
205. Juilfs, D. M., Fulle, H. J., Zhao, A. Z., Houslay, M. D., Garbers, D. L., and Beavo, J. A. (1997) A subset of olfactory neurons that selectively express cGMP-stimulated phosphodiesterase (PDE2) and guanylyl cyclase-D define a unique olfactory signal transduction pathway. *Proc Natl Acad Sci U S A* **94**, 3388-3395
206. Jin, S. L., Bushnik, T., Lan, L., and Conti, M. (1998) Subcellular localization of rolipram-sensitive, cAMP-specific phosphodiesterases. Differential targeting and activation of the splicing variants derived from the PDE4D gene. *J Biol Chem* **273**, 19672-19678
207. Verde, I., Pahlke, G., Salanova, M., Zhang, G., Wang, S., Coletti, D., Onuffer, J., Jin, S. L., and Conti, M. (2001) Myomegalin is a novel protein of the golgi/centrosome that interacts with a cyclic nucleotide phosphodiesterase. *J Biol Chem* **276**, 11189-11198
208. Mongillo, M., McSorley, T., Evellin, S., Sood, A., Lissandron, V., Terrin, A., Huston, E., Hannawacker, A., Lohse, M. J., Pozzan, T., Houslay, M. D., and Zaccolo, M. (2004) Fluorescence resonance energy transfer-based analysis of cAMP dynamics in live neonatal rat cardiac myocytes reveals distinct functions of compartmentalized phosphodiesterases. *Circ Res* **95**, 67-75

209. Stefan, E., Wiesner, B., Baillie, G. S., Mollajew, R., Henn, V., Lorenz, D., Furkert, J., Santamaria, K., Nedvetsky, P., Hundsrucker, C., Beyermann, M., Krause, E., Pohl, P., Gall, I., MacIntyre, A. N., Bachmann, S., Houslay, M. D., Rosenthal, W., and Klussmann, E. (2007) Compartmentalization of cAMP-dependent signaling by phosphodiesterase-4D is involved in the regulation of vasopressin-mediated water reabsorption in renal principal cells. *Journal of the American Society of Nephrology : JASN* **18**, 199-212
210. Boswell-Smith, V., Spina, D., and Page Clive, P. (2009) Phosphodiesterase inhibitors. *British Journal of Pharmacology* **147**, S252-S257
211. Baillie, G. S., Sood, A., McPhee, I., Gall, I., Perry, S. J., Lefkowitz, R. J., and Houslay, M. D. (2003) β -Arrestin-mediated PDE4 cAMP phosphodiesterase recruitment regulates β -adrenoceptor switching from G(s) to G(i). *Proceedings of the National Academy of Sciences of the United States of America* **100**, 940-945
212. Alto, N. M., Soderling, S. H., Hoshi, N., Langeberg, L. K., Fayos, R., Jennings, P. A., and Scott, J. D. (2003) Bioinformatic design of A-kinase anchoring protein-in silico: A potent and selective peptide antagonist of type II protein kinase A anchoring. *Proceedings of the National Academy of Sciences of the United States of America* **100**, 4445-4450
213. Gold, M. G., Lygren, B., Dokurno, P., Hoshi, N., McConnachie, G., Tasken, K., Carlson, C. R., Scott, J. D., and Barford, D. (2006) Molecular basis of AKAP specificity for PKA regulatory subunits. *Mol Cell* **24**, 383-395
214. Wang, Y., Ho, T. G., Bertinetti, D., Neddermann, M., Franz, E., Mo, G. C., Schendowich, L. P., Sukhu, A., Spelts, R. C., Zhang, J., Herberg, F. W., and Kennedy, E. J. (2014) Isoform-selective disruption of AKAP-localized PKA using hydrocarbon stapled peptides. *ACS Chem Biol* **9**, 635-642
215. Burns-Hamuro, L. L., Ma, Y., Kammerer, S., Reineke, U., Self, C., Cook, C., Olson, G. L., Cantor, C. R., Braun, A., and Taylor, S. S. (2003) Designing isoform-specific peptide disruptors of protein kinase A localization. *Proceedings of the National Academy of Sciences* **100**, 4072-4077
216. Carlson, C. R., Lygren, B., Berge, T., Hoshi, N., Wong, W., Tasken, K., and Scott, J. D. (2006) Delineation of type I protein kinase A-selective signaling events using an RI anchoring disruptor. *J Biol Chem* **281**, 21535-21545
217. Wang, Y., Ho, T. G., Franz, E., Hermann, J. S., Smith, F. D., Hehnly, H., Esseltine, J. L., Hanold, L. E., Murph, M. M., Bertinetti, D., Scott, J. D., Herberg, F. W., and Kennedy, E. J. (2015) PKA-type I selective constrained peptide disruptors of AKAP complexes. *ACS Chem Biol* **10**, 1502-1510

218. Verdine, G. L., and Hilinski, G. J. (2012) Stapled peptides for intracellular drug targets. *Methods in enzymology* **503**, 3-33
219. Faruque, O. M., Le-Nguyen, D., Lajoix, A. D., Vives, E., Petit, P., Bataille, D., and Hani, E. H. (2009) Cell-permeable peptide-based disruption of endogenous PKA-AKAP complexes: a tool for studying the molecular roles of AKAP-mediated PKA subcellular anchoring. *Am J Physiol Cell Physiol* **296**, C306-316
220. Calejo, A. I., and Tasken, K. (2015) Targeting protein-protein interactions in complexes organized by A kinase anchoring proteins. *Front Pharmacol* **6**, 192
221. Tsalkova, T., Mei, F. C., Li, S., Chepurny, O. G., Leech, C. A., Liu, T., Holz, G. G., Woods, V. L., Jr., and Cheng, X. (2012) Isoform-specific antagonists of exchange proteins directly activated by cAMP. *Proc Natl Acad Sci U S A* **109**, 18613-18618
222. Almahariq, M., Tsalkova, T., Mei, F. C., Chen, H., Zhou, J., Sastry, S. K., Schwede, F., and Cheng, X. (2013) A novel EPAC-specific inhibitor suppresses pancreatic cancer cell migration and invasion. *Mol Pharmacol* **83**, 122-128
223. Chen, H., Tsalkova, T., Mei, F. C., Hu, Y., Cheng, X., and Zhou, J. (2012) 5-Cyano-6-oxo-1,6-dihydro-pyrimidines as potent antagonists targeting exchange proteins directly activated by cAMP. *Bioorganic & medicinal chemistry letters* **22**, 4038-4043
224. Rehmann, H. (2013) Epac-inhibitors: facts and artefacts. *Sci Rep* **3**, 3032
225. Sayner, S. L., Alexeyev, M., Dessauer, C. W., and Stevens, T. (2006) Soluble adenylyl cyclase reveals the significance of cAMP compartmentation on pulmonary microvascular endothelial cell barrier. *Circ Res* **98**, 675-681
226. Schroder-Lang, S., Schwarzel, M., Seifert, R., Strunker, T., Kateriya, S., Looser, J., Watanabe, M., Kaupp, U. B., Hegemann, P., and Nagel, G. (2007) Fast manipulation of cellular cAMP level by light in vivo. *Nat Methods* **4**, 39-42
227. Steuer Costa, W., Yu, S.-c., Liewald, J. F., and Gottschalk, A. (2017) Fast cAMP Modulation of Neurotransmission via Neuropeptide Signals and Vesicle Loading. *Current Biology* **27**, 495-507
228. Ryu, M. H., Moskvina, O. V., Siltberg-Liberles, J., and Gomelsky, M. (2010) Natural and engineered photoactivated nucleotidyl cyclases for optogenetic applications. *J Biol Chem* **285**, 41501-41508

229. Lindner, R., Hartmann, E., Tarnawski, M., Winkler, A., Frey, D., Reinstein, J., Meinhart, A., and Schlichting, I. (2017) Photoactivation Mechanism of a Bacterial Light-Regulated Adenylyl Cyclase. *J Mol Biol* **429**, 1336-1351
230. Ash, C., Dubec, M., Donne, K., and Bashford, T. (2017) Effect of wavelength and beam width on penetration in light-tissue interaction using computational methods. *Lasers in Medical Science* **32**, 1909-1918
231. Ryu, M.-H., Kang, I.-H., Nelson, M. D., Jensen, T. M., Lyuksyutova, A. I., Siltberg-Liberles, J., Raizen, D. M., and Gomelsky, M. (2014) Engineering adenylate cyclases regulated by near-infrared window light. *Proceedings of the National Academy of Sciences of the United States of America* **111**, 10167-10172
232. Scheib, U., Broser, M., Constantin, O. M., Yang, S., Gao, S., Mukherjee, S., Stehfest, K., Nagel, G., Gee, C. E., and Hegemann, P. (2018) Rhodopsin-cyclases for photocontrol of cGMP/cAMP and 2.3 Å structure of the adenylyl cyclase domain. *Nature Communications* **9**, 2046
233. Berglund, K., Birkner, E., Augustine, G. J., and Hochgeschwender, U. (2013) Light-emitting channelrhodopsins for combined optogenetic and chemical-genetic control of neurons. *PloS one* **8**, e59759
234. Berglund, K., Clissold, K., Li, H. E., Wen, L., Park, S. Y., Gleixner, J., Klein, M. E., Lu, D., Barter, J. W., Rossi, M. A., Augustine, G. J., Yin, H. H., and Hochgeschwender, U. (2016) Luminopsins integrate opto- and chemogenetics by using physical and biological light sources for opsin activation. *Proceedings of the National Academy of Sciences of the United States of America* **113**, E358-E367
235. Park, S. Y., Song, S. H., Palmateer, B., Pal, A., Petersen, E. D., Shall, G. P., Welchko, R. M., Ibata, K., Miyawaki, A., Augustine, G. J., and Hochgeschwender, U. (2017) Novel luciferase-opsin combinations for improved luminopsins. *Journal of neuroscience research*
236. Tung, J. K., Gutekunst, C.-A., and Gross, R. E. (2015) Inhibitory luminopsins: genetically-encoded bioluminescent opsins for versatile, scalable, and hardware-independent optogenetic inhibition. *Scientific Reports* **5**, 14366
237. Insel, P. A., Maguire, M. E., Gilman, A. G., Bourne, H. R., Coffino, P., and Melmon, K. L. (1976) Beta adrenergic receptors and adenylate cyclase: products of separate genes? *Molecular pharmacology* **12**, 1062-1069
238. Hall, M. P., Unch, J., Binkowski, B. F., Valley, M. P., Butler, B. L., Wood, M. G., Otto, P., Zimmerman, K., Vidugiris, G., Machleidt, T., Robers, M. B., Benink, H. A., Eggers, C. T., Slater, M. R., Meisenheimer, P. L., Klaubert, D. H., Fan, F., Encell, L. P., and

- Wood, K. V. (2012) Engineered luciferase reporter from a deep sea shrimp utilizing a novel imidazopyrazinone substrate. *ACS Chem Biol* **7**, 1848-1857
239. Timney, B. L., Raveh, B., Mironska, R., Trivedi, J. M., Kim, S. J., Russel, D., Wentz, S. R., Sali, A., and Rout, M. P. (2016) Simple rules for passive diffusion through the nuclear pore complex. *The Journal of cell biology* **215**, 57-76
240. Cheng, K. P., Kiernan, E. A., Eliceiri, K. W., Williams, J. C., and Watters, J. J. (2016) Blue Light Modulates Murine Microglial Gene Expression in the Absence of Optogenetic Protein Expression. *Scientific Reports* **6**, 21172
241. Barrow, K. M., Perez-Campo, F. M., and Ward, C. M. (2006) Use of the cytomegalovirus promoter for transient and stable transgene expression in mouse embryonic stem cells. *Methods Mol Biol* **329**, 283-294
242. Stierl, M., Penzkofer, A., Kennis, J. T., Hegemann, P., and Mathes, T. (2014) Key residues for the light regulation of the blue light-activated adenylyl cyclase from *Beggiatoa* sp. *Biochemistry* **53**, 5121-5130
243. Feinstein, T. N., Wehbi, V. L., Ardura, J. A., Wheeler, D. S., Ferrandon, S., Gardella, T. J., and Vilardaga, J. P. (2011) Retromer terminates the generation of cAMP by internalized PTH receptors. *Nature chemical biology* **7**, 278-284
244. Gheorgheosu, D., Dehelean, C., Cristea, M., and Muntean, D. (2011) Development of the B16 Murine Melanoma Model. *Ann Rom Soc Cell Biol* **16**, 148-156
245. Fidler, I. J. (1975) Biological behavior of malignant melanoma cells correlated to their survival in vivo. *Cancer Res* **35**, 218-224
246. Cillo, C., Dick, J. E., Ling, V., and Hill, R. P. (1987) Generation of drug-resistant variants in metastatic B16 mouse melanoma cell lines. *Cancer Res* **47**, 2604-2608
247. Prezioso, J. A., Wang, N., Duty, L., Bloomer, W. D., and Gorelik, E. (1993) Enhancement of pulmonary metastasis formation and gamma-glutamyltranspeptidase activity in B16 melanoma induced by differentiation in vitro. *Clinical & experimental metastasis* **11**, 263-274
248. Bennett, D. C., Holmes, A., Devlin, L., and Hart, I. R. (1994) Experimental metastasis and differentiation of murine melanoma cells: actions and interactions of factors affecting different intracellular signalling pathways. *Clinical & experimental metastasis* **12**, 385-397

249. Hill, S. E., Rees, R. C., and MacNeil, S. (1990) A positive association between agonist-induced cyclic AMP production in vitro and metastatic potential in murine B16 melanoma and hamster fibrosarcoma. *Clinical & experimental metastasis* **8**, 461-474
250. Hill, S. E., Rees, R. C., and MacNeil, S. (1990) The regulation of cyclic AMP production and the role of cyclic AMP in B16 melanoma cells of differing metastatic potential. *Clinical & experimental metastasis* **8**, 475-489
251. Lester, B. R., Stadel, J. M., Buscarino, C., Sheppard, J., Greig, R. G., and Poste, G. (1987) Reconstitution of the Gs protein from B16 melanoma clones of high and low experimental metastatic potential into S49 cyc-membranes. *Biochem Biophys Res Commun* **147**, 443-451
252. Sheppard, J. R., Lester, B., Doll, J., Buscarino, C., Gonzales, E., Corwin, S., Greig, R., and Poste, G. (1986) Biochemical regulation of adenylate cyclase in murine melanoma clones with different metastatic properties. *International Journal of Cancer* **37**, 713-722
253. Kameyama, K., Vieira, W. D., Tsukamoto, K., Law, L. W., and Hearing, V. J. (1990) Differentiation and the tumorigenic and metastatic phenotype of murine melanoma cells. *Int J Cancer* **45**, 1151-1158
254. Murata, J., Ayukawa, K., Ogasawara, M., Fujii, H., and Saiki, I. (1997) Alpha-melanocyte-stimulating hormone blocks invasion of reconstituted basement membrane (Matrigel) by murine B16 melanoma cells. *Invasion & metastasis* **17**, 82-93
255. Kim, A., Son, M., Kim, K. I., Yang, Y., Song, E. Y., Lee, H. G., and Lim, J. S. (2009) Elevation of intracellular cyclic AMP inhibits NF-kappaB-mediated thymosin beta4 expression in melanoma cells. *Exp Cell Res* **315**, 3325-3335
256. Agarwal, K. C., and Parks, R. E., Jr. (1983) Forskolin: a potential antimetastatic agent. *Int J Cancer* **32**, 801-804
257. Watanabe, Y., Murata, T., Shimizu, K., Morita, H., Inui, M., and Tagawa, T. (2012) Phosphodiesterase 4 regulates the migration of B16-F10 melanoma cells. *Experimental and Therapeutic Medicine* **4**, 205-210
258. Greco, A., Albanese, S., Auletta, L., Mirabelli, P., Zannetti, A., D'Alterio, C., Di Maro, G., Orlandella, F. M., Salvatore, G., Soricelli, A., and Salvatore, M. (2016) High-Frequency Ultrasound-Guided Injection for the Generation of a Novel Orthotopic Mouse Model of Human Thyroid Carcinoma. *Thyroid* **26**, 552-558
259. Mancini, M., Vergara, E., Salvatore, G., Greco, A., Troncone, G., Affuso, A., Liuzzi, R., Salerno, P., Scotto di Santolo, M., Santoro, M., Brunetti, A., and Salvatore, M. (2009)

- Morphological ultrasound microimaging of thyroid in living mice. *Endocrinology* **150**, 4810-4815
260. Espana-Agusti, J., Tuveson, D. A., Adams, D. J., and Matakidou, A. (2015) A minimally invasive, lentiviral based method for the rapid and sustained genetic manipulation of renal tubules. *Sci Rep* **5**, 11061
261. Pfeifer, A., and Verma, I. M. (2001) Gene therapy: promises and problems. *Annual review of genomics and human genetics* **2**, 177-211
262. Bindels, D. S., Haarbosch, L., van Weeren, L., Postma, M., Wiese, K. E., Mastop, M., Aumonier, S., Gotthard, G., Royant, A., Hink, M. A., and Gadella, T. W., Jr. (2017) mScarlet: a bright monomeric red fluorescent protein for cellular imaging. *Nat Methods* **14**, 53-56
263. Hyun, H., Park, M. H., Owens, E. A., Wada, H., Henary, M., Handgraaf, H. J. M., Vahrmeijer, A. L., Frangioni, J. V., and Choi, H. S. (2015) Structure-inherent targeting of near-infrared fluorophores for parathyroid and thyroid gland imaging. *Nature Medicine* **21**, 192
264. Wada, H., Hyun, H., Kang, H., Gravier, J., Henary, M., Bordo, M. W., Choi, H. S., and Frangioni, J. V. (2017) Intraoperative Near-Infrared Fluorescence Imaging of Thymus in Pre-Clinical Models. *The Annals of thoracic surgery* **103**, 1132-1141
265. Neumann, S., Geras-Raaka, E., Marcus-Samuels, B., and Gershengorn, M. C. (2010) Persistent cAMP signaling by thyrotropin (TSH) receptors is not dependent on internalization. *Faseb j* **24**, 3992-3999
266. Schaap, P., van Ments-Cohen, M., Soede, R. D., Brandt, R., Firtel, R. A., Dostmann, W., Genieser, H. G., Jastorff, B., and van Haastert, P. J. (1993) Cell-permeable non-hydrolyzable cAMP derivatives as tools for analysis of signaling pathways controlling gene regulation in Dictyostelium. *J Biol Chem* **268**, 6323-6331
267. Moll, D., Prinz, A., Brendel, C. M., Berrera, M., Guske, K., Zaccolo, M., Genieser, H. G., and Herberg, F. W. (2008) Biochemical characterization and cellular imaging of a novel, membrane permeable fluorescent cAMP analog. *BMC biochemistry* **9**, 18
268. Shipunova, V. O., Shilova, O. N., Shramova, E. I., Deyev, S. M., and Proshkina, G. M. (2018) A Highly Specific Substrate for NanoLUC Luciferase Furimazine Is Toxic in vitro and in vivo. *Russian Journal of Bioorganic Chemistry* **44**, 225-228